Technische Universität München
Fachgebiet für Theoretische Chemie

# Density functional studies of acrolein hydrogenation on silver surfaces

**Amjad Basha Mohammad**

Vollständiger Abdruck der vom Department für Chemie der Technischen Universität München zur Erlangung des akademischen Grades eines

**Doktors der Naturwissenschaften (Dr. rer. nat. )**

genehmigten Dissertation.

Vorsitzender: Univ.-Prof. Dr. H. J. Neusser

Prüfer der Dissertation:
1. Univ.-Prof. Dr. N. Rösch
2. Univ.-Prof. Dr. K.−O. Hinrichsen

Die Dissertation wurde am 13.05.2008 bei der Technischen Universität München eingereicht und durch die Fakultät für Chemie am 03.06.2008 angenommen.

## Acknowledgements

First and foremost, I would like to thank my Doktorvater, Prof. Dr. Notker Rösch for giving me the opportunity to do my doctoral thesis in his research group. I am grateful for his support throughout these years.

I would like to thank Prof. Dr. Konstantin M. Neyman for his guidance and Dr. Zhao Xu Chen who has introduced me to this topic. The many discussions and constant help from Dr. Ilya V. Yudanov and Dr. Kok Hwa Lim were highly useful to finish my research work successfully. I thank Dr. S. Krüger for the many administrative supports and scientific discussions.

I appreciate the camaraderie shared among the past and present research group members: Dr. R. Deka, Dr. S. Majumder, Dr. K. Siriwong, Dr. C. Inntam, Dr. C. Bussai, Dr. G. M. Xiong, Dr. F. Schlosser, Dr. Q. Sun, P. Chuichay, Dr. A. Ivanova, Dr. G. N. Vyssilov, Dr. A. Genest, Dr. A. Matveev, Dr. G. Jezierski, A. Deka, R. S. Ray, R. Ramakrishnan, H. R. Miquel, M. Metzner, A. Kremleva, S. N. Derrar, S. Bosko, E. Vladimirov and those not mentioned here. They have not only made my stay enjoyable, but also taught me many things.

I am grateful too, for the financial support from Deutsche Forschungsgemeinschaft (DFG). My German friends were very helpful in improving my German language skills and also they enriched my awareness of German culture. I would also like to thank my brother Imdad for motivating me in many aspects of my life. I am indebted to my in-laws and relatives for their constant support throughout the years. I would also like to thank Mr. Reddy who helped me in the last moments of my thesis submission. The Indian community in Garching was very helpful in many ways.

Finally I would like to thank my wife Ruhi for her love, patience, understanding and the encouragement. My son Sharuq made my life very pleasant and enjoyable.

Amjad Basha Mohammad
Munich, Germany
6th May'2008

Dedicated with love to my parents

Shakira Begum and Mahbub Basha

# Abstract

The selective hydrogenation of the C=O bond is a challenge. Silver being a widely used oxidation catalyst, when supported on silica, Ag/SiO2, exhibits a rather high selectivity (~40 %) for allylic alcohol during acrolein hydrogenation, in comparison to group VIII metals such as Pt. The origin of atomically adsorbed hydrogen is a prerequisite for acrolein hydrogenation reaction. Hydrogen dissociative adsorption reaction is endothermic with an activation barrier of about 120 kJ/mol. Oxygen binds strongly on silver and the dissociative adsorption of hydrogen on oxygen reconstructed silver surfaces like p(nx1)O/Ag(110), $O_{oss}$/Ag(111) and O/Ag(110), is highly exothermic with the barriers ranging from ~70 kJ/mol to as low as 10 kJ/mol. Oxygen pretreatment increased the selectivity towards allyl alcohol, to more than 50%. The most efficient mechanism for hydrogen activation found is dissociative adsorption near an isolated O atom at the Ag(110) surface where each oxygen produces two adsorbed hydrogen atoms and the oxygen is removed in the form of water.

Mechanism of acrolein hydrogenation to propenol or propanal is studied on O/Ag(110) as this is the only surface which shows exothermicity. Acrolein hydrogenation is also studied on $O_{oss}$/Ag(111) surface as it is less endothermic with respect to other surfaces. The calculated barriers suggest that the $O_{oss}$/Ag(111) surface yields a high selectivity to allyl alcohol even though the reaction may be slow due to high hydrogenation barriers of acrolein and the intermediates.

# Zusammenfassung

Die selektive Hydrierung der C=O Bindung stellt ein große Herausforderung dar. Silber wird gewöhnlich als Oxidationskatalysator vewendet. Im Vergleich zu den Metallen der Gruppe VIII wie Pt, besitzt Silber geträgert auf Siliciumdioxid, $Ag/SiO_2$, bei der Acrolein Hydrierung eine relativ hohe Selektivität (40%) zu allylischem Alkohol. Für die Hydrierung ist die Bildung eines atomar adsorbierten Wasserstoffatoms Vorraussetzung. Die dissoziative Adsorption von Wasserstoff ist endotherm und besitzt eine Aktivierungsbarriere von 120 kJ/mol. Sauerstoff wird stark an Silber gebunden und die dissoziative Adsorption von Wasserstoff an Sauerstoff–veränderten Silberoberflächen wie *p*(nx1)O/Ag(110), $O_{oss}$/Ag(111) and O/Ag(110) ist stark exotherm mit einer Aktievierungsbarriere von bis ~10 kJ/mol bis 70 kJ/mol. Die Vorbehandlung mit Sauerstoff erhöht die Selektivität bezüglich allylischem Alkohls auf über 50%. Der effizienteste Mechanismus für die Wasserstoffaktivierung ist die dissoziative Adsorption nahe eines isolierten Sauerstoffatoms auf der Ag(110)-Oberfläche, da jedes Sauerstoffatom zwei adsorbierte Wasserstoffatome bildet und Sauerstoff als Wasser von der Oberfläche entfernt wird.

Der Mechanismus der Acrolein Hydrierung zu Propenol oder Propanal wurde an O/Ag(110) untersucht, da nur diese Oberfläche Exothermizität aufweist. Die Acrolein Hydrierung wurde auch an einer $O_{oss}$/Ag(111) Oberfläche untersucht, da sie bezüglich der anderen Oberflächen am wenigsten endotherm ist. Die berechneten Barrieren deuten darauf hin, dass die $O_{oss}$/Ag(111) eine hohe Selektivität für allylischen Alkohol ergibt, auch wenn wegen der hohen Hydrierungsbarrieren von Acrolein und er übrigen Intermediate die Reaktion langsam verläuft .

# Table of Contents

# Chapter 1
# Introduction

A catalyst is a material that facilitates the conversion of reactants to the desired products without itself being consumed [1]. Usually, it also increases the rate of a reaction by lowering the corresponding barrier(s) of activation. Catalysts play a crucial role in nature and in activities of man. Many aspects of daily life are affected by catalysts, from the purification of breathing air to the formation of fuel used for cars. Apart from the actual products, also intermediates produced during catalytic processes are used in many industries. In general there are two types of catalytic processes: heterogeneous and homogeneous. In heterogeneous catalytic processes, the catalyst and the reactants are in two different media, e.g., the catalyst is a supported metallic particle, the reactants may be in the gas phase, and the reaction occurs at the metal-gas interface. In homogeneous catalysis catalyst and reactants are in the same phase. The bulk of products of chemical industry is produced in heterogeneous catalytic processes.

Catalytic reactions typically comprise different important basic steps, e.g., physisorption, chemisorption, dissociation and activation, diffusion, recombination and desorption. In the case of acrolein hydrogenation over silver surfaces, acrolein in the gas phase has to react with the surface, and in this process the first reaction step is physisorption whereby the molecules are weakly bound to a surface, mostly through Van der Waals forces [1]. In subsequent steps, these molecules and their transformation products bind to the surface through molecule-metal bonding, a process referred to as chemisorption [1]. The energy required to break such bonds is referred to as “binding

energy". Usually the next step in a catalytic cycle is bond dissociation or activation of the required functional group or an intermediate which is bound to the surface. On the surface of a catalyst, there are defect sites like kinks and steps which are often more active in bond breaking than sites on an ideal surface. Almost all desired reactions happen at such defect sites. Therefore, one has to explore not only ideal surfaces, which are easier to study, but also surface defects and impurities etc. After the activation of a molecule, intermediate species formed on the surface will diffuse on the surface depending on how low the energy barrier for diffusion is. Finally one also has to take into account reverse reactions, like the recombination of intermediate species to the reactants.

The desorption energy of the products is also important in the catalytic cycle, and once the desired product is removed from the surface the active sites will be free for the next catalysis cycle. However, there are few catalysts which allow many cycles; they perish upon few cycles of catalytic reactions. Related to the life time of a catalyst are also problems like active sites getting blocked by other products of reactions due to unfavourable side reactions, rendering the catalyst inactive after some time. This undesirable process is termed catalyst "poisoning"; for example, in petroleum refining the supported metal catalyst produces 200–800 barrels of products per pound of catalyst [2].

To understand the mechanism of a catalytic process all these steps may be modelled by quantum chemical calculations. Most calculations related to heterogeneous catalysis are done using methods which are based on density functional theory (DFT) [3,4]. These calculations are useful in providing the necessary atomistic level of understanding to the experimentalist who is facing a lot of problems in characterizing the catalyst at the atomic level. Experimentalists and theoreticians who work on designing catalysts have three important issues in mind: the catalyst should produce the desired products, show high activity, and maintain its activity for a long time.

The task of the present study was to examine by means of quantum chemical calculations the hydrogenation of acrolein, $CH_2$=CH–CH=O (Figure 1.1), over supported silver particles, modelled as extended silver surfaces. Selective catalytic hydrogenation of organic molecules containing a number of unsaturated functional groups is an important

step in the industrial preparation of fine chemicals and has been attracting much interest in fundamental research in catalysis [5], e.g., allylic alcohols obtained by preferred hydrogenation of the C=O group of unsaturated aldehydes are valuable intermediates for the production of perfumes, flavouring and pharmaceuticals [5].

Acrolein or propenal is one of the simplest α,β-unsaturated aldehydes (Figure 1.1). Acrolein is useful in producing polyester resin, acrylic acid and glycerol [6–8]. Acrolein has also been used in World War I as a chemical weapon [9]. When skin is exposed to acrolein it causes serious damage [10].

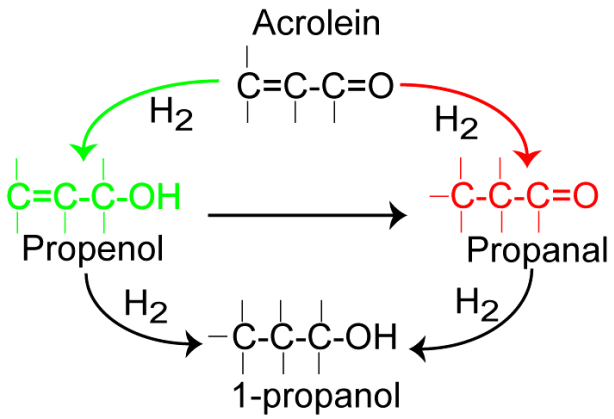


**Figure 1.1:** Schematic representation of acrolein hydrogenation cycle

Hydrogenation is a chemical reaction where hydrogen attacks multiple bonds of unsaturated organic compounds, yielding new molecules. The reverse reaction is dehydrogenation. Such reactions happen in the gas phase at high temperatures, and one of the roles of the catalyst is to decrease the temperature at which the reaction occurs. In the presence of most of the conventional group VIII metal hydrogenation catalysts, α,β-unsaturated aldehydes are hydrogenated predominantly to saturated aldehydes by reduction of the C=C group or to saturated alcohols [11]. Recently, also silver has been shown to be an active hydrogenation catalyst with an unexpected selectivity for unsaturated alcohol [11]. Gold particles also show a similar type of catalytic selectivity to allyl alcohol [12], but silver gained more attention because it is much cheaper.

In acrolein hydrogenation, these reaction steps are modelled according to the Horiuti-Polanyi mechanism [1], where hydrogen prefers to attack the double bond in sequential order, i.e. it first either attacks the C=O or the C=C bond. Usually the carbon atoms in organic compounds tend to have the most stable configurations by getting attached to two hydrogen atoms and maintaining single bonds with the rest of the chain. In the case of unsaturated aldehydes there will be double or triple bonds which are open for hydrogen attacks. In acrolein hydrogenation it is desirable to find catalysts which will control the intermolecular selectivity by hydrogenating preferentially the C=O group while keeping the olefinic double bond intact (Figure 1.1, reaction to propenol).

In order to prevent consecutive hydrogenations to the saturated alcohol, 1-propanol and the isomerization of the allylic alcohol, the catalyst has to suppress these reaction pathways, i.e., the reaction pathways marked in red and black color in Figure 1.1. In the gas phase, hydrogenation of the C=O bond is disfavoured with respect to hydrogenation of the adjacent C=C bond, both thermodynamically and kinetically [13]. Thus, the selective hydrogenation of the C=O bond represents a challenge which is somewhat facilitated for higher aldehydes $R_1R_2C$=CH-CH=O, where bulky substituents $R_i$, interacting with the catalyst, may sterically hinder the activation of the C=C bond [13–16]. Acrolein as the lowest α,β-unsaturated aldehyde does not exhibit such steric hindrance and the transformation to unsaturated alcohols is even more difficult, the selectivity is generally low, ~2% [17].

Silver is very well known as an oxidation catalyst [18,19], but Claus et al. showed that when supported on silica, $Ag/SiO_2$, exhibits a rather high selectivity (~40 %) for allylic alcohol during acrolein hydrogenation [20], in comparison to the group VIII metals such as Pt (~2 %) [13]. In support of the above finding, some experimental studies [12,21,22] substantiated the crucial role of Ag as an active component in the selective hydrogenation.

Apart from the present work on silver, the research group of Sautet et al. is working on DFT studies of acrolein hydrogenation on the surface of Pt and related alloys [23]. Recently, Loffreda et. al. with the help of DFT calculations found that it is more

favourable to hydrogenate the C=O bond on Pt(111) surface compared to the C=C bond for acrolein hydrogenation. However, poor selectivity of allylic alcohol is still observed on the Pt(111) surface because the allylic alcohol binds too strongly to the Pt catalysts, making it the rate determining step for the formation of allylic alcohol [23].

The aim of the present work is to use the density functional computational approach to help clarify the chemical process which makes silver to behave unusually as a hydrogenation catalyst. To achieve this goal, this study first and foremost will

(1) look into hydrogen dissociative adsorption on silver surfaces and the role of oxygen, possibly present on such surfaces, and

(2) study acrolein hydrogenation on clean and oxygen reconstructed silver surfaces

This dissertation is organized as follows. In Chapter 2, the experimental background and previous theoretical works are presented. Chapter 3 presents the theoretical background and the computational method with which the results to be presented subsequently have been obtained. In Chapter 4, hydrogen activation, adsorption and diffusion on well-defined silver surfaces is discussed. In Chapter 5, the adsorption and diffusion of oxygen on surfaces of silver catalysts as well as its effect on the activation of hydrogen are explored in detail. Chapter 6 is devoted to acrolein adsorption and hydrogenation on silver surfaces and oxygen reconstructed silver surfaces.

# Chapter 2
# Status of the field

In this section a summary of the existing work related to experimental and theoretical investigations of acrolein hydrogenation is presented. Upon hydrogenation of lower α,β-unsaturated aldehydes like acrolein and crotonaldehyde using group VIII metals like Pt, Rh, or Pd, supported on silica, the unsaturated aldehydes are converted mostly to the saturated aldehydes and only to a much smaller degree to unsaturated alcohols [11,24]. Using high resolution electron energy loss spectroscopy (HREELS) and temperature programmed desorption (TPD) experiments, oxidation of π–allyl ($\eta^3$-$C_3H_5$) over Ag(110) surface has been shown to yield acrolein (-59 kJ $mol^{-1}$), the corresponding half hydrogenated intermediate (Horiuti-Polanyi mechanism) (-239 kJ $mol^{-1}$), and allyl alcohol (-71 kJ $mol^{-1}$). The corresponding large (in absolute terms) adsorption enthalpies, given in parentheses, point to a strong interaction of these species with silver surfaces [25]. These results stimulated Claus and co-workers to use silver catalysts for acrolein hydrogenation reactions and to look for possibilities for their modifications [26]. Claus et al. used a fully computer controlled fixed-bed micro reactor system (CCRS) [27] to carry out gas phase hydrogenations of α,β-unsaturated aldehydes (acrolein, crotonaldehyde) on Ag catalysts. The possibly better catalysts Ag and also Au will be reviewed in the following sections. Selectivity depends on many factors like method of preparation of catalyst, availability of hydrogen on catalyst, pressure, temperature, and oxygen pretreatment of the catalyst. All these factors will be explained in detail in the following sections.

## 2.1 Experimental studies

### 2.1.1 Catalyst preparation and characterization techniques

Catalyst preparation is a very important initial step. Different methods have lead to different selectivities for acrolein hydrogenation (Table 2.1). Several standard preparatory methods have been used also for silver catalyst preparation for acrolein hydrogenation. The sol-gel process is a procedure for making glass or ceramic like materials [28]. It process involves the transition of a system from a liquid into a solid phase. A series of hydrolysis and polymerization reactions are done on the precursor until it forms a colloidal suspension, then the particles condense in a new phase, the gel, in which a solid macromolecule is immersed in a solvent [28]. Using the sol-gel technique one can produce high-surface-area materials and also microporous materials. These high-surface-area microporous crystalline materials play a crucial role in many applications of surface science, ranging from gas separation [29] to heterogeneous catalysis [30]. Using this method the catalyst $Ag/SiO_2$-SG was prepared [31] for acrolein hydrogenation; it consists of silver particles supported in silica gel. Incipient wetness impregnation (IW) is another technique used by Claus et al. in synthesizing the catalyst [32]. Thereby, the metal precursor is dissolved in an aqueous or organic solution. That solution is then added to a catalyst support which exhibits the same pore volume as the volume of solution that was added. Capillary action draws the solution into the pores. The catalyst is then calcined (thermal treatment process) and dried to drive off the volatile components within the solution, depositing the metal on the catalyst surface. In the following sections different designators will be used to designate the various catalysts by their preparation technique, e.g., $Ag/TiO_2$-LTR and $Ag/TiO_2$-HTR (Table 2.1) were prepared using the IW method. The catalyst $Ag/TiO_2$-LTR was reduced by hydrogen at a low temperature, 473 K, and $Ag/TiO_2$-HTR was reduced at a high temperature, 773 K [33]. Other methods for catalyst preparation were deposition-precipitation (DP); for instance, the catalyst $Ag/SiO_2$-DP was prepared according to this method [20]. Using only precipitation, the catalyst $Ag/SiO_2$-P was prepared [22]. Even further techniques have been used, e.g., sputtering where silver is sputtered on an aluminium foil [20]. All these catalysts were reduced in a flow of hydrogen which in turn generated metallic silver,

These catalysts were characterized with different methods, depending on the specific requirement and the type of the catalyst. Upon chemical analysis of all the catalysts prepared, it was observed that silver is present in its metallic form [22]. The various preparation methods yielded different sizes of silver particles. In catalysts prepared with the sol-gel technique, silver particles are between 2 and 5 nmM; they are smaller than particles prepared by other methods, e.g. impregnation and precipitation [31]. With the help of X-ray diffraction (XRD) it was shown that silver is present in crystalline form in the catalysts prepared by silver sputtering and electrochemical deposition [20]. A study by X-ray photoelectron spectroscopy (XPS, also known as electron spectroscopy for chemical analysis or ESCA), showed that the catalyst prepared by precipitation exhibits a silver oxide ($Ag_2O$) phase [20]. This is an important result because in further sections oxygen species on Ag surfaces will be shown to potentially play an important significant role in the mechanism of acrolein hydrogenation. From ESR results, it was concluded that on silver catalysts supported on $TiO_2$, at 77 K, partial reduction of the $TiO_2$ support is favored [34]. Also these above ESR studies illustrated that a distribution of the silver nanoparticles is present, not just two distinct particle sizes. Considerably smaller nanoparticles were observed at increased temperatures around 293 K.

### 2.1.2 Hydrogen adsorption on silver

It is important to study the interaction of hydrogen with silver before one examines the hydrogenation of acrolein because atomically adsorbed hydrogen is a prerequisite for the hydrogenation of acrolein. Dissociation of molecular hydrogen $H_2$ on metals to form atomic H species is a crucial step in numerous technologically important processes; just to mention hydrogen storage [35]. Differently from many other metals, $H_2$ dissociation on clean planar silver surfaces appears to be unlikely according to a variety of surface science [36–40] and theoretical [41–43] studies. This contradicts experimental findings which showed silver, well-known to catalyze *oxidation* reactions [44], also is an efficient *hydrogenation* catalyst which transforms $\alpha,\beta$-unsaturated aldehydes to unsaturated alcohols [11]. At low temperatures like 100 K, only physisorption of $H_2$ is observed on the Ag(111) surface indicating that $H_2$ dissociation on silver is an activated process and

there is no dissociative adsorption of hydrogen for exposures up to $10^4$ L [36]. From experimental results, the binding energy of $H_2$ on Ag surfaces was estimated to be 15 kJ $mol^{-1}$ [37]. Hydrogen molecular adsorption was not at all observed on Ag(110) at 90 K [39].

Based on the finding that $H_2$ does not dissociate on Ag(111) at 100 K the upper limit for the binding energy of H atoms at this surface was estimated at 218 kJ $mol^{-1}$, i.e. half of the $H_2$ dissociation energy in gas phase [39]. Also, on the more open Ag(110) surface dissociative adsorption of $H_2$ is found to be a strongly activated process [38]. As $H_2$ cannot be activated under common experimental conditions on clean low-index surfaces of silver, one has to discuss alternative activation sites, either sites on higher-index surfaces, which contain more active low-coordinated metal centres, or surface sites formed by impurities, e.g. atomic oxygen [45,46].

On the other hand the silver catalysts supported on silica ($Ag/SiO_2$) which has been prepared using IW and precipitation methods are able to activate hydrogen, and the existence of atomic hydrogen on these surfaces has been studied by isotopic exchange [22]. Deuterium has been pulsed over hydrogen pretreated silver catalysts and in the outlet of the chemical reactor $H_2$ and HD has been detected. These results show the presence of hydrogen on surface. The catalyst $Ag/SiO_2$-IW was able to activate gas-phase hydrogen and to stabilize hydrogen atoms on catalyst surface and the adsorption of hydrogen is completely reversible [20]. In this experiment atomic hydrogen was even observed at high temperature in vacuum; hydrogen seems to interact strongly with highly dispersed silver. The two different catalysts prepared by two different methods have different ratio of $HD/H_2$, which indicates that hydrogen activation depends on the size distribution of the metal particles [22].

Thus, it is possible that the hydrogen activation takes place at defect sites or at kinks, since it is known that hydrogen dissociation is not possible at low index surfaces of silver single crystals [47]. Hydrogen atoms may then diffuse and occupy more stable adsorption sites, for example in case of flat surface facets of nanoparticles. Due to the weak interaction of hydrogen with single crystal silver surfaces and the relatively strong

interaction with nanoparticles at high pressures, the catalytic properties of silver are modified [22]. There is no clear information in which form hydrogen exists on Ag surfaces. Hydrogen might exist either in molecular form or dissociatively adsorbed hydrogen or subsurface hydrogen as indicated at higher values of coverage [48].

For comparison also Au surface may be discussed, which is also very active as catalyst for hydrogen dissociation (Table 2.1). Small surface strain on gold, induced by the support may be responsible for the hydrogen activation [49]. It was concluded that the supported gold particles may be responsible for the activation of hydrogen and the hydrogenation properties of supported gold catalysts [46].

There are also speculations that hydrogen activation occurs at special sites at the interface between the support and metal [50]. However, Boudart and coworkers [51] demonstrated that it is possible to hydrogenate acrolein using unsupported Ag. But taking into account the evidence as discussed above that $H_2$ activation by pure silver is not very probable, also in this case impurities may be involved as active sites for $H_2$ dissociation. Hence, given the right temperature, pressure, and silver structure or defects, $H_2$ can be activated. It is one of the goals of the present work to explore Ag surface structures which facilitate hydrogen availability on silver catalysts.

### 2.1.3 Acrolein hydrogenation

Acrolein hydrogenation has successfully been performed on Ag catalysts by the group of Claus [21]. Hydrogen and acrolein are used as reactants. Experiments were performed in a pressure range of 0.5 to 20 MPa and a temperature range of 453-595 K under steady-state conditions of the catalysts. As important characteristic parameters of catalysts, the selectivity (S) of the reaction product can be calculated from the moles of product formed per moles of acrolein converted. Turn-over frequencies (TOF) were determined from the number of chemisorbed oxygen species per surface area of a metallic particle; the latter quantity was estimated via the particle as derived from transmission electron microscopy (TEM).

It has to be noted that thermodynamics favours hydrogenation of the C=C over the C=O bond of unsaturated aldehydes. The C=C bond is more reactive than the C=O functional group on group VIII metal surfaces [52]. This is one of the reasons that in the presence of most of conventional monometallic hydrogenation catalysts, based on Pt, Rh, or Pd on silica or alumina as supports, lower α,β-unsaturated aldehydes such as acrolein and crotonaldehyde are hydrogenated mostly to the saturated aldehydes and only to a small extent to unsaturated alcohols [11,24]. For acrolein hydrogenation allyl alcohol and propanal are the main hydrogenation products. The selectivity with respect to allyl alcohol and propanal is almost independent of the degree of acrolein conversion. However, the product distribution depends strongly on the pressure applied: the higher the total pressure, the higher the concentration of allyl alcohol [22]. In addition it is observed that partial pressures of hydrogen and acrolein influence the catalytic performance more than the total pressure. Keeping the total pressure constant, and changing the partial pressure of either acrolein or hydrogen, increases the selectivity to allyl alcohol. On the other hand, increase in the total pressure of the reaction mixture by adding argon without changing the partial pressures of hydrogen and acrolein does not have any considerable effect on the selectivity.

As stated above, the selectivity depends on the preparation method of the catalyst. In comparison to other catalyst preparatory methods, the catalyst prepared by the sol-gel technique ($Ag/SiO_2$-SG) showed a selectivity of 44 % to allyl alcohol and maintained this selectivity for longer times [22] (Table 2.1). The lowest selectivity towards allylic alcohol was observed over the catalysts prepared by the precipitation method. However, with time there is a constant deactivation as well as decrease in selectivity. For instance after 12.5 h of time, selectivity towards allyl alcohol decreased from 44 % to 36 % in case of catalysts prepared by the sol-gel method. The support could be involved in the catalytic reaction; for example, acrolein adsorbs readily on silica gel. The interaction of the carbonyl group of acrolein via hydrogen bonding with isolated silanol groups and with a pair of vicinal surface silanol groups, respectively, results in strong interaction of acrolein with silica [53]. Also a support free silver catalyst was prepared using the precipitation method; its selectivity to allyl alcohol and propanal did not depend on the presence of a support in the catalyst [22].

Prior to hydrogenation, acrolein is adsorbed on the surface. Acrolein binds weekly on silver surfaces and IRAS investigations of silver films showed that the adsorption geometry of acrolein depends on the coverage [54]. Oxygen pretreated Ag(110) surfaces exhibiting electropositive surface sites in the vicinity of adsorbed oxygen favours the coordination via the C=O functional group [55,56].From their IRAS results [54], Itoh and co-workers proposed four types of structures of acrolein on silver films at 90 K. In all four cases the molecular plane is parallel to the surface. In two structures, acrolein was proposed to interact directly with the silver substrate, while the others were assigned to physisorbed states, i.e. they form molecular layers on top of the first two forms where acrolein is having chemical interaction with the substrate. At higher exposures, multilayer structures are formed [54].

Reflection-absorption spectroscopy on Pt single crystals found that there acrolein is lying flat on the surface and binds through the C=O functional group [57]. The C=O functional group is oriented parallel to the surface [57]. A partly hydrogenated product of acrolein hydrogenation, propionaldehyde, has been detected by *in situ* XAS studies [20]. This could indicate, that at low pressure addition of the second hydrogen is slow and rate determining, whereas the adsorption and addition of the first hydrogen are fast steps [20]. Besides the factors discussed above, very recent experiments by Claus et al. [58] showed that the degree of reduction of silver by hydrogen also has a strong influence on the activity and selectivity in acrolein hydrogenation. Claus et al. found that the oxygen pretreatment on a deactivated $Ag/SiO_2$ catalysts significantly increased the hydrogenation activity and improved the selectivity, especially at lower reaction pressures [58].

In Figure 2.1, four samples are selected depending on the way in which they were reduced with hydrogen and how the pretreatment by oxygen was done. Out of the first two, the catalyst H2-325 was reduced with hydrogen at 325 °C and the catalyst Air-250 was pretreated with oxygen ex-situ at 250 °C. The other two remaining catalysts were pretreated with oxygen and later reduced with hydrogen at two different temperatures (Air-250 H2-250; Air-250 H2-325). The selectivity to allyl alcohol was the highest for the catalyst which had been strongly reduced with hydrogen at 325 °C after oxidation

(Air-250H2-325)).

**Table 2.1:** Performance of Ag hydrogenation catalysts in acrolein conversion in comparison to Au and Pt. Selectivity (S), reaction temperature (T) and pressure (P).

| Catalyst | T, K | P, MPa | S, % | Ref |
|---|---|---|---|---|
| $Ag/TiO_2$-LTR IW | 473 | 2 | 42 | [32] |
| $Ag/TiO_2$-HTR IW | 473 | 2 | 27 | [32] |
| Ag-In/$SiO_2$ | 513 | 2 | 60 | [26] |
| | | 4 | 61 | [26] |
| $Ag/SiO_2$-IW | 523 | 1 | 40 | [20] |
| | | 2 | 45 | [20] |
| | 533 | 0.1 | 30 | [20] |
| $Ag/SiO_2$-DP | 523 | 1 | 35 | [20] |
| | | 2 | 40 | [20] |
| $Ag/SiO_2$-S | 523 | 1 | 20 | [20] |
| | | 2 | 25 | [20] |
| | 533 | 0.1 | 13 | [20] |
| Ag/Al-S | 648 | 0.1 | 8 | [20] |
| $Ag/SiO_2$-IW | 523 | 1 | 40 | [22] |
| $Ag/SiO_2$-P | | 0.5 | 32 | [22] |
| | | 1 | 35 | [22] |
| | | 1.5 | 36 | [22] |
| $Ag/SiO_2$-SG | | 2 | 44 | [22] |
| $Au/ZrO_2$ | 513 | 2 | 41 | [12] |
| $Pt/ZrO_2$ | | | 4 | [12] |
| Au/ZnO | 593 | 2 | 34 | [59] |
| Au-In/ZnO | | | 63 | [59] |
| Au - powder | 513 | 2 | 7 | [59] |
| $Au/SiO_2$ | 533 | 2 | 23 | [46] |

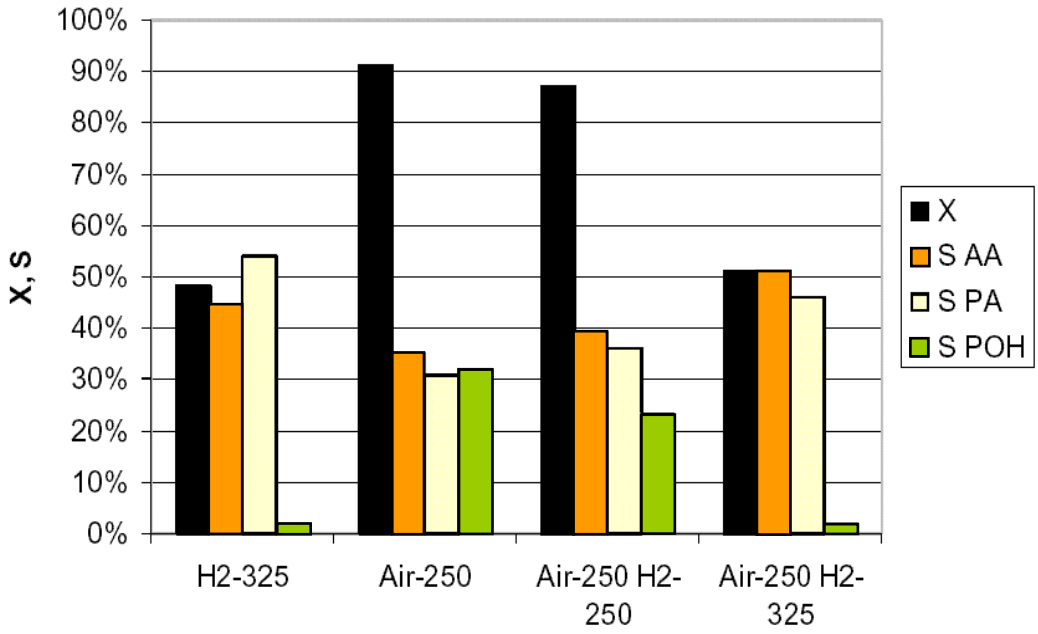


**Figure 2.1:** Conversion and selectivity to the main products in the gas phase hydrogenation of acrolein over differently pretreated $Ag/SiO_2$ catalysts at 10 bar. AA: allyl alcohol, PA: propionaldehyde, POH: propanol, X: conversion (ratio between amount converted to products in comparison with the total input to the reaction), S: selectivity (ratio between the desired product formation and the total input to the reaction). Catalyst preparation: H2-325 – reduction with hydrogen at 325 °C, Air-250 – pretreatment of oxygen, Air-250 H2-250 – reduced catalyst at 250 °C after oxidation, Air-250 H2-325 – reduced catalyst at 325 °C after oxidation. Adapted from Ref. 60.

The data displayed in Figure 2.1 suggest that the selectivity of the catalysts correlates with their conversion rates. The selectivity also depends on the preparation of the catalyst; for example, catalyst Air-250 H2-325 has a higher selectivity than catalysts Air-250 or H2-325. In the case of H2-325, the catalyst was treated by hydrogen, the conversion was very low and so was the selectivity; similarly, for Air-250 the conversion was found to be high and so was the selectivity is also high. With both oxygen pretreatment and hydrogen reduction at 325 °C the selectivity increased to ~ 50%. The overall hydrogenation activity increased two- to three-fold after oxidative pretreatment [60]. Thus, a used catalyst which is no more active can be regenerated by an oxygen treatment [2]. All these findings suggest that oxygen might play an important role in the catalysis of acrolein hydrogenation. Hence, in this thesis, we will first explore the

dissociative adsorption of hydrogen on clean and oxygen reconstructed silver surfaces, prior to the actual study of acrolein hydrogenation.Interaction of oxygen with silver has been studied extensively, still the nature of oxygen on silver is not clear [44,61–68]. Surface science studies under ultra-high vacuum (UHV) conditions provided more detailed structural information. In particular, an added-row reconstruction of the Ag(110) surface by adsorbed oxygen is experimentally well-established [69–73]: Ag-O-Ag-O chains develop along the [001] direction. The interaction between the chains is repulsive and ordered ($n\times1$) structures ($n$ = 2–8) have been observed, with $n$ larger for lower oxygen coverage. This added-row $p(n\times1)$O/Ag(110) system appears to be the only surface phase of oxygen on silver with a well-defined structure. The chemisorption of atomic oxygen on the Ag(111) surface at temperatures between 400 K and 500 K produces a $p$(4x4) pattern over a range of coverages up to a saturation of 0.51±0.04 ML [74]. Still the structure of the silver oxide over layer formation on Ag(111) is not clear and debatable [75,65].

It is well known that small atoms can diffuse into the crystal lattices (sub-surface sites) of transition metals in appreciable quantities, affecting bulk properties and causing various macroscopic phenomena, such as corrosion and embrittlement [76]. Also surface properties may be affected because of impurities residing in interstices near the surface. A recent STM study of the Pd(111) surface by Rose et al. suggests the existence of subsurface carbon and oxygen [77] and studies of H in Ni(111) point to the unique reactivity of subsurface H for the hydrogenation of surface species [78-80]. Oxygen subsurface may be viewed as an initial stage in the corrosion and the growth of metal oxides [81]. The most stable oxide of silver, $Ag_2O$, decomposes at 460 K and at atmospheric pressure. Silver oxide catalysts get destabilized due to the temperature treatment used during preparation. Note that other oxidic structures may be more stable, e.g. ruthenium oxide is stable up to temperatures greater than 1000 K [82]. At low coverages ($\theta$ = 0.05±0.03 ML), O atoms are known to occupy subsurface octahedral sites below the first Ag layer [83]. However, it has been shown that on-surface adsorption at low coverage is significantly more favourable [84,85]. Compared to on-surface oxygen adsorption on Ag(111), which exhibits a strong decrease in adsorption energy with increasing coverage, subsurface oxygen shows a weak dependence on coverage [84]. The

octrahedral site is favoured for all coverages ranging from 0.11 to 1 ML [84]. The effect of sulfurization on the selectivity of allyl alcohol during acrolein hydrogenation is small, as reported by Ponec et al. [13]; yet, a substantial effect was observed by Hutchings et al. [86] who reported a selectivity of 46% allyl alcohol. Thus the role of sulfurization remains controversial.

Besides the well known group VIII metals and Ag also other catalysts like Au and mixed metal catalysts have been found to be efficient hydrogenation catalysts [59]. Controlled reactions of organometallic precursorscompounds with surfaces of metals or metal oxides can give bimetallic particles with quite different hydrogenation properties compared to the corresponding monometallic catalysts. Claus et al. [11] achieved the highest selectivity to crotyl alcohol (75 %) in the gas phase hydrogenation of crotonaldehyde using catalyst based on group VIII metals which was modified by a second metal. With this motivation Lucas et al. [26] developed an indium-silver supported catalyst with indium being less in weight percentage compared to silver, Ag-In/$SiO_2$ (Table 2.1). This catalyst gave a selectivity of 60 % with respect to allyl alcohol. Moreover this catalyst is extremely suitable for liquid phase hydrogenation of acrolein under moderate hydrogenation conditions [26].

Catalytic properties of gold supported catalysts used for acrolein hydrogenation depend on the occurrence of multiply twinned particles (MTPs) and the degree of particle rounding (particle with almost no facets) [59]. MTPs cause a lowering of the selectivity to allyl alcohol. In silver catalysts the metal particles do not exhibit a completely spherical shape, but are truncated, and to a certain extent MTPs occur even at very small size [87]. Hydrogenation of acrolein over an Au/$SiO_2$ catalyst prepared by incipient wetness is compared with other catalysts in Table 2.1. This catalyst gave high selectivity to crotyl alcohol in comparison with allyl alcohol. In case of Au/$TiO_2$ catalysts prepared by deposition-precipitation methods the selectivity to the unsaturated alcohol was decreased to 60 – 70 % when using crotonaldehyde, to 30% in case of acrolein. Until now apart from gold on oxide supports, silver catalysts are the only candidates which convert acrolein to allyl alcohol with selectivities one order of magnitude higher than group VIII hydrogenation catalysts.

There are several questions which remained unanswered by the experimentalists. To get a better understanding of the chemical process at a molecular level, theoretical works were carried out which will be reviewed in the next section.

## 2.2 Theoretical studies

There are not many theoretical studies of acrolein hydrogenation on metal catalysts, specifically for silver there is no work in literature so far. However, hydrogen and oxygen adsorption behaviour on metals has been studied extensively. This is of interest also for the present study. The hydrogen molecule binds to the Ag(111) surface by 10 kJ $mol^{-1}$, as obtained with the local density approximation (LDA) [41]. DF calculations at the gradient-corrected (GGA) level yielded binding energies of H atoms that vary slightly with the exchange-correlation approximation, ~200 kJ $mol^{-1}$ (PW91 functional) [88] and ~185 kJ $mol^{-1}$ (RPBE functional) [89] for H adsorption at 3-fold hollow sites of the Ag(111) surface [43]. Such an energy gain by H adsorption is not sufficient for dissociating $H_2$ from the gas-phase onto the Ag(111) surface, which requires an energy expense of 436 kJ $mol^{-1}$ (experiment) [90] or 439 kJ $mol^{-1}$ (DF calculations with PBE and PW91 functionals [91]). On the Ag(100) surface, a rather high activation barrier of 105 kJ $mol^{-1}$ for hydrogen dissociation has been determined from DF calculations with the PW91 functional [42]. DF calculations of Mavrikakis et al. determined an activation barrier of 107 kJ $mol^{-1}$ for hydrogen dissociation on the Ag(111) surface [43]. These results are in line with the experimental finding that hydrogen does not dissociate at clean silver surfaces (see above) and needs to probe into the presence of impurities like oxygen on the surface.

At low oxygen exposure the Ag(110) surface gets reconstructed and results in added row structure as discussed above in the experimental Section 2.3. There are few theoretical studies which tried to model the added row structure [92,93]. Structural

characteristics obtained in DF LDA calculations [92] are different from those of DF GGA calculations [93]; results obtained at the GGA level are closer to experiment. A more detailed study of the structural differences will be presented in Chapter 3 of this thesis. Using the DACAPO code [94,95], Mavrikakis et al. determined oxygen to be less stable in sub-surface octahedral sites than at the three-fold hollow sites of the Ag(111) surface [43]. Also, the same DF calculations showed that the hydrogen activation energy is 107 kJ $mol^{-1}$ on the clean Ag(111) surface with 1/2 hydrogen coverage i.e. two hydrogen atoms per four silver atoms. A reduced barrier of 71 kJ $mol^{-1}$ was calculated with sub surface oxygen on Ag(111) surface, with oxygen coverage of ½. In this case the final state comprised two hydrogen atoms which occupy one hcp and one fcc site next to the subsurface oxygen. This demonstrates that there is some important role of oxygen in decreasing the activation energy of hydrogen.

A study by Khanra et al. for the Ag(111) surface [96], using the concept of bond order conservation and Morse potentials (BOC-MP), yielded a high selectivity to allyl alcohol in comparison to the Pt(111) surface. On clean silver surfaces like Ag(111), acrolein has binding energy of about 10 kJ $mol^{-1}$ [97]. On the Ag(110) surface, it binds also with ~ 10 kJ $mol^{-1}$, while the binding energy is ~ 20 kJ $mol^{-1}$ on the stepped surface Ag(221) [97]. In these calculations five layer models were used with 0.17 ML acrolein coverage on Ag(110) and with 0.08 ML coverage of acrolein on Ag(221) surface. All these calculations were performed with the plane-wave based Vienna ab initio simulation package (VASP) [98-100] using the PW91 exchange-correlation functional [101]. So far DF calculations on acrolein hydrogenation has been studied in detail only for Pt(111) surface by Sautet et al. [23]. These calculations employed a four layer substrate slab model with a 0.11 ML coverage of adsorbates, which were placed on only one side of the slab. Optimization of the adsorbates together with the top two layers of the substrate was undertaken. Sautet et al. were interested in the Pt surface because of the high availability of hydrogen atoms on that surface.

On Ag surfaces the trans isomer of acrolein was calculated 10 kJ $mol^{-1}$ more stable than the cis isomer of acrolein [97]. As the overall interaction of acrolein with this substrate is weak, comparison to the relative abundance in the gas phase seems possible.

Indeed, these computational results for acrolein at Ag surfaces agree well with experiments in the gas phase where, at room temperature, 96 % of acrolein molecules exhibit the *trans* form [102]. In all model calculations of this work, the trans form of acrolein was used.

Considerable coverage effects have been found for acrolein adsorption on the Pt(111) surface. With increasing acrolein coverage the binding energy decreases [103], iat 0.08 ML coverage the binding energy is 99 kJ $mol^{-1}$ and at 0.25 ML coverage it is reduced to 79 kJ $mol^{-1}$. Thus, on Pt(111) the adsorption of acrolein is rather strong compared to Ag surfaces. A low selectivity to allyl alcohol was identified because of the strong binding of allyl alcohol, ~ 200 kJ $mol^{-1}$ at the Pt(111) surface, in comparison to the binding of propanal, ~ 170 kJ $mol^{-1}$ [23]. Despite of the low barriers for acrolein hydrogenation, i.e. less than 100 kJ $mol^{-1}$, the selectivity to allyl alcohol is very low due to the larger binding energy of this product at Pt (111).

## 2.3 Summary

From the discussion of the experimental results it is obvious that silver can be used as hydrogenation catalyst. Even though silver is inert to hydrogen activation it has a good selectivity for allyl alcohol in acrolein hydrogenation. The selectivity depends on the total pressure of the reactants acrolein and hydrogen. Not only the pressure influences the selectivity but also oxygen pretreatment and hydrogen reduction. Availability of hydrogen on silver surface is a key factor for the acrolein hydrogenation. Dissociation of hydrogen may be facilitated by defect sites or edges and then it diffuses to attack the acrolein. Claus et al. observed that the catalysts which has been oxygen pretreated shows a good selectivity to allyl alcohol, and also observed an increment in selectivity on hydrogen reduced catalysts. Adsorbed oxygen is a possible candidate for facilitating hydrogen dissociative adsorption. Also there are speculations about the existence of sub-surface oxygen. Another factor which influences the selectivity is the catalyst prepara-

tion. For example, catalysts prepared by the sol-gel method show the largest selectivity.

Later on we will present results of a detailed study of how hydrogen behaves on stepped surfaces like (110) and (221), and flat surfaces like (111). Impurities on or below the surface also help to lower the activation energy for hydrogen dissociative adsorption on silver surface. Theoretical studies of Mavrikakis et al. showed that subsurface oxygen lowers the activation energy of hydrogen over Ag(111) surface. Following this direction oxygen on Ag(110) surface and sub surface Ag(111) surfaces has been studied in this thesis. The effect of presence of oxygen on Ag surfaces will be discussed in detail in Chapters 4 and 5.

Sautet et al. studied computationally acrolein hydrogenation over the surface Pt(111). Due to the high binding energy of allyl alcohol the selectivity to allyl alcohol is very low on Pt(111), even though the hydrogenation reaction barriers are relatively low. On Ag surfaces ((111), (110) and (221)) acrolein binds very weakly, with a binding energy of ~ 10 to 20 kJ $mol^{-1}$ and molecular hydrogen also binds very weakly.

The aim of this thesis is to contribute to resolving open questions in regard to acrolein hydrogenation by silver catalysts. What facilitates hydrogen dissociation by reducing the activation barrier over Ag surfaces? Do surface defects, impurities or subsurface oxygen play a role? Answers to these questions will help to understand the process of hydrogen activation. Further questions related to the mechanism of acrolein hydrogenation are: What is the thermodynamic force which drives the reaction in favour of allyl alcohol? To answer this, one needs to determine pertinent intermediates and reaction energies of elementary steps of acrolein hydrogenation as well as the corresponding activation energies. All these questions were addressed in this thesis.

# Chapter 3
# Methods and Computational Details

This chapter provides an overview over the computational methods used and the corresponding choice of parameters. After a small introduction to the electronic structure method, then the computational parameters and models used are discussed. Finally the procedures applied in transition state search are sketched.

## 3.1 Electronic structure method

All electronic calculations carried out in this work are based on Density Functional Theory (DFT) [3,4]. This theory describes the total energy of a solid or a molecule as a functional of the electron density. Hohenberg and Kohn showed [3] that the energy of a system is a unique functional of the electronic density. Modern methods on the basis of DFT, which now are extensively used for solving many chemical and physical problems, have been established by Kohn and Sham (KS) [4]. The exchange-correlation functional of KS theory and the corresponding effective one-electron potential $V_{xc}$ are not exactly known. Therefore, approximations such as the generalized gradient approximation (GGA) or hybrid functionals [104] are used.

All calculations described in the subsequent chapters were performed with the plane-wave based Vienna ab initio simulation package, VASP [98-100], applying the GGA in the form of the exchange-correlation functional PW91 [101]. Specifically, the

projector augmented wave method, as implemented in VASP [105,106], was used to describe the interaction between atomic cores and electrons. Monkhorst-Pack grids [107] of the size (5x5x1) in reciprocal space were combined with a generalized Gaussian smearing technique [108], for integration over the Brillouin zone. The size of k-grids has been tested for the adsorption of hydrogen atoms on the top site of Ag(110) where the

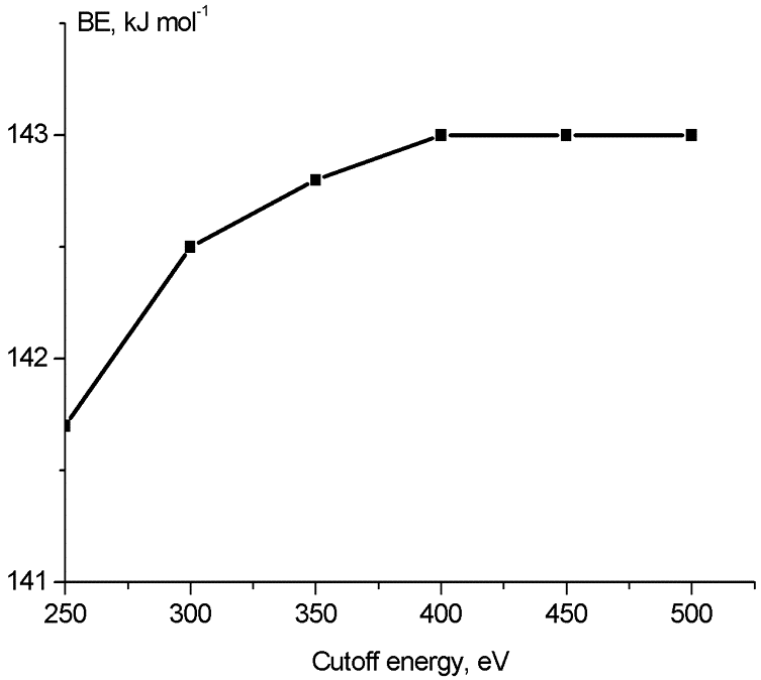


**Figure 3.1:** Binding energy of a hydrogen atom on the Ag(110) surface as function of the energy cutoff parameter, at a surface coverage of 1/4. Ag(110) is modelled by a slab of two metal layers. A (5x5x1) k-point grid was applied.

binding energy of H atoms was calculated for different k-grids, starting from (3x3x1) to (7x7x1). The binding energy converged to 143 kJ $mol^{-1}$ from (5x5x1). An energy cut-off of 400 eV which determines the size of the plane wave basis set has been used throughout all calculations. Test calculations for H adsorbed on Ag(110) showed that this value indicates convergence of binding energies within 1 kJ $mol^{-1}$ (Figure 3.1). During structure optimizations, all forces of the atoms relaxed (see below) were converged to at least 0.02 eV/Å.

## 3.2 Characteristic energies

The binding energy (BE) of an adsorbed molecule, defined as the energy required for breaking the bond between the adsorbate and the surface, is calculated according to the following expression,

$$BE = E_{tot}(ads) + E_{tot}(sub) - E_{tot}(ads+sub) \quad (3.2.1)$$

Here, $E_{tot}$ refers to the total energy of a system under consideration. $E_{tot}(ads+sub)$ is the total energy of the system where adsorbates are bound to the substrate in their optimized positions. $E_{tot}(ads)$ and $E_{tot}(sub)$ are the total energies of the adsorbate in the gas phase and of the clean substrate, respectively.

The reaction energy (RE) is the difference between the summed total energies of products and reactants

$$RE = E_{tot}(products) - E_{tot}(reactants) \quad (3.2.2)$$

A reaction is exothermic if the reaction energy is negative; alternatively, a reaction is endothermic if the reaction energy is positive.

## 3.3 Surface models

The metal Ag exhibits a face-centred cubic crystal structure with an optimized lattice parameter of 414 pm, compared to the experimental value of 409 pm [109]. The calculated inter-atomic distance between two Ag atoms is 293 pm, compared to a value of 289 pm in experiment. In this work the super cell approach has been applied to model silver surfaces as periodically repeated slabs. The thickness of a slab is an important parameter in these models. Test calculations justified that five-layer slab models of silver surfaces provide sufficiently accurate structures and energy characteristics. Thus, five-layer slab models represent an acceptable compromise between accuracy and

computational economy. The results displayed in Figure 3.2 make it obvious that one should select slabs with an odd number of layers as models because for such slab models the binding energies of an H atom on Ag(110) surface is rather stable, while models with an even number of layers tend to converge towards the odd ones, but only slowly. In support of this choice, it should be noted that also in some other studies [42,110-112] slab models with five substrate layers have successfully been used.

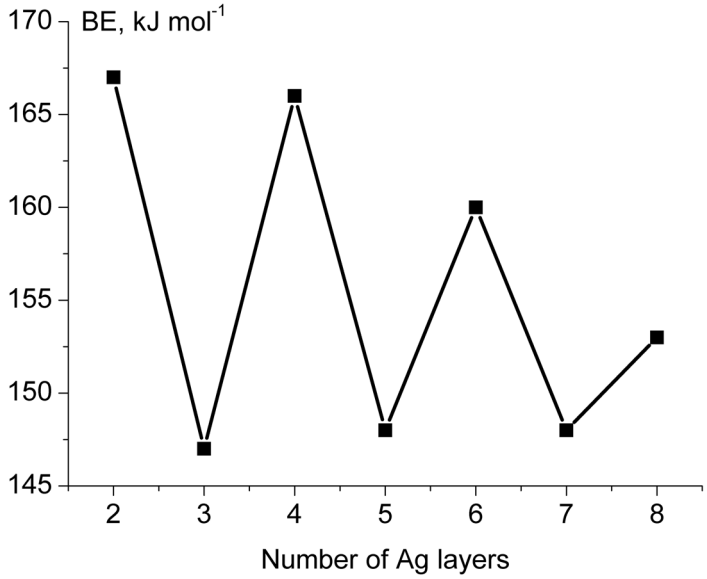


**Figure 3.2:** Adsorption energy of atomic hydrogen at on-top sites of Ag(110) slab models with various numbers of metal layers. The surface coverage in these test calculations was 1/4.

Models of Ag surfaces contain one atom per layer and unit cell for the surfaces Ag(111) and Ag(110) and three atoms per layer for the (221) surface. These minimum unit cells have been extended to a (2x2) unit cell which includes four atoms per layer for the (110) and (111) surfaces and to a (4x3) unit cell containing twelve atoms per layer for the (221) surface; these models provide enough space to model the envisaged adsorbates like acrolein and they allow one to consider surface coverages as low as 1/4 for Ag(110) and Ag(111) and 1/12 for the (221) surface. In super cell calculations, model slabs are separated by a vacuum spacing, determined as the difference between the thickness of the slab and the height of the unit cell. A vacuum spacing of ~1 nm (after introduction of the

adsorbates) was adopted to separate the periodically repeated slabs. Adsorbates were placed on one side of each slab only.

### 3.3.1 Surface relaxation

To examine the effect of surface relaxation, a slab of nine layers was optimized modelling the Ag(110) surface. From one to six surface layers of the slab were relaxed. For all models, the first layer relaxed inward by about 11 pm and the second layer moved outward by about 6 pm (Table 3.1). The third and fourth layers do follow the same oscillatory trend, but the magnitude of the relaxation is smaller. The spacing between layers five and six changed at most 0.2 % compared to the bulk, which shows that the surface relaxation does not extend not deeper into the bulk. These computational results are in quite good agreement with a LEED study of layer relaxation on Ag(110) [113]. Lead by these results, a five layer slab with two relaxed surface layers was regarded as a sufficiently reliable model. Test calculations for five layer model (Table 3.2) show that the interlayer distance between the top two layers of the Ag(110) surface decreased by 12 pm and the distance between the second and third layers increased by 7 pm. Thus, one obtains an adequate model if one allows the top two layers of a five-layer slab to relax while keeping the bottom three layers fixed is at their bulk terminated geometry.

Similarly, on a five-layer slab model of the Ag(111) surface the top three layers have been relaxed and the interlayer distances changed by at most 2 pm. For a five-layer slab model of the Ag(221) surface, with the top three layers relaxed, the second-layer atoms changed their positions by less than 2 pm. The first-layer atoms showed larger displacements; the edge atoms moved 6 pm toward the “bulk” while the terrace atoms moved 1–7 pm in opposite direction. With these changes, the distance between the first-layer Ag atoms shortened to 289 pm on average in comparison to the bulk Ag-Ag distance of 293 pm. This relaxation effect is in quite good agreement with the rule “that the interlayer spacing between surface and first subsurface layer contracts, while the interlayer spacing between the subsurface layers and its deeper neighbouring layers

expands" [114]. In subsequent adsorption studies, five layer slabs with two relaxed surface layers were used as reference. Rösch et al. justified the adequacy of this type of models for Pd surfaces [115,116].

**Table 3.1:** Relative relaxation of interlayer distances (%) and change in total energy (eV) of the Ag(110) surface modelled by a nine-layer slab in comparison to the bulk.

| Relaxed layers [a] | $E_{total}$ | $\Delta_{12}$ | $\Delta_{23}$ | $\Delta_{34}$ | $\Delta_{45}$ | $\Delta_{56}$ | $\Delta_{67}$ |
|---|---|---|---|---|---|---|---|
| 1/9 | -92.78 | -5.04 | | | | | |
| 2/9 | -92.80 | -6.87 | 3.75 | | | | |
| 3/9 | -92.80 | -6.84 | 3.84 | -0.15 | | | |
| 4/9 | -92.81 | -7.98 | 4.64 | -0.99 | 0.73 | | |
| 5/9 | -92.81 | -8.00 | 4.60 | -1.01 | 0.60 | 0.16 | |
| 6/9 | -92.81 | -8.05 | 4.58 | -1.00 | 0.59 | 0.17 | 0.00 |
| Expt[b] | | -7±2 | 1±2 | -2±2 | | | |

a -x/9 means that x surface layers of the nine layer slab have been relaxed.

b – Ref. [113]

$\Delta_{ij} = (d_{ij} - d_{bulk})/d_{bulk} \times 100$, $d_{bulk} = 146$ pm for Ag(110)

**Table 3.2:** Absolute ($d_{ij}$) and relative ($\Delta_{ij}$) relaxation of interlayer distances (in pm and %, respectively), and change in total energy (eV) of Ag(110) surface modelled by a five-layer slab in comparison to the bulk. For comparison results of a nine-layer slab model with six layers (6/9) relaxed is also shown.

| Relaxed layers | $E_{total}$ | $d_{12}$ | $\Delta_{12}$ | $d_{23}$ | $\Delta_{23}$ | $d_{34}$ | $\Delta_{34}$ |
|---|---|---|---|---|---|---|---|
| 1/5 | -49.07 | -7.8 | -5.33 | | | | |
| 2/5 | -49.09 | -11.7 | -8.00 | 6.6 | 4.50 | | |
| 3/5 | -49.09 | -11.7 | -8.05 | 6.7 | 4.58 | -0.1 | -0.07 |
| 6/9 | | -11.7 | -8.05 | 6.7 | 4.58 | -1.4 | -1.00 |

## 3.4 Transition state search

### 3.4.1 Methods applied

Finding a transition state (TS) is not an easy process. It consumes quite a bit of computational and human time since automated procedures are not available. For a rather small system like hydrogen activation on the Ag(110) surface, a constrained transition state search has been used to check whether this procedure can reduce the search time compared to the well established nudged elastic band (NEB) method [117]. Details will be given below.

In NEB, the search for TS is started by interpolating a series of structures, which are referred to as images, between the initial (IS) and final states (FS). The transition state search is then transformed into a minimization problem. On the potential energy surface the initial and final images are kept fixed throughout the search. To get the minimum energy path (MEP), structures of all images are then optimized. During the optimization iteration, the forces on the nuclei are decomposed into components normal to and along the reaction path under investigation and the later one are set to zero. In this way movements along the reaction path are avoided; especially upon optimization of an image, the structure might converge to either IS or FS on the MEP. In addition, a harmonic artificial potential is applied to restrict the separation of images during optimization. The described NEB procedure results in a MEP and approximate TS as the highest energy on the MEP.

Normal mode analysis was used to verify that the approximate TS obtained from the NEB method exhibits exactly one imaginary frequency. By diagonalizing the Hessian matrix of force constants which were approximated via finite differences of forces, the vibrational frequencies were obtained. For this purpose, atomic centres of the adsorbates were moved by ±3 pm along each of the Cartesian directions. In line with the model approach chosen, the substrate was kept fixed during the normal mode analysis because the effects of the substrate on the vibration frequencies were deemed to be small and hence negligible.

### 3.4.2 Application of nudged elastic band method

Before a TS search, one has to determine first the IS and FS of the reaction. The most stable adsorbed structures of the reactants are chosen as IS and the most stable co-adsorbed complexes of the products as FS. For example, in the case of hydrogen dissociative adsorption on Ag (110), in the IS the hydrogen molecule is located 350 pm above the surface and, in the FS, hydrogen atoms are located at two short bridge sites.

Usually interpolation between initial and final states is used to get a starting image which approximates the transition state. Of course, one can also choose more structures by interpolation between IS and FS. In this case a larger amount of computational time is required. To speed up the calculations and to obtain good starting approximations for the images, the surface models in this work were reduced to two-layer substrate models for the Ag(110) surface and to three-layer substrate models for the Ag(111) surface incorporating subsurface oxygen. The vacuum thickness was kept at 1 nm, but the energy cut-off was reduced to 300 eV. The search strategy was simplified because the intermediate structures are not of interest herein and the only aim is locating structure that approximates the transition state. With all the above restrictions, only one image for each NEB calculation was used. After each NEB run, the structure was analyzed, e.g., for H-H bond breaking by comparing the H-H distance to the values in the IS and FS structure. The total energy of the optimized image was compared to IS and FS energies to see whether one has to replace the initial or the final state structure for the next image search. Apart from structural and energetic comparisons also gradients along the approximate reaction path were checked. Normally 8 to 10 NEB steps were required before approximate TS ($TS^{approx}$) was obtained. To make sure that the obtained structure was close to the TS, a normal mode analysis was carried out. Also for acrolein hydrogenation the above procedure was applied. In this more demanding cases, 10 to 20 steps were necessary to reach a $TS^{approx}$ structure.

Once the $TS^{approx}$ structure was obtained, then full surface models as described in Section 3.2 were used for refinement, following again the procedure described above.

Normally, the final accurate TS structure was obtained with about four NEB steps using the complete models.

### 3.4.3 Constrained search for transition state

All transition state searches in this study were done by using the NEB method of VASP, but for comparison also a constraint search approach was tried out. This methodology has been applied only for hydrogen activation. The main reason to try an alternative approach was that the potential energy surface for $H_2$ adsorption is rather flat; therefore, as a first step, approximate TS configurations are located with the help of a constrained search, and subsequently the nudged elastic band method [117] was applied. Also the full NEB TS search was applied to cross check both types of results. For the example of hydrogen activation on the Ag(110) surface with a final state of both hydrogen atoms occupying short bridge sites, the structural parameters for the transition state obtained with NEB are r(H-H) = 155 pm for the H-H distance and z(H-H) = 149 pm for the height of $H_2$ above the surface. With the constrained search strategy, one obtained r(H-H) = 160 pm; z(H-H) = 148 pm. The activation barriers in both the cases agreed within 1 kJ $mol^{-1}$. The constrained search results were very useful in reducing the number of images in the NEB calculations. However, the computational time consumed by the constrained search is similar to the time needed for a full NEB calculation. The drawback of the constrained search is that the end result is not an exact transition state because there is a limitation for the degrees of freedom inspected.

The detailed procedure for the constrained search was as follows. The initial state at 350 pm distance of $H_2$ above the Ag(110) surface was chosen and a final state with H atoms adsorbed at two-short bridge sites. The interatomic distance of the hydrogen atoms was then relaxed while the height of the molecule above the surface was kept fixed. A series of interatomic distances were measured by bringing the hydrogen molecule closer to the surface, varying its height above the surface.

From Figure 3.3 one can see that the total energy corresponding to the height 150 pm indicates an approximate transition state. A refined search has been performed in this

area by establishing taking a matrix for height values ranging from 140 pm to 150 pm, in steps of 5 pm, and the hydrogen interatomic distance ranging from 80 pm to 160 pm, in steps of 5 pm. As a result Figure 3.4 was obtained. The three lines drawn in the plot are achieved by polynomial fitting of the original data. From this plot it is clear that an approximate transition state is located at an interatomic distance of about 160 pm.

Finally, the constrained TS search was refined by scanning the interatomic distance of the molecule above the surface by a fine grid. The HH bond length r was varied in steps of 1 pm between 153 and 164 pm. In Figure 3.5 at a height of 148 pm from the surface the transition state is indicated. This figure is drawn keeping the inter-atomic distance fixed and varying the height of the molecule in steps of 5 pm in the range 140 pm to 150 pm. One can see that the total energy at the inter-atomic distance of 160 pm from Figure 3.4 is similar to the total energy at a height of 148 pm in Figure 3.5. The energy of -54.53 eV corresponds to the transition state and yields a barrier height of 130 kJ $mol^{-1}$, the same value as obtained with the NEB approach.

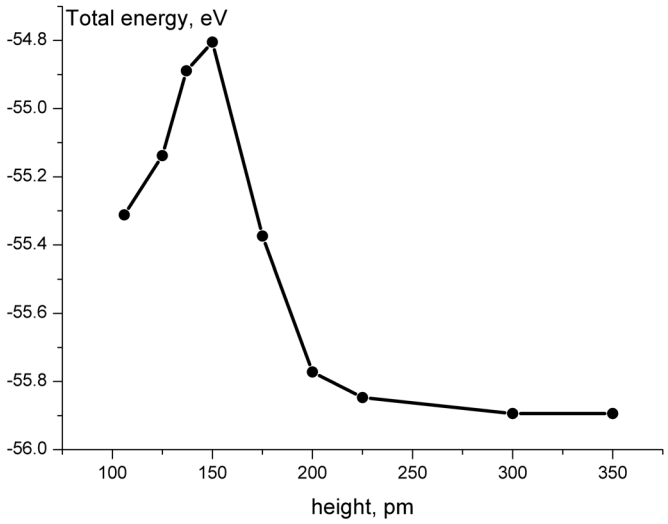


**Figure 3.3:** Cut through the potential energy surface of dissociative adsorption of a hydrogen molecule over the Ag(110) surface, keeping the centre of mass of the molecule fixed at various heights above the surface and relaxing only the interatomic distance.

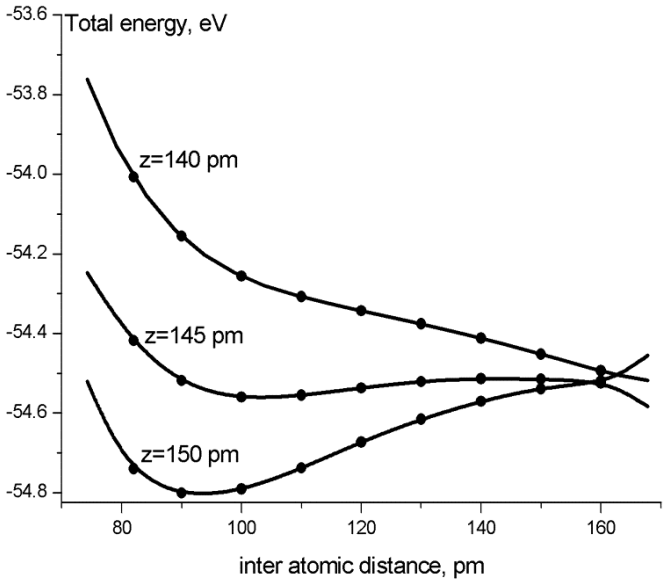


**Figure 3.4:** Total energy as function of the inter-atomic distance, keeping the height z of the hydrogen molecule fixed over the Ag(110) surface. Curves are smoothed using polynomial fitting.

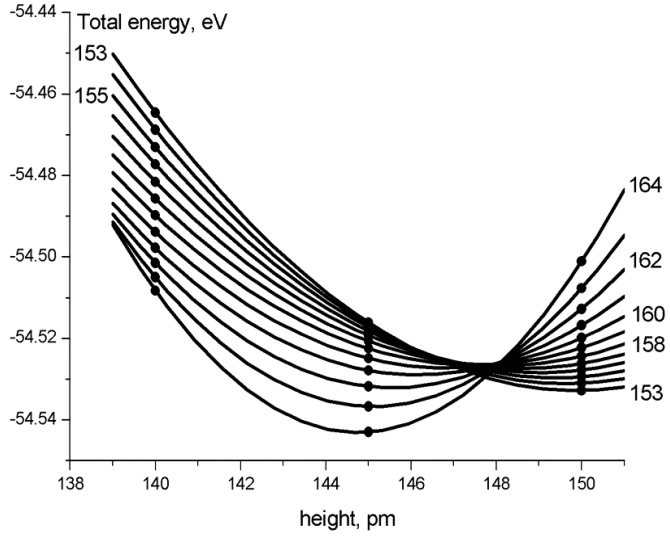


**Figure 3.5:** Total energy of a hydrogen molecule above the Ag(110) surface as function of the height above the surface, the keeping the inter atomic distance d fixed at values between 153 and 164 pm. From curve to curve, the value of d varies by 1 pm. Curves are smoothed using polynomial fitting.

# Chapter 4

# Hydrogen activation, adsorption and diffusion on silver surfaces

This study addresses the problem of $H_2$ dissociation on well-defined silver surfaces. It is motivated by hydrogenation reactions on silver surfaces, also where oxygen adsorbates may be present on the catalyst surface, e.g. generated by aldehyde decomposition [45]. Apart from clean surfaces, model surfaces with well-defined overlayers of oxygen were also considered. As $H_2$ cannot be activated under common experimental conditions on clean low-index surfaces of silver, one has to discuss alternative activation sites, either sites on higher-index surfaces, which contain more active low-coordinated metal centres, or surface sites formed by impurities, e.g. atomic oxygen [46]. In this chapter, the activation of molecular hydrogen on clean Ag surfaces and Ag surfaces exposed to oxygen is compared. Employing density functional slab models, hydrogen activation, adsorption and diffusion on Ag(111), Ag(110) and Ag(221) surfaces has been studied. To examine the effect of the surface morphology on the activation of hydrogen, adsorption of $H_2$ was considered: (i) on the most stable surface Ag(111), (ii) on the more open surface Ag(110), and (iii) on the stepped surface Ag(221). Then, the reaction path of $H_2$ dissociation on the Ag-O chains of the reconstructed $p(n\times1)$O/Ag(110) surface was investigated.

## 4.1 Models

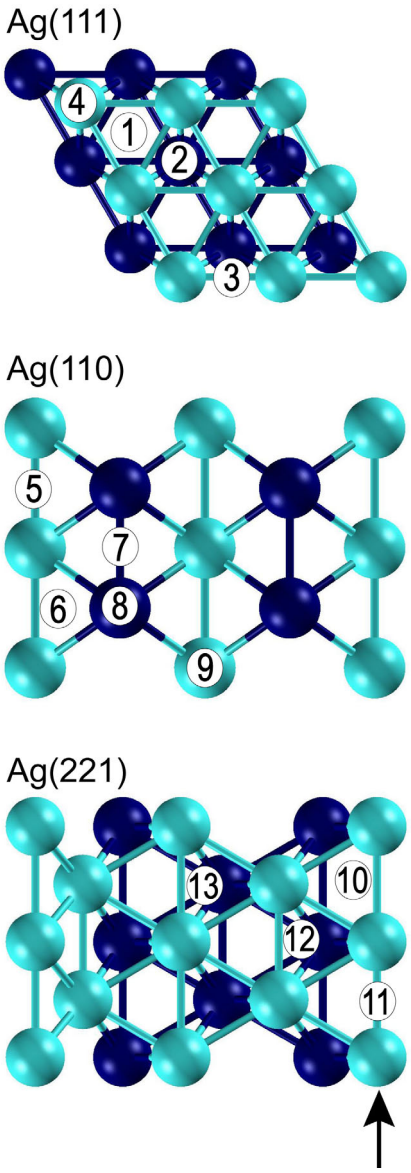


**Figure 4.1:** Sketches of the top view of the adsorption sites studied at the (111), (110) and (221) surfaces of silver. For clarity, only two Ag layers are shown (Ag1, Ag2). Light blue – top-layer Ag atoms (Ag1); dark blue – second-layer Ag atoms (Ag2). Ag(111): **1** – fcc, **2** – hcp, **3** – bridge, **4** – top; Ag(110): **5** – short bridge, **6** – 3-fold hollow, **7** – long bridge, **8** – 4-fold hollow, **9** – top; Ag(221): **10** – edge 3-fold hollow-1, **11** – edge bridge, **12** – edge 3-fold hollow-2 and **13** – terrace 3-fold hollow. The arrow at the bottom of the Ag(221) sketch points along a step edge.

Hydrogen adsorption was studied on Ag(111) at top, bridge and 3-fold hollow sites. On Ag(110) surface adsorption studies were performed at top site, short bridge, long bridge, 3-fold hollow and 4-fold hollow as shown in Figure 4.1. Also hydrogen activation has been studied on combinations of two sites as the final adsorption positions. Also adsorption was studied on stepped surface (221) at edge bridge, terrace 3-fold hollow, 3-fold hollow with one bridge atom and two terrace atoms, 3-fold hollow with two bridge atoms and one terrace atom.

## 4.2 Hydrogen activation, adsorption and diffusion over silver surfaces

The experimental value for the binding energy of a hydrogen molecule (in the gas phase) is 436 kJ $mol^{-1}$, with a H–H bond distance of 74 pm [118]. Calculations on $H_2$ using GGA and LDA approximations showed that LDA overestimates the binding energy by 39 kJ $mol^{-1}$ compared to the experimental value, whereas GGA gives 439 kJ $mol^{-1}$ in excellent agreement with experiment. According to calculations, $H_2$ molecules are essentially unbound on all Ag surfaces considered: the adsorption energy $E_{ad}$ is at most about -2 kJ $mol^{-1}$. This agrees with the experimental observations that $H_2$ does not adsorb on Ag(110) at 90 K [38] and adsorbs only very weakly on Ag(111) surface with $E_{ad}$ = -15 kJ $mol^{-1}$ [38]. As already mentioned, dissociative adsorption of $H_2$ at the three Ag surfaces studied is an endothermic process, requiring about 40 kJ $mol^{-1}$. The two more open surfaces Ag(110) and Ag(221) do not exhibit any propensity for a more favourable thermodynamics of $H_2$ dissociation than the close-packed surface Ag(111). Therefore, this process was explored in detail at clean silver surfaces only for the example of Ag(110).

### 4.2.1 Adsorption of H on the Ag(111) surface

On Ag(111), adsorption complexes at 3-fold hollow sites were found to be the most stable: there is no clear preference between fcc **1** or hcp **2** sites. Normal mode analysis confirmed that these structures correspond to local minima of the potential energy surface. The calculated adsorption energy, -198 kJ $mol^{-1}$, is essentially the same as the value obtained in earlier slab model DF PW91 calculations, about -200 kJ $mol^{-1}$ [42]. Note, that according to experimental estimates, the H binding energy on silver is less than -218 kJ $mol^{-1}$ [39], i.e. $H_2$ dissociation is endothermic. HREELS (high-resolution electron-energy-loss spectroscopy) data are most consistent with adsorption complexes at 3-fold hollow sites [119]. Adsorption complexes of H at bridge positions **3** are slightly less stable, having an adsorption energy of -187 kJ $mol^{-1}$.

Calculated vibrational modes of these complexes feature one imaginary frequency, indicating that the bridge sites **3** represents a TS for H diffusion between the 3-fold hollow sites **1** and **2**. Top sites **4** are least favourable for atomic H on Ag(111), with $E_{ad}$ = -150 kJ $mol^{-1}$; a vibrational analysis identified this structure as a saddle point with two imaginary frequencies, i.e. a local maximum for lateral motion. The calculated binding energies of H among the sites **1** to **4** vary by only ~50 kJ $mol^{-1}$ and the estimated barrier for H diffusion between the local minima **1** and **2** via the bridge site **3** is merely 11 kJ $mol^{-1}$. One expects from these results that atomic hydrogen exhibits a notable mobility on the Ag(111) surface already at rather low temperatures. The calculated H-Ag distances of the adsorption complexes H/Ag(111), ranging from 166 to 192 pm (Table 4.1), show an anti-correlation with the coordination number of the adsorbate.

### 4.2.2 Adsorption of H on the Ag(110) surface

It is surprising that calculations on the adsorption of atomic hydrogen at Ag(110) showed similar strong binding energies at the short bridge **5** (-196 kJ $mol^{-1}$) and at the long bridge **7** (-193 kJ $mol^{-1}$). Both adsorption complexes are local minima according to a vibrational

**Table 4.1:** Parameters of adsorption complexes of atomic H on high-symmetry sites of various Ag surfaces.[a]

| Substrate | Site[b] | H-Ag, pm | $E_{ad}$, kJ mol$^{-1}$ |
|---|---|---|---|
| Ag(111) | **1** fcc | 192 | -198 |
| | **2** hcp | 192 | -198 |
| | **3** bridge | 183 | -187 |
| | **4** top | 166 | -150 |
| | Exp.[c] | | -218 |
| Ag(110) | **5** short bridge | 181 (180[d]) | -196 (-192[d]) |
| | **6** 3-fold hollow[d] | 185, 201[e] | -204 |
| | **7** long bridge | 208, 200[e] | -193 |
| | **8** 4-fold hollow | 178 | -169 |
| | **9** top | 166 | -147 |
| Ag(221) | **10** edge 3-fold hollow-2[f] | 191, 200[e] (192, 200)[h] | -202 (-198)[h] |
| | **11** edge bridge | 182 (183)[h] | -199 (-195)[h] |
| | **12** edge 3-fold hollow-1[g] | 194, 194[e] (195, 195)[h] | -198 (-192)[h] |
| | **13** terrace 3-fold hollow | 190, 196[e] (190, 196)[h] | -193 (-186)[h] |

[a] Energies of adsorption $E_{ad}$ (a negative sign implies favourable adsorption) and lengths of the shortest H-Ag bonds. Unless specially stated, the coverage of H was 1/4 of a monolayer, except for Ag(221) where the standard coverage was 1/8.

[b] See Figure 4.1.

[c] Ref. [39].

[d] Surface coverage 1/2.

[e] The adsorption site comprised two non-equivalent Ag atoms.

[f] Formed by two edge and one terrace Ag atoms.

[g] Formed by one edge and two terrace Ag atoms.

[h] Surface coverage 1/12.

analysis. At the long bridge site **7**, H is located essentially at the height of the top layer Ag1 of the substrate. The distances, H-Ag2 = 200 pm, of adsorbed H to the Ag atoms of the second substrate layer are shorter than those to the top-layer Ag atoms, H-Ag1 = 208 pm. This finding may be interpreted as an adsorption complex of H involving the four Ag

atoms that form the long bridge site **7**: two atoms belong to the first layer Ag1 and the other two to the second layer Ag2 (Figure 4.1)

As suggested by experimental findings [37], calculations were also done for adsorption at the 3-fold hollow site **6** where H is displaced from the short bridge **5** toward a 4-fold hollow position **8** (Figure 4.1), however, no stable structure with 1/4 surface coverage of hydrogen was found. At higher coverage, H atoms may occupy 3-fold hollow sites **6** to minimize H-H repulsion as observed experimentally at coverage of 1/3 or larger [37]. Indeed, according to calculations this is the case at hydrogen coverage of 1/2: the zigzag ordering of hydrogen atoms along the $[1\bar{1}0]$ direction (corresponding to a confirmed local minimum) is by 12 kJ $mol^{-1}$ per H atom more stable than the structure with hydrogen at the short bridge (Table 4.1).

The 4-fold hollow site **8** binds H somewhat weaker, $\Delta E_{ad}$ = -169 kJ $mol^{-1}$, but it represents a saddle point with two imaginary vibrational frequencies. In that adsorption complex, the distance of H to the nearest Ag1 atom of the surface layer, 256 pm, is much longer than the H-Ag2 contact, 178 pm, to a metal atom of the second layer; this finding indicates that on this site H interacts predominantly with a single Ag atom of the second layer of the substrate and the H-Ag2 distance is just 12 pm longer than that with Ag atom of the top sites **4** and **9**. Atomic hydrogen adsorption on Ag(110) was calculated to be least stable at the top site **9**, with $\Delta E_{ad}$ = -147 kJ $mol^{-1}$ (with two imaginary frequencies again a saddle point of lateral motion). In fact, the H-Ag distances of adsorption complexes with the same coordination of H are quite similar as well for these two surfaces (Table 4.1). The transition state of H diffusion from the short bridge site **5** to the long bridge site **7** was identified using the nudged elastic band method. The resulting TS is less stable than the IS by only 14 kJ $mol^{-1}$, thus even more stable than the adsorption complex on the 4-fold hollow site **8**. Therefore, H diffusion on Ag(110) surface also appears to be very facile.

## 4.2.3 Hydrogen Activation on the Ag(110) surface

The calculated results for selected reaction pathways of $H_2$ dissociation on Ag(110) are shown in Table 4.3. The corresponding activation energies $E_a$, and geometric parameters of the transition and final states are also included in Table 4.3. A configuration where the $H_2$ molecule practically does not interact with the substrate, namely 300 pm above the top crystalline plane was chosen as initial state. Many combinations of stable H adsorption sites seem possible as final state of $H_2$ dissociation because the potential energy surface of atomic H adsorption on Ag is quite flat. The FS (with hydrogen coverage of 1/2) was chosen as combinations of various stable adsorption complexes (Table 4.3; Figure. 4.1; Figure. 4.3), namely the short bridge site **5**, the long bridge site **7**, and 3-fold hollow site **6**. All selected FSs have been shown to be local minima with the help of a normal mode analysis. Based on these structures for coverage 1/2, single-point calculations were also carried out at coverage 1/3. The zigzag FS configuration of hydrogen atoms at 3-fold hollow sites, **6**/**6**, turned out to be the least endothermic among the configurations studied, with $E_r$ = 33 and 49 kJ $mol^{-1}$ for coverage of 1/2 and 1/3, respectively. Note, that reducing the surface coverage from 1/2 to 1/3 generally makes $H_2$ dissociation slightly more endothermic except for the long-bridge/ long-bridge configuration **7**/**7** along one trough where the reaction energy is essentially the same for both coverage values (Table 4.2). This implies that more energy (~10 kJ $mol^{-1}$) is required for initial $H_2$ dissociation when the surface is free of adsorbed H, but the differences are small and within the accuracy of the computational method employed.

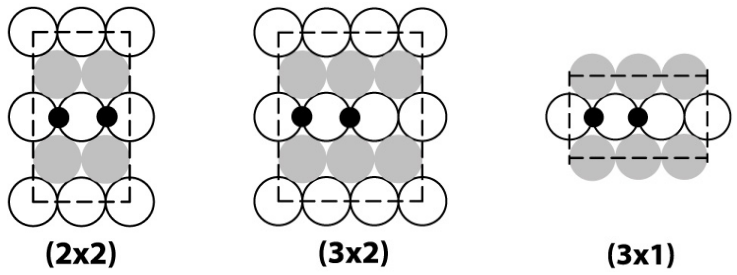


**Figure 4.2:** Schematic representation of unit cells of the Ag(110) surface. The two black dots represent the final state of hydrogen coadsorption on the Ag(110) surface.

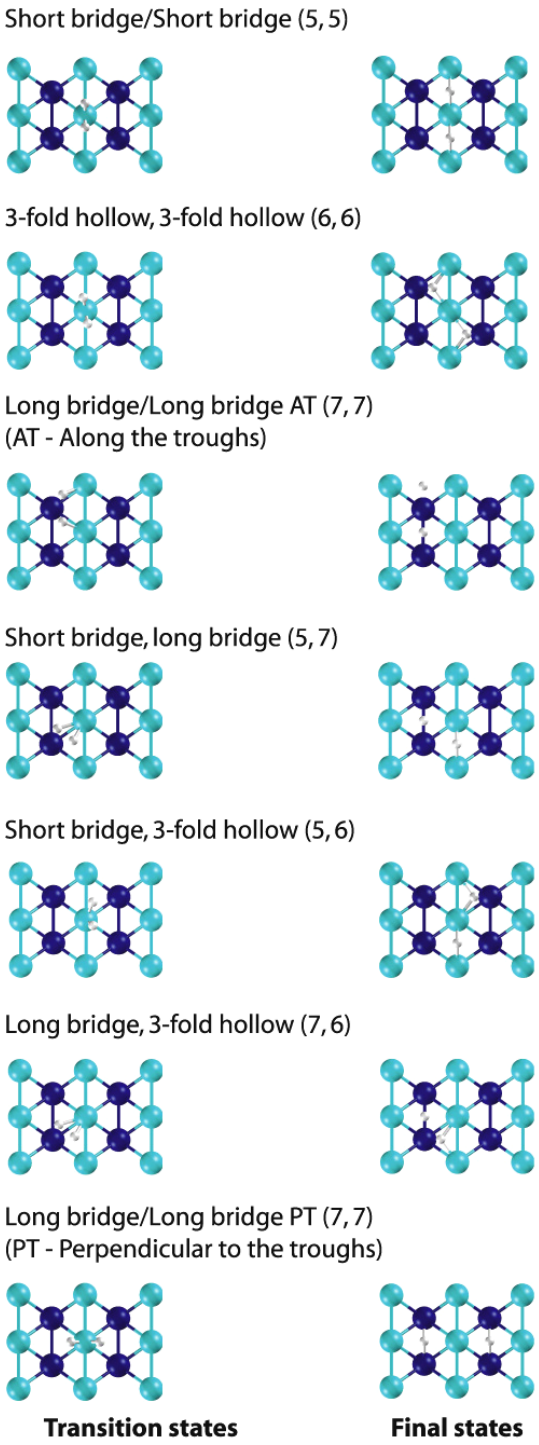


**Figure 4.3:** Structures of various transition states of hydrogen activation over Ag(110) surface and the corresponding final states of the adsorbates. The structures are arranged in the order as they are given in Table 4.3.

**Table 4.3:** Calculated activation energies $E_a$ and reaction energies $E_r$ (kJ $mol^{-1}$) of $H_2$ dissociation for various final states on the Ag(110) surface at coverage 1/2 (see also Figure 1).[a] Selected distances (pm) of the transition state (TS) and the final state (FS) are also shown.[b]

| | TS | | | | FS | | |
|---|---|---|---|---|---|---|---|
| | H-H | z(H) | H-Ag | $E_a$ | H-H | H-Ag | $E_r$ |
| short bridge **5** / short bridge **5** | 155 | 149 | 168 | 132 (134) | 293 | 180 | 57 (61) |
| 3-fold **6** / 3-fold **6**[c] | 151 | 155 | 172 | 133 (134) | 361 | 185 | 33 (49) |
| long bridge **7** / long bridge **7**[d] | 171 | 100 | 183 | 162 (160) | 293 | 190 | 68 (67) |
| short bridge **5** / long bridge **7** | 136 | 107, 50 | 178, 183 | 122 (127) | 277 | 180, 200 | 54 (63) |
| short bridge **5** / 3-fold **6** | 152 | 121, 158 | 170, 168 | 129 (131) | 318 | 180, 185 | 44 (55) |
| long bridge **7** / 3-fold **6** | 152 | 137, 130 | 167, 169 | 138 (143) | 347 | 190, 185 | 52 (58) |

[a] Values in parentheses are obtained in single-point calculations at coverage 1/3 for structures determined at coverage 1/2.

[b] H-H and H-Ag are interatomic distances and z(H) is the height of H atom above the Ag(110) surface.

[c] Zigzag ordering of H atoms.

[d] Complex oriented along the troughs.

For selected transition states, the calculations were extended to different unit cells of (3x2) and (3x1), apart from the regular (2x2) unit cells (Figure 4.2). However, this did not result in any big effect on either the binding energy of the hydrogen atom or on the transition state of hydrogen activation.

The lowest activation energies calculated for $H_2$ dissociation on Ag(110) with surface coverage at 1/2 is about 125 kJ $mol^{-1}$. This value is comparable to the reported lowest activation energies of 106 kJ $mol^{-1}$ on the Ag(100) surface [42], but notably higher than on other transitional metal surface. For instance, a vanishing activation barrier was calculated for the surface Pt(111) [43]. Reducing the surface coverage from 1/2 to 1/3 does not change the activation energies by more than 5 kJ $mol^{-1}$ for all the

configurations studied. On the basis of the present results, one should consider the activation energies of the final states **5**/**6**, **6**/**6**, and **5**/**7** (Table 4.3; Figure 4.3) as very similar, on average ~125 kJ $mol^{-1}$. The present results are consistent with the low dissociation probability of $H_2$ determined experimentally at silver surfaces [39].

In summary, the calculations showed that $H_2$ dissociation is kinetically and thermodynamically unfavourable on clean surfaces of silver. Thus, other sites are likely responsible for the activation of hydrogen on silver, e.g. reaction centres induced by the presence of surface oxygen species.

### 4.2.4 Hydrogen adsorption on Ag(221) surface

On the stepped surface Ag(221) [4(111)× (111)], adsorption sites **10**, **11** and **12** located at the step edges were considered. These sites were selected because the low-coordinated edge atoms usually form more active centres [116]. In addition, the terrace 3-fold hollow site **13** as a reference to characterize the mobility of the adsorbates was also considered. The optimized adsorption complexes at all these sites were confirmed as local minima. Atomic H at the edge hollow sites **10** and **12** as well as at the edge bridge sites **11** feature very similar energy of adsorption, -198 to -202 kJ $mol^{-1}$ (Table 4.1, Figure. 4.1). These values are close to those calculated for the most favourable sites of the surfaces Ag(111) and Ag(110). The reactivity of terraces of the Ag(221) surface is similar to that of the (111) surface. This is manifested by the energy of H adsorption on the terrace 3-fold hollows **13**, -193 kJ $mol^{-1}$ that essentially matches the adsorption energy of atomic H at the 3-fold hollow sites **1** and **2** of the Ag(111) surface. Note that the interaction of H with the terrace site **13** is only slightly weaker than with the edge sites **10** to **12**. Consequently, one can expect facile mobility of atomic H also on this stepped Ag(221) surface, just as on the Ag(111) and Ag(110) surfaces. Inspection of Table 4.1 reveals that H-Ag distances are very similar to those of sites with the same coordination on the other surfaces studied. Reducing the surface coverage to 1/12 of a monolayer does not reveal any noticeable change in the adsorption geometries and binding energies of hydrogen atoms (Table 4.1).

## 4.3 Hydrogen adsorption on *p*(*n*×1)O/Ag(110) surface

### 4.3.1 *p*(n×1)O/Ag(110) added row formation

The Ag(110) surface is especially interesting because oxygen can adsorb in several molecular forms at low temperatures [120] as well as at higher temperature giving a series of added-row structures of the form (nx1), where n = 2–7, induced by dissociatively adsorbed oxygen [121]. These latter structures, which can be seen as function of coverage, have been identified by low-energy electron diffraction (LEED). Earlier, Ag(110)-(2x1)-O structures were studied using low-energy ion scattering (LEIS) [122] which lead to the conclusion that oxygen occupies long-bridge sites, with reference to the second layer of Ag(110) surface.

Similar (2x1)-O phases are formed on Cu(110) [123-126] and Ni(110) [127-129] and there has been considerable debate about their structure [123-129]. There were many arguments for interpreting this structure either as missing row or as added row reconstruction [71,130,131], but STM studies on Cu(110)-(2x1)-O surface showed that the formation of a (2x1) structure occurs by addition of Cu-O rows on the surface, growing from step edges [126,132]. Therefore, the term "added-row" reconstruction is appropriate, although the structure may also be viewed as a "missing-row" structure [69]. An STM study of the O/Ag(110) system similarly suggested that the LEED patterns from this surface correspond to the formation of Ag-O-Ag-O chains along [001] direction, on top of the Ag(110) crystal surface; i.e., there is an added row [133].

There is a relationship between the added row formation process and the mass transport mechanism at step edges for the O/Ag(110) system. It has been shown that mobile added atoms exist on the terrace even prior to oxygen exposure [134]. Additional Ag adatoms are readily supplied by step edges via thermal detachment at a nominal rate of three atoms/sec per step site at room temperature [134]. At higher oxygen pressures, the supply of Ag adatoms from the step edge cannot keep up with the rate of over layer formation. Nonetheless, at a pressure above $10^{-5}$ mbar, the formation of an oxygen over layer is sustained by the creation of pits on large (110) terraces. These pits reveal the

second “substrate extraction” channel for Ag adatoms, in addition to the supply via step edges. The mass transport mechanism at Ag(110) steps provides reactive nucleation centres, i.e., mobile Ag adatoms, distributed across the terraces. The reaction sites during oxidation are thus distributed across the terraces not localized at steps.

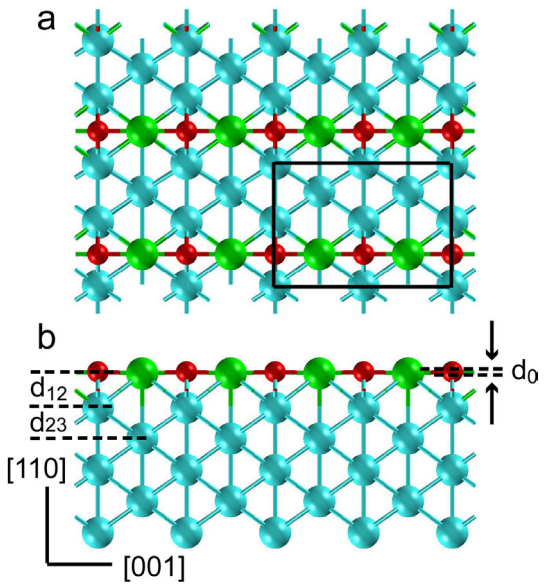


**Figure 4.4:** Top view (a) and side view (b) of the added-row $p(2 \times 1)$O/Ag(110) structure. Red spheres – O atoms, green spheres – Ag atoms of the added row, blue sphere – Ag substrate atoms. Selected interlayer distances in relaxed structures: $d_0$ – height of the oxygen atoms above the Ag atoms of the added row; $d_{12}$ – height of Ag atoms of the added row above the top crystal plane of the Ag substrate; $d_{23}$ – height of the top Ag plane of the substrate above the subsurface Ag plane. The rectangle indicates the smallest surface elementary cell considered.

To start the discussion, $p(2\times1)$O/Ag(110) surface is considered, which is characterized by the smallest unit cell among the $(n\times1)$ reconstructed added-row structures. The surface for $n = 2$ is sketched in Figure. 4.4; added-row Ag atoms are positioned at 4-fold hollow sites of the non-reconstructed Ag(110) surface and O atoms occupy short bridge sites on it.

Table 4.4 compares the calculated geometric parameters of the reconstructed $p(2\times1)$O/Ag(110) surface with experimental data [70,71[71]] and results of previously

reported calculations [92,93]. The Ag and O atoms of the added row apparently form almost linear chains with the intermediate Ag atoms of the added row; it is found that O atoms to be displaced by only 7 pm ($d_0$) from the axis of the added Ag atoms in the direction away from the substrate, in agreement with the geometry of photoelectron

**Table 4.4:** Comparison of calculated and experimental distances[a] (pm) characterizing the added-row *p*(2×1)O/Ag(110) surface; for the designations, see Figure. 4.4.

| | PED[b] | LEIS[c] | SEXAFS[d] | LDA[d] | LDA[e] | GGA[f] | GGA[g] |
|---|---|---|---|---|---|---|---|
| $d_0$ | 3 ±5 | -3 ±8 | ±20±20 | 59 | 15 | 7 | 7 |
| $d_{12}$ | 155 ±6 | 166 ±3 | 167±40 | 142 | 138 | 161 | 161 |
| $d_{23}$ | 133 ±6 | 132 ±3 | | 128 | 134 | 138 | 144 |
| $r_{nn}$ | 204.4±0.2 | 204.5±0.5 | 205± 3 | 213 | 208 | 205 | 207 |
| $r_{nnn}$ | 216 ±10 | 223 ±8 | 221± 3 | 242 | 220 | 224 | 227 |

[a] For the interlayer distances $d_0$, $d_{12}$, and $d_{23}$, see Figure 4.4; $r_{nn}$ – distance between O and the nearest Ag atoms, $r_{nnn}$ – distance between O and the next-nearest Ag atoms.

[b] Photoelectron diffraction (PED), Ref. [69].

[c] Low energy ion-scattering (LEIS), Ref. [71].

[d] Surface extended X-ray adsorption fine structure (SEXAFS), Ref. [92].

[d] DF LDA calculation, substrate of 4 layers, Ref. [92].

[e] DF LDA calculation, substrate of 5 layers, our work.

[f] DF GGA calculation, substrate of 4 layers, Ref. [93].

[g] DF GGA calculation, substrate of 5 layers, our work.

diffraction (PED) study (Table 4.4), which is particularly sensitive to the parameter $d_0$ [69]. The only notable difference with respect to the PED experiment is the computed distance $d_{23}$, 144 pm, which is ~10 pm (longer) out of the experimentally determined range. Probably, for a more quantitative description of the $d_{23}$ values one should consider a thicker slab and allow relaxation of more surface layers. The results of the present study agree quite well with all recently communicated experimentally derived structures [69,71,92] and with the structure of a DF PW91 slab model study [93].

However, the structural characteristics obtained in an earlier DF LDA model investigation [92] (using the Perdew-Zunger exchange-correlation functional [135]) differ

considerably, but do so also from the values of other studies listed in Table 3.1. Most noticeable is deviation of the $d_0$ value, which is ~50 pm longer in the previous LDA work [92] than in the present work and a former DF study [93], the latter two carried out with the PW91 functional. At the same time the $d_{12}$ value of Ref. 92 is ~20 pm shorter compared to present PW91 result.

To check on these discrepancies, the structure of the surface *p*(2×1)O/Ag(110) was optimized at the LDA level [135] (Table 4.4). Indeed, the present results using LDA agree only qualitatively with those of the previous LDA calculation [92]. Also, it is observed that in LDA study the distance $d_0$ is longer and the distance $d_{12}$ shorter compared to the results obtained using PW91. Likely, the differences between the two LDA structures have to be attributed to different representations of the Kohn-Sham orbital, namely by localized functions in Ref. 92 and the PAW technique in the present study [105,106]. The differences between the present LDA and GGA (PW91) results are somewhat surprising as one often observes that LDA structures are closer to experiment than the corresponding ones of PW91.

The optimized structure of the added row surface system changed only in a minor way when the interval between the added rows increases, i.e. on going from the *p*(2×1)O/Ag(110) to the *p*(4×1)O/Ag(110) structure [93]. The corresponding change of the calculated vibrational frequency of O atoms was about 10 $cm^{-1}$, in line with experimental estimates of the effect of reduced oxygen coverage [93]. This implies that the adsorption propensity and, thus, the reactivity of the Ag-O chains should not change significantly at lower oxygen coverage. In the following, this expectation for the case of hydrogen adsorption is studied.

### 4.3.2 Hydrogen adsorption on *p*(n×1)O/Ag(110) added row

Compared to a clean Ag(110) surface, a reconstructed added-row *p*(*n*×1)O/Ag(110) surface which is discussed in the previous subsection, offers three new types of positions for the adsorption of atomic hydrogen, on O and Ag atoms of the added rows, and on the

terrace next to added row. The energy of H adsorption on-top of an added-row Ag centre of *p*(2×1)O/Ag(110) is calculated to be -77 kJ $mol^{-1}$; in that structure, each Ag centre of the added rows is occupied with one atom H. The significantly weaker interaction energy indicates a notable destabilization compared to on-top adsorption complexes of the oxygen-free surfaces Ag(110) and Ag(111), with $E_{ad}$ of about -150 kJ $mol^{-1}$. In contrast, the interaction with O centres was calculated to be very strong, $E_{ad}$ = -331 kJ $mol^{-1}$, in the system with 1H:1O where each of the O centres forms an H adsorption complex. For a system with the lower coverage 1H:2O, the adsorption energy is calculated at -317 kJ $mol^{-1}$. This trend in binding energies is likely due to the more flexible structure of the added Ag-O row, when the O atoms are fully hydrogenated compared to the more rigid added Ag-O structure where some O atoms are not hydrogenated. Note that, at 1H:1O coverage, all O atoms are bound to two Ag atoms of the added row, whereas the O centres not hydrogenated at 1H:2O coverage are bound to two substrate Ag atoms and two added row Ag atoms. The binding energies were calculated for hydrogen atoms at different sites of the *p*(2x1)O/Ag(110) surface, e.g., on top of silver atom, long bridge, short bridge, 4-fold hollow, 3-fold hollow sites on terraces of this surface. Hydrogen atoms are bound to the added row surface less stable by ~30 kJ $mol^{-1}$ compared with sites of the clean Ag(110) surface. The least stable site is on top of silver, as it was observed also on a clean Ag(110) surface.

On going from the (2×1) to the (3×1) and (4×1) periodic structures, where the distance between the added rows increases, the adsorption energy at full coverage, 1H:1O, changes only slightly, from -331 kJ $mol^{-1}$ to -328 and -329 kJ $mol^{-1}$, respectively. Indeed, even in the (2×1) structure the distance between neighbouring added rows, 585 pm, is large enough to prevent any noticeable adsorbate-adsorbate interaction between different rows.

For clean silver surfaces, dissociation of $H_2$ molecules involving oxygen centres of added rows is exothermic by more than 200 kJ $mol^{-1}$. Hydrogen adsorption induces significant changes in the structure of the added row. Oxygen centres with hydrogen adsorbed shift away from the substrate; the Ag-O distance increases from 207 pm, without adsorbate, to 226 pm.

## 4.3.3 Hydrogen activation on *p*(n×1)O/Ag(110) added row

The reaction path for $H_2$ dissociation on Ag-O added rows of the *p*(*n*×1)O/Ag(110) surfaces is discussed here. The *p*(2×1)O/Ag(110) structure which features the most compact unit cell was selected for this purpose. Hydrogen molecules physisorb on this surface; the calculated energy of adsorption, $E_{ad}$ ~ -2 kJ $mol^{-1}$, is negligible. Therefore, the initial state (IS) of $H_2$ dissociation (and the energy reference) was represented by almost free $H_2$ molecules at 300 pm above the added Ag-O rows (Figure 4.5).

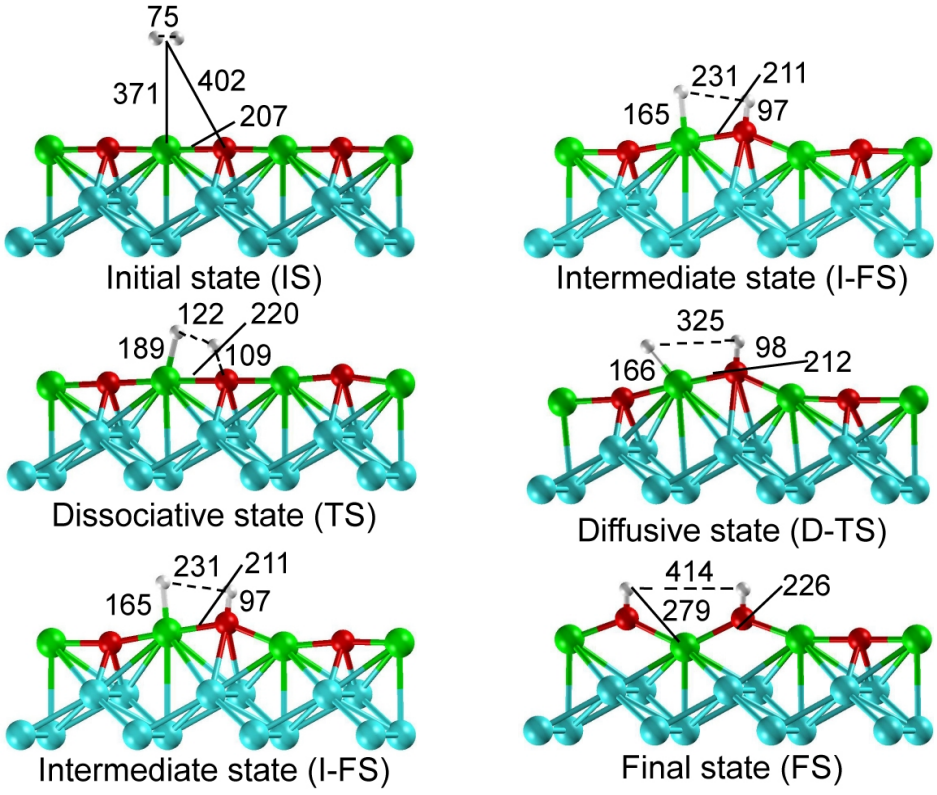


**Figure 4.5:** The $H_2$ dissociation on the added-row *p*(2×1)O/Ag(110) surface for the coverage H:O = 2:3. The panel (a) shows (IS) the initial state with $H_2$ in the gas phase above the surface, ($TS_{diss}$) the transition state for $H_2$ dissociation, (I-FS) the intermediate state with one atom H adsorbed at O and another one at the neighbouring Ag centre and (b) shows the ($TS_{diff}$) the transition state for H diffusion from the centre Ag to a neighbouring unoccupied O, and (FS) the final state with both H adsorbed at O sites.

**Table 4.5:** Calculated geometric parameters and relative energies of initial states (IS), transition states for $H_2$ dissociation ($TS_{diss}$), intermediates (I), transition states for diffusion of one atom H form Ag to O ($TS_{diff}$), and final states (FS) for the dissociation of hydrogen at the $p(2\times1)$O/Ag(110) surface. Energy values in parentheses are for $p(3\times1)$O/Ag(110) structures, calculated in a single-point approximation.

| | Interatomic distances, pm | | | | E, [a] kJ mol$^{-1}$ | |
|---|---|---|---|---|---|---|
| | H-H | Ag-H | O-H | Ag-O | | |
| **H : O = 1 : 1** | | | | | | |
| IS | 75 | 371 | 402 | 207 | 0 | |
| $TS_{diss}$ | 122 | 189 | 109 | 220 | 71 | (69) |
| I | 231 | 165 | 97 | 211 | 32 | (29) |
| $TS_{diff}$ | 325 | 166 | 98 | 212 | 44 | (43) |
| FS | 414 | 279 | 98 | 226 | -224 | (-218) |
| **H : O = 2 : 3** | | | | | | |
| IS | 75 | 372 | 404 | 207 | 0 | |
| $TS_{diss}$ | 122 | 189 | 109 | 220 | 76 | |
| I | 233 | 166 | 98 | 213 | 46 | |
| $TS_{diff}$ | 324 | 168 | 98 | 212 | 63 | |
| FS | 414 | 284 | 98 | 227 | -205 | |

[a] Energy change relative to the IS.

According to the present study, the activation of $H_2$ on the added row proceeds in two steps (Figure. 4.5). First, $H_2$ dissociates and the two atomic H species bind to neighbouring O and Ag atoms of an added row. The calculated activation energy of this dissociation step is 71 kJ mol$^{-1}$ relative to the above mentioned IS where $H_2$ is essentially free (Table 4.5). This activation barrier is reduced almost to a half of that calculated for $H_2$ dissociation on the clean Ag(110) surface (Table 4.3). The H–H distance in the corresponding transition state $TS_{diss}$, 122 pm, elongates to 231 pm in the intermediate state after complete splitting of the H–H bond, to better match the Ag–O distances of 207–226 pm (Table 4.5). That intermediate state is destabilized by 32 kJ mol$^{-1}$ with respect to the IS, due to the relatively weak binding, -77 kJ mol$^{-1}$ (see above), of an H atom at an Ag centre of the added row. In the second step, this weakly bound H atom moves from Ag to a neighbouring (vacant) O centre. The activation energy of this

transition state $TS_{diff}$ characterizing a diffusive motion is very small, only 12 kJ $mol^{-1}$. moves from Ag to a neighbouring (vacant) O centre. The activation energy of this transition state $TS_{diff}$ characterizing a diffusive motion is very small, only 12 kJ $mol^{-1}$. As already discussed, the resulting FS lies 224 kJ $mol^{-1}$ lower in energy than the IS (Table 4.5). To examine an eventual effect of adsorbate-adsorbate interaction, a model with lower coverage of adsorbed hydrogen – one $H_2$ molecule per (2×3) unit cell, was also studied, where in the end one of three O adsorption sites remains unoccupied. The data in Table 4.5 shows that the reaction path is affected only slightly, both structurally and energetically, by this reduction of the hydrogen coverage along the added row. In addition, the effect of a reduced oxygen coverage was estimated, by studying $H_2$ activation on the structure *p*(3×1)O/Ag(110) with a (3×2) unit cell where the distance between the rows was increased; here, a previous model was used where in the final state all oxygen centres are occupied by hydrogen atoms. As expected, also in this case, there were no essential changes of the characteristics of the reaction path (Table 4.5, values in parentheses). Thus, the reaction profile is almost independent of the hydrogen coverage along the added rows and the distance between the added rows. Therefore, it seems justified to generalize the present mechanism of $H_2$ activation also to very low oxygen coverage, as long as local fragments resembling added-row structures are formed.

## 4.4 Conclusions

In this chapter, a study of hydrogen activation and adsorption on clean and oxygen reconstructed silver surfaces has been reported. It was found that the clean silver surface is almost inert to the hydrogen activation, whereas the presence of oxygen notably decreases the activation energy.

Atomic hydrogen is strongly bound to the Ag(110) surface at short and long bridge sites, both being stable sites with almost the same binding energy. Hydrogen adsorption at 4-fold hollow and top sites is not stable. Diffusion of hydrogen over the

surface is rather facile as the barriers are very low. On the Ag(111) surface the 3-fold hollow sites are most stable with the same binding energy as on Ag(110). The stepped surface Ag(221) exhibits different absorption modes, but the strongest adsorption site is a 3-fold hollow near the edge with a binding energy similar to that on Ag(110) surface.

Hydrogen dissociation is thermodynamically and kinetically unfavourable on clean silver surfaces: it is endothermic by ~40 kJ $mol^{-1}$ and the activation barrier about 125 kJ $mol^{-1}$. In contrast, dissociation of $H_2$ on –Ag-O- added-row chains of reconstructed *p*(nx1)O/Ag(110) surfaces is highly exothermic (by 200-220 kJ $mol^{-1}$) and proceeds in two steps with low activation barriers: (i) dissociation of $H_2$ on an Ag-O pair with activation energy of ~70 kJ $mol^{-1}$, and (ii) diffusion of a hydrogen atom from a silver atom to the more favourable neighbouring vacant oxygen position with an activation barrier of ~10 kJ $mol^{-1}$. On the basis of these results, the presence of atomic oxygen species on silver surfaces seems to be essential for their propensity to activate molecular hydrogen.

# Chapter 5

# Oxygen adsorption and diffusion on silver surfaces – its effect on Hydrogen activation

This chapter reports on computational studies of oxygen adsorption and diffusion over Ag(111), Ag(110) and Ag(221) surfaces. All results were obtained with density functional slab models. For the hydrogenation of acrolein important factors are the presence of hydrogen and its availability for the reaction to take place with less effort. In contrast to platinum group metals, hydrogen is not readily available on silver surfaces since dissociation of molecular hydrogen is an activated process. Under reaction conditions oxygen is available in different forms and one of them is adsorbed oxygen. This chapter is discusses the role of oxygen on silver surfaces for the dissociation of hydrogen.

In nature silver is available always as silver oxide and is well-known to be an oxidation catalyst [44].This is due to unusual interaction with oxygen, and many surface science studies have been performed trying to understand the chemical and physical properties [68,69,71,74,92,136,137]. There is a number of well established structures of oxygen-reconstructed silver surfaces [68,69,71,74,92,136,137], for instance, added row structures over Ag(110) surface [69,71,92]. It is also well known that small atoms can diffuse into the lattices of transition metals in appreciable quantities, affecting bulk properties and causing various macroscopic phenomena, such as corrosion and embitterment [76]. When these impurities reside in interstices near the surface, they may directly affect surface properties. The following subsections present a detailed study about the diffusion of oxygen from the surface to sub-surface sites over flat (111) and

stepped surfaces like (110), (221). Subsequently, it is shown that oxygen plays a crucial role lowering the hydrogen dissociation energy, to as low as ~ 20 kJ $mol^{-1}$.

## 5.1 Models

For Ag(110), the following adsorption sites have been studied: top, short bridge, long bridge, 4-fold hollow and sub-surface sites which is exactly below long bridge and below 3-fold hollow. For Ag(111) and Ag(221) surface, the following adsorption sites were studied: 3-fold hollow and octahedral sub-surface site (oss). For Ag(111) surface, nine atoms per layer were used, for the stepped Ag(221) [4(111)×(111)] surface, twelve atoms per layer and for Ag(110), four atoms per layer have been used. For surfaces with subsurface oxygen, oxygen atoms were inserted at the octahedral position between the top and second layers of metal slab. The tetrahedral subsurface position would be too small for location of oxygen atom [138,115].

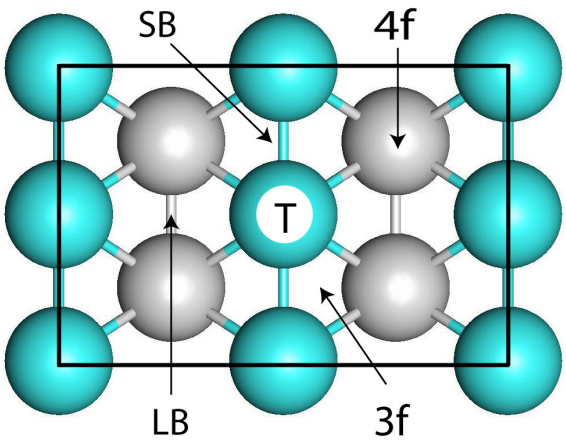


**Figure 5.1:** Adsorption sites for oxygen on a Ag(110) surface: short bridge (SB), long bridge (LB), top (T), three-fold hollow (3f), four-fold hollow (4f). A rectangular frame traces the projection of a unit cell onto the surface plane. Only atoms of the two top layers of the 5-layer slab are shown.

In the original publication [121] the oxygen coverage $\theta_O$ is 1 ML, which corresponds to a saturated (2×1)O/Ag(110) surface. However, in the following oxygen coverage is defined as the ratio of O atoms to Ag atoms in the surface layer, i.e. $\theta_O$ = 0.5 ML corresponds to the ordered phase (2×1)O/Ag(110).

## 5.2 Oxygen adsorption on Ag(110) surface

On the non-reconstructed Ag(110) surface, calculations showed that atomic O can form three stable adsorption complexes which are quasi-degenerate (Table 5.1, Figure 5.1): at long bridges (LB) in [001] direction with an adsorption energy of -351 kJ mol$^{-1}$, at four-fold hollow (4f) sites in the troughs with an adsorption energy of -353 kJ mol$^{-1}$, and at three-fold hollow sites (3f), located at the sides of the troughs, with an adsorption energy of -359 kJ mol$^{-1}$. The two quasi-degenerate sites along the troughs, LB and 4f, are separated by a small, almost symmetric barrier, 7 kJ mol$^{-1}$ from the 4f side (Figure 5.2),

**Table 5.1:** Calculated interatomic distances O-Ag, heights h(O) of the atom O above the surface (110) plane (both in pm), and adsorption energies $E_{ad}$ (kJ mol$^{-1}$) of atomic oxygen on the unreconstructed Ag(110) surface for a coverage $\theta_O$ = 1/4.

| Site [a] | O-Ag | h(O) | $E_{ad}$ |
|---|---|---|---|
| LB [b] | 221, 232 | 32 | -351 |
| 3f [b] | 215, 222 | 60 | -359 |
| 4f | 222 | 54 | -353 |
| SB [c] | 204 | 134 | -309 |
| T [c] | 193 | 193 | -207 |

[a] See Figure 5.1 for the definition of the adsorption sites.

[b] Distances to the nearest-neighbour Ag atoms of the first and the second layer, respectively.

[c] Not a local minimum (see text).

whereas the barrier from the LB site toward the most stable site 3f is hardly 1 kJ mol$^{-1}$(Figure 5.2). Vibrational frequency analyses confirmed all three sites as local minima, but revealed adsorption complexes at short-bridge (SB) sites, with adsorption energy of -309 kJ mol$^{-1}$, to be saddle points of the potential energy surface.

For adsorption complexes with oxygen on top of silver centres (T), with $E_{ad}$ = -207 kJ mol$^{-1}$, two imaginary vibrational frequencies were calculated; thus they represent local maxima of the potential energy with respect to lateral motion. The O-Ag distances to Ag centres of the first and second layers are 215 and 222 pm, respectively, for oxygen adsorbed at 3f sites; the corresponding values for the LB complex are 221 and 232 pm, and the distances in 4f complex are 222 pm. The oxygen centres are located at heights of 60 pm (3f), 54 pm (4f) and 32 pm (LB) above the top layer plane of the surface (Table 5.1).

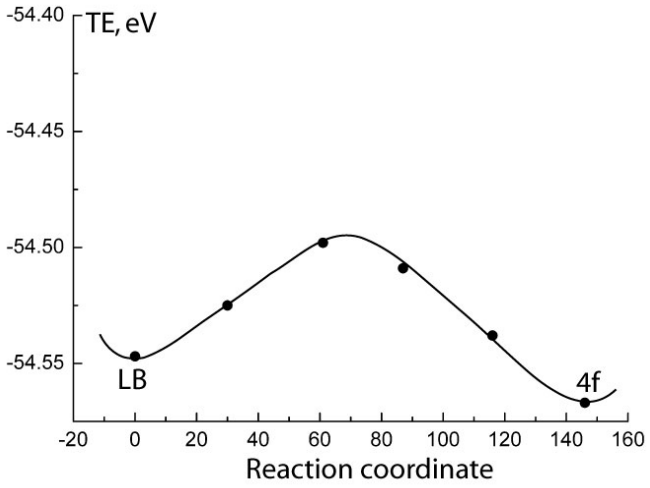


**Figure 5.2:** Potential energy surface (total energy, TE) showing the atomic oxygen diffusion barrier from long bridge site (LB) to 4-fold hollow (4f).

Previous computational studies [139,140] on the adsorption of oxygen at Ag(110) surface reported at LB and 4f sites as preferred, but neither study specified the topology of the potential energy surface nor considered the 3f site. In quantitative agreement with the present results, the binding energy of atomic oxygen on the four-fold hollow site had previously been calculated at about 340 kJ mol$^{-1}$, with oxygen located at 57 pm above the top crystal plane [141].

From experimental data [121], the adsorption energy of atomic O on Ag(110) surface is about -416 kJ $mol^{-1}$. This estimate is for an oxygen coverage of $\theta_O$ = 0.15 ML. In this coverage range, formation of ordered added-row phases (7×1) ($\theta_O$ = 0.143) and (6×1) ($\theta_O$ = 0.166) was observed [121]. Early surface extended X-ray-absorption fine-structure (SEXAFS) studies [71,142] assumed oxygen atoms to be adsorbed on the Ag(110) at long-bridge sites at 2 pm above the top crystal plane. However, with the help of STM results, later on ordered ($n$×1) phases were identified as reconstructed, with added rows running along the [001] direction [131,133]. Thus, the above experimental adsorption energy estimate [121] probably corresponds to oxygen in a more stable added-row structure rather than to adsorption on the unreconstructed Ag(110) surface.

At such low coverage that added-row moieties are not yet formed adsorption complexes LB, 4f, and 3f of oxygen exhibit very similar features (Table 5.1). Thus, any of them appears to be similarly adequate as representative model of $H_2$ activation at the unreconstructed Ag(110) surface. (2×2) surface unit cells as used here have been justified elsewhere [143] for studying adsorption of small molecules on metal surfaces.

## 5.3 Oxygen diffusion into Ag(110) sub-surface

Oxygen underneath an LB site on Ag(110) (Figure 5.1), was reported to be ~20 kJ $mol^{-1}$ more strongly bound than at the LB site; also, a calculated activation barrier of 86 kJ $mol^{-1}$ for oxygen diffusion from the LB to the sub-LB position was reported, which corresponds to a barrier of ~66 kJ $mol^{-1}$ for the reverse movement [139]. Attempts to reproduce these findings failed. The binding energies of oxygen, reported in Ref. 139 for all sites (LB, 4f, SB, top), are about 250 kJ $mol^{-1}$ larger than obtained in the present study and other works. According to the present study, oxygen leaves the sub-LB site for the more stable LB site without any activation barrier.

**Table 5.2:** Calculated binding energies $E_{ad}$(fcc) of atomic O at three-fold hollow fcc sites and the corresponding interaction energies $E$(oss) at octahedral subsurface (oss) sites of Ag(110) (Figure 5.1), Ag(111) and Ag(221) (Figure 5.4) slabs, as well as energies $E$(fcc→oss) for fcc→oss oxygen transfer, and the corresponding activation barriers $E_a$. All energies are in kJ mol$^{-1}$.

| Surface | site | $E_{ad}$(fcc) | $E$(oss) | $E$(fcc→oss) | $E_a$(fcc→oss)[a] |
|---|---|---|---|---|---|
| Ag(110) | 3f | -359 | -278 | 81 | 81 (~0) |
| Ag(111) | fcc | -358 | -292 | 66 | 80 (14) |
| Ag(221) | fcc 1 | -363 | -292 | 70 | 70 (~0) |
| | fcc 2 | -348 | -299 | 49 | 51 (2) |
| | fcc 3 | -342 | -284 | 57 | 76 (19) |

[a] Values in parentheses are activation barriers for reverse diffusion, from subsurface sites to the surface.

Oxygen in the interstitial oss site underneath the SB site of Ag(110) (Figure 5.1) represents a local minimum of the potential energy surface. However, this complex is 81 kJ mol$^{-1}$ higher in energy than oxygen adsorbed at the neighbouring surface 3f site (Table 5.2); the reverse process does not encounter a notable activation barrier, but a vibrational analysis identified the subsurface complex as a local minimum.

There is a significant structural stress due to the incorporation of oxygen in subsurface. Nearest-neighbour distances between Ag centres close to $O_{oss}$ are elongated to 340–350 pm, from 293 pm. In these models, the top three layers of the Ag(110) slab are relaxed (one layer more than in regular model discussed in Chapter 3) to determine more precisely the optimized positions of Ag centres close to oss sites.

## 5.4 Oxygen adsorption and diffusion on Ag(111) surface

As discussed in Chapter 4, oxygen-induced reconstruction of Ag(110) surface leads to a *p*(nx1)O/Ag(110) added-row structure. Similarly, the Ag(111) surface reconstructs in the

presence of oxygen; the oxygen-induced surface reconstruction leads to the ordered phase *p*(4×4)O/Ag(111) (Figure 5.3) which has been extensively studied both experimentally [68,74,75] and theoretically [84,144-146]. Recently the atomistic structure of the *p*(4×4)O/Ag(111) phase has been revisited [146,65,66]. While originally this phase was interpreted as a $Ag_{1.83}O$ structure, formed by hexagonal -Ag-O- rings and related to an epitaxial over layer of the oxide $Ag_2O$, recent STM studies, supplemented by DF modelling, suggested the formation of silver terraces bridged by oxygen centres [65,66]. In any case, these different interpretations of the *p*(4 × 4) phase have in common the local structural motif Ag-O-Ag-O of an O centre bridging two Ag centres. The added silver atoms occupy the 3-fold hollow and top sites (fcc and hcp represented as F and H, where as top site as T in Figure 5.3) and the oxygen atoms occupy the 3-fold hollow sites created by the added silver atoms at F, H and T of Figure 5.3. In regular fashion oxygen is above and below (represented as U and L in Figure 5.3) the plane of these three silver centres.

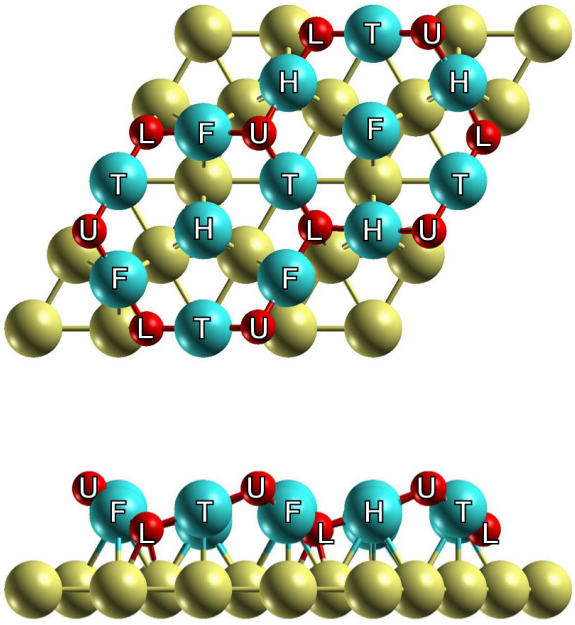


**Figure 5.3:** Top (upper panel) and side view (lower panel) of $Ag_{1.8}O$ on top of Ag(111) surface. Yellow spheres – Ag(111) substrate, blue spheres – Ag atom from $Ag_{1.8}O$ structure, red spheres – O. T – top site, F – fcc site, H – hcp site of Ag(111) substrate, U – upper O atom and L – lower O atom.

This motif resembles the models considered in the present study for the added-row $p(2\times1)$O/Ag(110) surface. In fact, the oxygen coverage of $p(2\times1)$O/Ag(110) surface, 1/2, is similar to the value of 3/8 of the oxide-covered surface $p(4\times4)$O/Ag(111). Additional arguments, that results obtained for the added-row modified Ag(110) surface may be generalized to the Ag(111) surface partly covered by oxygen, come from photoelectron spectroscopy. The binding energy (ionization potential) of O1s core levels of the $p(4\times4)$O/Ag(111) structure differs only ~0.1 eV from that of the $p(2\times1)$O/Ag(110) structure [67,68], in line with DF estimates [66]. Because of these similarities of the surfaces, further calculations on $p(4\times4)$O/Ag(111) surface has not been done in the context of the present work.

On the Ag(111) surface, a similar picture for oxygen diffusion from the fcc three-fold hollow sites to oss sites can be drawn as in the case of Ag(110). At an oxygen coverage of 0.11 ML, adsorption at the surface three-fold hollow fcc site is 66 kJ $mol^{-1}$ more favourable than in the corresponding oss site, $E$(oss) = -292 kJ $mol^{-1}$ (Table 5.2). The calculated activation barrier for oxygen diffusion fcc$\rightarrow$oss is 80 kJ $mol^{-1}$; therefore, the reverse process is also activated, by 14 kJ $mol^{-1}$. The results of the present study agree very well with those of a previous computational study for the same oxygen coverage [84], where 5-layer slab models had been used, and to check the effect of slab thickness the calculations were done with 4-layer models in this present work. That earlier study also addressed the effect of oxygen surface coverage on the stability of subsurface species on Ag(111); for coverage up to 0.5 ML, surface positions were calculated to be favoured over subsurface sites [84].

## 5.5 Oxygen adsorption and diffusion on Ag(221)

Now the discussion moves on to the stepped surface (221) where oxygen diffusion to subsurface sites has been inspected. This surface exhibits (111) terraces terminated by steps. Three types of fcc sites and the corresponding oss sites were considered (Figure

5.4), distinguished by their location on the terrace with respect to a step. The unit cell shown in Figure 5.4, with single oxygen species, corresponds to oxygen coverage of 1/12. In view of the more open structure of Ag(221) compared to the ideal Ag(111) surface, one may expect more flexibility for incorporating oxygen species in the subsurface region. On first glance, on Ag(221), the energy profiles for oxygen subsurface diffusion fcc→oss are similar to that on Ag(111) (Table 5.2). This holds in particular for fcc sites 1 near the top of a step, except that the corresponding oss site, a very shallow local minimum, exhibits essentially no barrier for $O_{oss}$ atoms to be released to the surface. fcc sites 2 and 3 further "inward" on the terrace are notably less bound, up to 20 kJ $mol^{-1}$, while the associate oss sites show much

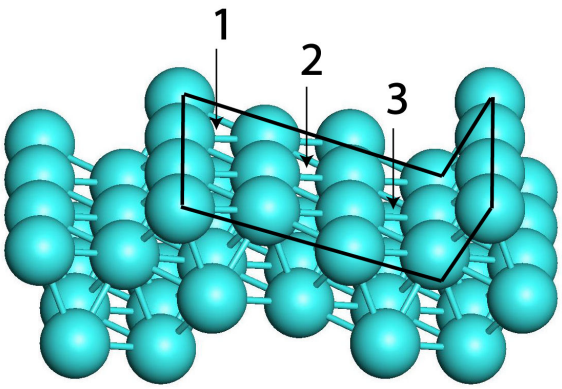


**Figure 5.4:** Three-fold hollow fcc sites **1**, **2**, **3** on a (111) terrace of the Ag(221) surface which were considered as starting points for oxygen diffusion to subsurface oss sites. The frame traces a unit cell in the top layer. Only the two top layers of the 5-layer slab are shown.

smaller variations in stability. This significantly reduces the associated energy change upon oxygen release to the surface, which has to overcome small activation barriers, up to 19 kJ $mol^{-1}$ (site 3, Figure 5.4). As in the case of Ag(110) and Ag(111), occupation of oss positions of Ag(221) by oxygen induces significant structural stress: nearest-neighbour distances among Ag atoms surrounding the oss site reach 330–350 pm.

All Ag surface systems considered in this section show subsurface oxygen species to be unstable (in the absence of adsorbed oxygen). Recall that according to DF and *ab*

*initio* thermodynamics modelling on oxygen at Ag(111), bulk-dissolved oxygen also was calculated to be energetically disfavoured at low oxygen concentrations compared to surface oxygen [84]. Yet, oxygen species in subsurface interstitial positions of silver, even if only as metastable complexes, cannot be excluded under (hydrogenation) reaction conditions.

## 5.6 $H_2$ activation and diffusion on *p*(2x1)O/Ag(110) surface

In Chapter 4, hydrogen activation was studied keeping the hydrogen molecular axis parallel to the added row and in this section the hydrogen molecular axis is oriented perpendicular to the added row and positioned on top of oxygen atom. In this way the final state is one hydroxyl formation on added row and the other hydrogen is located on short bridge site of terrace and the reaction energy is calculated to be exothermic by 75 kJ $mol^{-1}$. Using the NEB method, the calculated activation barrier is 140 kJ $mol^{-1}$ with r(H-H) = 123 pm, and oxygen getting lifted from its normal position. This barrier is two times higher than the barrier when the molecular axis of hydrogen is kept parallel to the added

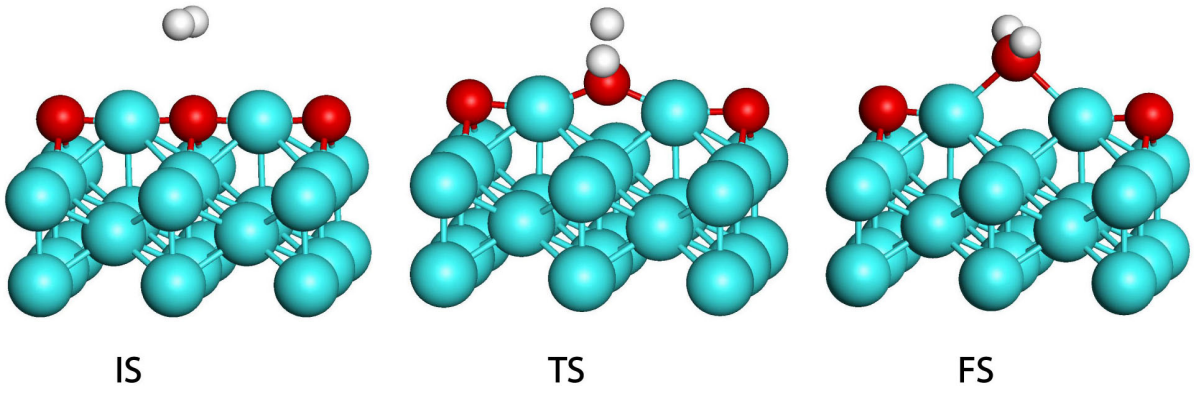


**Figure 5.5:** Hydrogen activation on *p*(2x1)O/Ag(110) surface with hydrogen axis oriented in perpendicular direction to the added row. IS – initial state; TS – transition state; FS – final state.

row chains. As formation of water is more exothermic than formation of terrace hydrogen, there is a high possibility that hydrogen diffusion happens over the surface and forms water molecule with the hydroxyl group of added row with a diffusive activation barrier of 80 kJ $mol^{-1}$. However the formation of hydroxyl and one terrace H is weak in reaction energy when compared to the formation of water the reaction energy of which is ~140 kJ $mol^{-1}$. Thus, in competition when hydrogen dissociates on oxygen, it forms water and removes oxygen from the surface.

**Table 5.3:** Calculated reaction energies $E_r$ and corresponding barriers $E_a$ (kJ $mol^{-1}$) for $H_2$ dissociation on silver surfaces with pre-adsorbed oxygen. Selected interatomic distances (pm) in the transition states of $H_2$ dissociation are also shown.

| Substrate | | Final state [a] | $E_r$ | $E_a$ | H-H | O-H | Ag-H |
|---|---|---|---|---|---|---|---|
| O/Ag(110) | | $OH_*$ + $H_*$ | -99 | 47 | 93 | 134 | 207 |
| OH/Ag(110) | | $H_2O_*$ + $H_*$ | -48 | 10 | 89 | 147 | 226 |
| *p*(2×1)O/Ag(110) | step 1[b] | $OH_{*ar}$ + $H_{*ar}$ | 32 | 71 | 122 | 109 | 189 |
| | step 2[b] | 2 $OH_{*ar}$ | -256 | 12 | | | |
| | 1st alternative, step 2[b] | $OH_{*ar}$ + $H_*$(LB) | -118 | 11 | | | |
| | 2nd alternative, step 2[b] | $OH_{*ar}$ + $H_*$(SB) | -120 | 11 | | | |
| *p*(2×1)O/Ag(110) | step 1[b] | $H_2O_{*ar}$ | -150 | 137 | 123 | 103 | 268 |
| | step 2[b] | $H_2O$ desorption | 20 | – | | | |
| | alternative step 2[b] | $OH_{*ar}$ + $H_*$(SB) | 77 | 156 | | | |
| *p*(2×1)OH/Ag(110) | | $H_2O_{*ar}$ + $H_*$ | -50 | 22 | 89 | 144 | 192 |
| Ag(111)/$O_{sub}$, $\theta_{oss}$ = 0.25 ML | | 2 $H_*$ | 15<br>-13[c] | 98 | 142 | | 172; 208 |
| Ag(111)/$O_{sub}$, $\theta_{oss}$ = 0.5 ML | | 2 $H_*$ | -80[c] | 71[c] | 109[c] | | |

[a] Adsorption complexes are indicated by $_*$ (or $_{*ar}$ if formed on the added row of a reconstructed surface).

[b] Reaction energies $E_r$ for each step, i.e. the initial state of the first step comprise $H_2$ while the initial state of the second step is the final state of the first step.

[c] Values from Ref. 147. In that work, different parameters were used in the models: energy cut-off 340 eV vs. our 400 eV; k-grid: 18 special Chadi-Cohen k-points vs. our 5x5x1 Monkhorst-Pack grid.

As discussed in Chapter 4, migration of H atoms was also considered, formed as intermediates after the first step of $H_2$ dissociation, from added-row Ag centres to the Ag(110) terrace (Figure 5.6), as alternative to migration to nearest-neighbour oxygen centres. The activation barriers for these alternative directions are almost the same, 12 kJ $mol^{-1}$ in $[1\,\bar{1}\,0]$ direction to the O centre, and 11 kJ $mol^{-1}$ in [100] direction to the neighbouring Ag(110) ridge. However, diffusion of H from the added row Ag site to O is 138 kJ $mol^{-1}$ more exothermic than movement to the neighbouring LB site [*p*(2×1)O/Ag(110), Table 5.3], whereas diffusion to the SB position at the ridge of the Ag(110) substrate is almost iso-energetic (cf. first and second alternatives of step 2; Table 5.3 and Figure. 5.6).

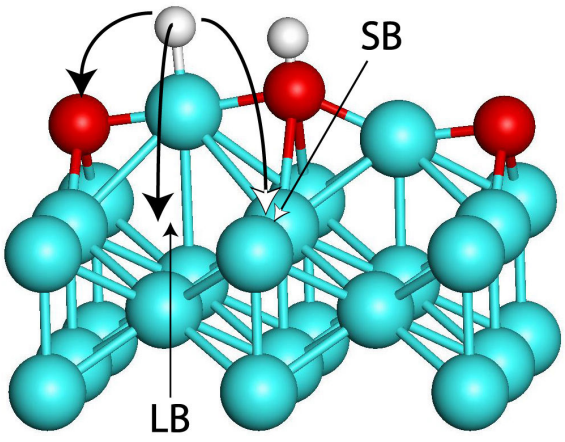


**Figure 5.6:** Alternative directions for transfer of a hydrogen atom from an Ag centre; situation after the assumed dissociation of an $H_2$ molecule at an Ag-O pair of the added row on a *p*(2×1)O/Ag(110) surface.

An alternative mechanism for the activation of hydrogen involves the formation of $H_2O$ from one OH group on an added row (the fully hydroxylated added row is discussed in the next paragraph), releasing the second H atom to an oxygen-free area of the Ag surface. To this end, the axis of the dissociating $H_2$ molecule is kept perpendicular to the added row above OH, along the $[1\,\bar{1}\,0]$ direction (Figure 5.6). However, it was found that this $H_2$ dissociation pathway with activation energy of 137 kJ $mol^{-1}$ leads directly to formation of a water molecule; this process is exothermic by -150 kJ $mol^{-1}$ (Table 5.3).

With an adsorption energy about -20 kJ $mol^{-1}$, the water molecule formed is weakly bound on the added row and it easily desorbs. Dissociation of $H_2O$ to produce an OH group sitting within the added row and a hydrogen atom on the metallic part of the surface is endothermic by 77 kJ $mol^{-1}$ and exhibits a high activation barrier of 156 kJ $mol^{-1}$. Note that water formation is by about 70 kJ $mol^{-1}$ less favourable than formation of two OH groups in the added row. Thus, the mechanism releasing one hydrogen atom per dissociated $H_2$ molecule to an oxygen-free part of the catalyst surface is kinetically unfavourable on the reconstructed surface. The most likely result when molecular hydrogen from the gas phase interacts with an added-row structure is complete hydrogenation of the added row.

A fully hydroxylated added row surface was considered for studying the dissociation of $H_2$ via interaction with an OH group, previously formed on an added row. In fact, in experiment a OH(1×2)/Ag(110) structure has been observed to form by $H_2O$ dissociation on *p*(4×1)O/Ag(110) [148]. An oxygen-covered Ag(110) surface is extremely reactive to water, even below room temperature [148]. However, the exact structure of the ordered hydroxyl layer OH(1×2) formed in this way [or OH(1×*n*/2) in the more general case of an initial *p*(*n*×1)O/Ag(110) phase] remains under discussion. Although -OH-Ag-OH- chains, preserving the added-row motif of an oxygen-covered

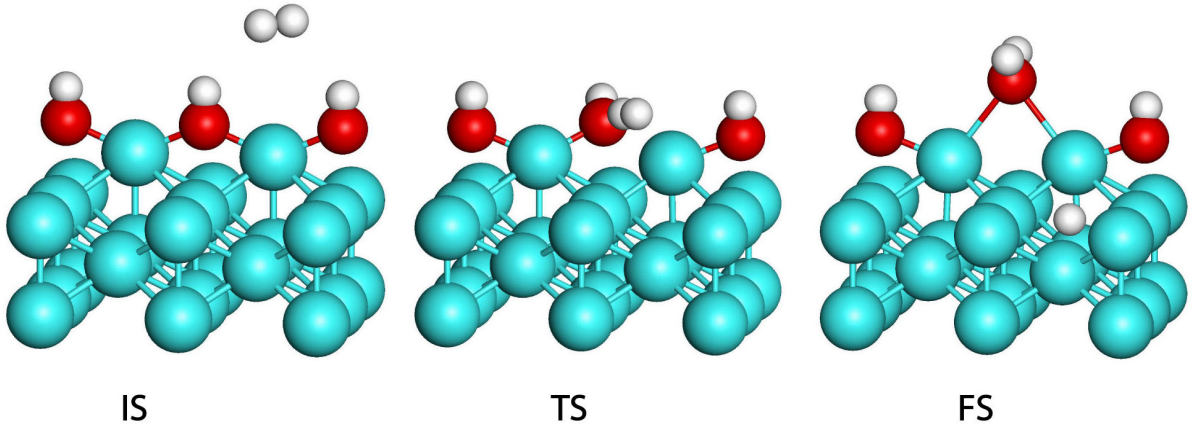


**Figure 5.7:** Hydrogen activation on *p*(2x1)OH/Ag(110) surface. IS – initial state; TS – transition state; FS – final state.

surface, were suggested as a possibility [149], very recently it has been suggested that the added rows dissolve, forming a hydroxyl layer that comprises just OH rows on Ag(110) substrate [148]. The models considered in this study comprised two types of surface hydroxyl groups: (*i*) OH on the unreconstructed Ag(110), (*ii*) hydroxylated added rows. In the next section 5.7 hydrogen activation on OH adsorbed on Ag(110) surface will be discussed, here the discussion on added row continues.

For this purpose, the added-row structure *p*(2×1)OH/Ag(110) as model (Figure. 5.7) was selected, which formally can be obtained by full hydrogenation of a *p*(2×1)O/Ag(110) structure. A very low activation barrier, 22 kJ $mol^{-1}$, was determined for the dissociation of $H_2$ via interaction with OH groups of the added row; this reaction was calculated to be exothermic, by -50 kJ $mol^{-1}$ (Table 5.3). Thus, a hydrogen atom can be released to a silver terrace via dissociation of $H_2$ on a previously formed OH group of an added row.

The H atoms, which are present on terraces of the added-row surface, may recombine with OH groups of the added rows, resulting in the formation of water molecules. The activation barrier of this process was calculated at 85 kJ $mol^{-1}$ and the reaction energy at -66 kJ $mol^{-1}$. Similar values, 76 kJ $mol^{-1}$ and -81 kJ $mol^{-1}$, respectively, were calculated on a Ag(111) surface relative to isolated OH and H(fcc) adsorbates [150]

## 5.7 $H_2$ activation and diffusion on O/Ag(110)

Atomic O centres at LB sites of Ag(110) (Figure 5.1) were chosen to model $H_2$ dissociation (Figure 5.8). In the TS, one H atom interacts with an oxygen centre (O-H distance 134 pm) and the other H atom is located above a silver ridge, at Ag-H = 207 pm (Table 5.3). The barrier for $H_2$ dissociation, 47 kJ $mol^{-1}$, is much lower than calculated for

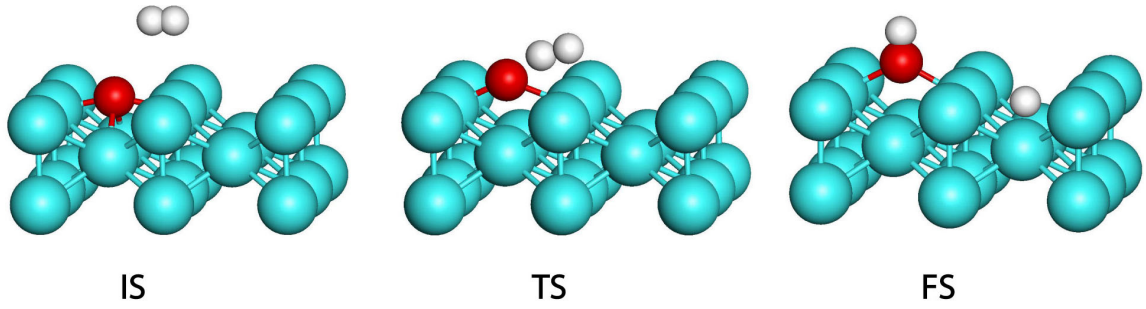


**Figure 5.8:** Hydrogen activation on O/Ag(110) surface where oxygen is adsorbed at long bridge site. IS – initial state; TS – transition state; FS – final state.

clean Ag(110), ~120 kJ mol$^{-1}$, and even notably lower than for the added-row structure *p*(2×1)O/Ag(110), ~70 kJ mol$^{-1}$. The H-H distance in the TS, 93 pm (Table 5.3), is significantly shorter than calculated for the TSs on *p*(2×1)O/Ag(110) (122 pm) and clean Ag(110) (136 pm). This finding indicates that $H_2$ dissociation at O/Ag(110) proceeds via an early transition state. The reaction was calculated exothermic, by -99 kJ mol$^{-1}$. After breaking the H-H bond, the hydrogen centre above the silver ridge moves to a LB site above a trough (Figure 5.8). The potential energy surface of an H atom on clean Ag(110) is rather flat with adsorption energy differences between LB, SB and 3f sites of at most 10 kJ mol$^{-1}$ (see Section 4.2). Therefore, an H atom can easily diffuse over the clean Ag(110) terrace to approach a target organic reactant or intermediate to be hydrogenated.

### 5.7.1 Activation of hydrogen on OH/Ag(110)

Hydroxyl groups formed on Ag(110) via interaction of adsorbed oxygen with $H_2$ molecules were considered as possible sites for activating a second $H_2$ molecule. Such a reaction produces $H_2O$ and one more H atom, released to a silver terrace and available as subsequent hydrogenation agent (Figure 5.9). The position of the OH group differs significantly from that of the original O centre. While oxygen adsorbed above the trough is almost in the plane of top silver atoms (Figure 5.8, left side), the O centre of an OH

group in the same position is 110 pm above that plane (Figure 5.8, right side). Moreover, a hydroxyl group at a SB position

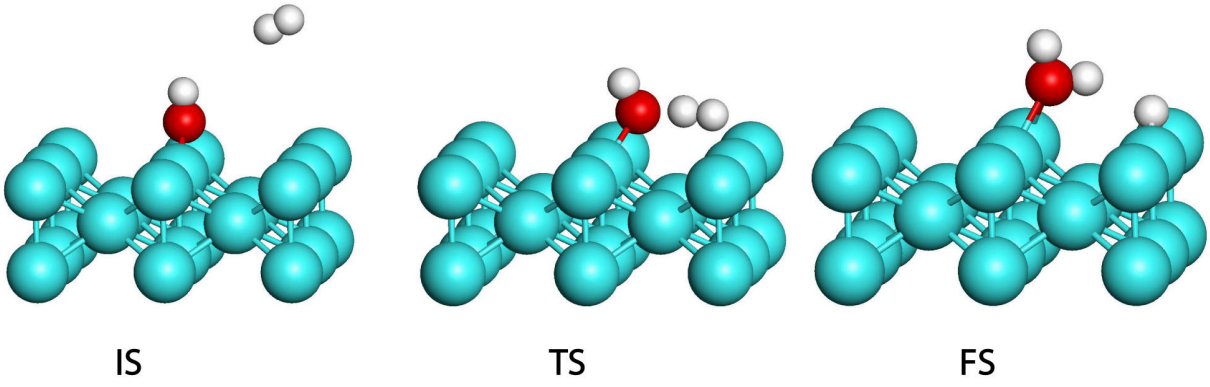


**Figure 5.9:** Hydrogen activation on OH/Ag(110) surface where OH is adsorbed at short bridge site. IS – initial state; TS – transition state; FS – final state.

is slightly more stable, ~5 kJ $mol^{-1}$, than a hydroxyl group at a LB site; therefore, $H_2$ dissociation on OH at a SB site (Figure 5.9) was calculated. Interestingly, the calculated activation barrier for $H_2$ dissociation is extremely low, only 10 kJ $mol^{-1}$. The geometric characteristics of the TS complex are similar to those calculated for the previous case of $H_2$ dissociation at an adsorbed O centre (Table 5.3). $H_2$ activation at an OH group is also exothermic, by -48 kJ $mol^{-1}$. The resulting H species binds at a SB position of the ridge neighbouring the ridge where the reacting OH was located (Figure 5.9). As on adsorbed O, the produced H atom can easily diffuse from its SB site to a clean Ag(110) terrace. Similar to other noble metal surfaces [151], e.g. Ag(111) [150], the $H_2O$ molecule formed is weakly bound on Ag(110), about -20 kJ $mol^{-1}$ at top site of the ridges, and thus desorbs easily.

The mechanism for the production of active H atoms considered here involves an isolated O centre adsorbed on Ag(110) surface, which is able to activate two $H_2$ molecules, thereby producing two H atoms adsorbed at oxygen-free Ag(110) terraces and an $H_2O$ molecule. The overall reaction $O(ads) + H_2(gas) \rightarrow H_2O(gas) + 2H(ads)$ is

exothermic by -126 kJ $mol^{-1}$; both $H_2$ dissociation steps exhibit small activation barriers of 47 and 10 kJ $mol^{-1}$, respectively.

## 5.8 Water adsorption on Ag(110) surface

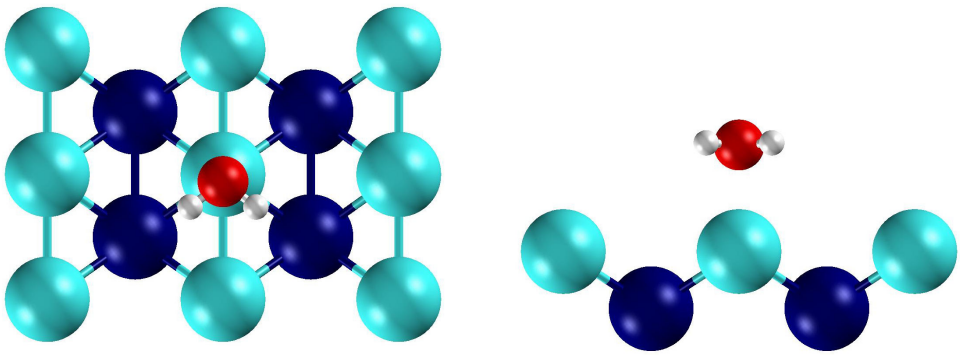

**(a)** **(b)**

**Figure 5.10:** Structure showing (a) top and (b) side views of water adsorbed at an on top site of Ag(110) surface, which is the most stable site for water adsorption.

On all metal surfaces $H_2O$ adsorbs preferentially at atop sites and lies parallel to the surface [151]. The results of the present study are in agreement with this general conclusion. $H_2O$ binds weakly to all surfaces and the adsorption energies range from 0.1 eV to 0.4 eV and are in the following sequence Au < Ag < Cu < Pd < Pt < Ru < Rh [151].

**Table 5.4:** Comparison of adsorption complexes of water at different sites on the Ag(110) surface.. Angle in degrees, distances in pm, and the binding energies in kJ $mol^{-1}$.

| Sites | ∟HOH | ∟AgOH | r(O-H) | r(O-Ag) | BE |
|---|---|---|---|---|---|
| Top | 104.8 | 95.2 | 98 | 252 | 20 |
| Bridge | 102.0 | 64.5[a] | 98 | 319 | 4 |
| 4-fold hollow | 102.3 | 64.5 | 98 | 350 | 6 |

a – This angle is measured with respect to the first layer of the substrate but not directly with the Ag atom.

The experimental characterization of $H_2O$ monomers is difficult, complicated by facile $H_2O$ cluster formation. Cluster formation is problematic because it masks the true $H_2O$-metal interaction, making it difficult to reach any definitive conclusion about $H_2O$-metal bonding. Despite of many theoretical studies in this area [151-155] a clear picture on the nature of $H_2O$-metal bonding thus far has not been reached. Some studies predict adsorption at atop sites while others predict adsorption at higher coordination sites [151-155].

Two factors have to be considered when discussing the stability of adsorbed water molecules: (i) the water-surface interaction and (ii) inter-water hydrogen bonding. $H_2O$ deforms slightly after adsorption: the O-H bond elongates from 97 pm in the gas phase, to 98 pm and the HOH angle opens slightly to 104.8° from 104.6° in the gas phase. These structural changes are in quiet good agreement with the structure mentioned by King et al [151]. The structural data, calculated in the present study, agree well with the experimentally determined structural parameters of water, where interatomic distance, r(O-H) = 96 pm and the angle ∠HOH = 104.5° [156-158].

A brief list of available calculations for water adsorption on different metal surfaces is collected in Table 5.5. From this compilation one can see that water adsorbs very weakly on metal surfaces, only on Pt(111) and Rh(111) surfaces it has higher binding energies of about 50 kJ $mol^{-1}$. In the present study the calculated binding energy is only 20 kJ $mol^{-1}$ on top site of Ag atom, showing that water is very weakly bound to the Ag(110) surface. At other sites of this surface, e.g. bridge and four-fold hollow, $H_2O$ essentially does not bind at all. In the present study, the structure of water molecule adsorbed at a bridge site agrees well with the structure obtained by King et al.[ 151].

The dissociation energy of an O-H bond of water was calculated at 534 kJ $mol^{-1}$ for molecules in the gas phase. This value agrees well with the experimental value of 531 kJ $mol^{-1}$ [159]. Thus, water requires a high energy to dissociate into hydroxyl and hydrogen. According to the following set of reactions describing the thermodynamics of water on the Ag(110) surface, about 118 kJ $mol^{-1}$ are necessary to dissociate water into a hydroxyl

and a hydrogen atom, both adsorbed on the surface. Obviously, the reaction is highly endothermic.

**Table 5.5:** Comparison of results from different studies related to the adsorption of water molecules at metal surfaces

| Reference | Surface | Site | BE kJ $mol^{-1}$ | r(O-Ag) pm |
|---|---|---|---|---|
| [152] – Cluster model (GAUSSIAN92 | Cu(100)) | top | 24 | 260 |
| | | bridge | 19 | 250 |
| | | 4f-hollow | 16 | 300 |
| | Au(100) | top | 28 | 270 |
| | | bridge | 26 | 250 |
| | | 4f-hollow | 19 | 250 |
| [160] – Exp | Cu(100) | | 36 | |
| [153] – Slab model VASP | Pt(111) | | 53 | |
| | Rh(111) | | 55 | |
| [154] – Slab model VASP | Ru(0001) | Top | 39 | 228 |
| | | bridge | 9 | 255 |
| | | 4f-hollow | 6 | 256 |
| | Rh(111) | Top | 39 | 232 |
| | | bridge | 12 | 257 |
| | | 4f-hollow | 11 | 270 |
| | Pd(111) | Top | 29 | 242 |
| | | bridge | 14 | 274 |
| | | 4f-hollow | 12 | 277 |
| | Pt(111) | Top | 28 | 243 |
| | | bridge | 12 | 311 |
| | | 4f-hollow | 11 | 312 |
| | Au(111) | Top | 10 | 267 |
| | | bridge | 3 | 280 |
| | | 4f-hollow | 2 | 280 |
| [155] | Ni(111) | top | 23 | 226 |
| | | bridge | 9 | 302 |
| | Ni(221) | top | 39 | 212 |
| | | bridge | 24 | 246 |
| [151] – Slab model CASTEP | Rh(111) | top | 40 | 231 |
| | Pd(111) | | 32 | 228 |
| | Pt(111) | | 34 | 236 |
| | Cu(111) | | 23 | 225 |
| | Au(111) | | 12 | 302 |
| | Ru(0001) | | 36 | 229 |

The mechanism may be summarized as follows:

| | | |
|---|---|---|
| $H_2$/Ag + O/Ag | → OH/Ag + H/Ag | (-117 kJ $mol^{-1}$) |
| OH/Ag | → O/Ag + H/Ag | (183 kJ $mol^{-1}$) |
| $H_2$/Ag + OH/Ag | → $H_2O$/Ag + H/Ag | (-60 kJ $mol^{-1}$) |
| $H_2O$/Ag | → HO/Ag + H/Ag | (118 kJ $mol^{-1}$) |

Thus, the thermodynamics of the overall reaction is:

| | | |
|---|---|---|
| $2H_2(g)$ + O/Ag(110) | → $H_2O^*$ + 2H* | (-170 kJ $mol^{-1}$) |
| $H_2O^*$ + 2H* | → $H_2O(g)$ + 2H* | (18 kJ $mol^{-1}$) |

With these reaction thermodynamics it is clear that the availability of hydrogen is possible over the Ag(110) surface, but under the conditions that there is oxygen on the surface. Also each oxygen results in two hydrogen atoms and finally oxygen will be out of the surface in the form of water. This whole process is explained in the above global reaction.

## 5.9 $H_2$ activation on $O_{oss}$/Ag(111) Surface

### 5.9.1 Adsorption

The Ag(111) surface with $O_{oss}$ atoms underneath the top layer of Ag atoms has been selected as model of $H_2$ activation near subsurface oxygen, but one should keep in mind that more complicated structures may occur under real catalytic conditions [161,162]. However, detailed structural information from experiment on such species is lacking. The goal of the calculations was to estimate the effect of subsurface oxygen occlusion (at low concentrations) on the surface chemistry of hydrogen.

The analysis was started with the adsorption of atomic H near an $O_{oss}$/Ag(111) complex (Figure. 5.11). The three-fold hollow fcc and hcp sites on (111) surfaces of fcc metals usually exhibit very similar propensity for adsorption of H; for instance, in a very

recent study [163] H adsorption at fcc sites of Pd(111) was calculated just 6 kJ $mol^{-1}$ stronger than at hcp sites while on Cu(111) both adsorption complexes were calculated degenerate [143]. For the Ag(111) surface the results are identical with adsorption energies, -198 kJ $mol^{-1}$, for atomic H at fcc and hcp sites at an H coverage of 1/4 ML.

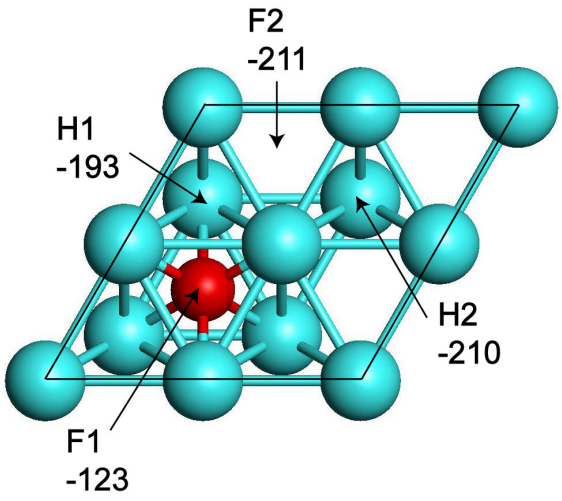


**Figure 5.11:** Three-fold hollow hcp (**H1**, **H2**) and fcc (**F1**, **F2**) adsorption sites of atomic hydrogen on a Ag(111) surface, modified by oxygen centres (red) occupying subsurface oss sites at a coverage of ¼ ML. The solid frame indicates a (2×2) surface unit cell. Calculated adsorption energies of single atoms H are also shown (in kJ $mol^{-1}$). Two adjacent **F2** sites represent the final state for the hydrogen activation process studied (see text).

Experimentally, the concentration of subsurface O atoms can be assumed to be very low [58,60]. This situation has been represented by the model $O_{oss}$/Ag(111) with the coverage $\theta_{oss}$ = 1/4 ML and a $p(2\times2)$ unit cell (Figure. 5.11). Two fcc (**F1**, **F2**) and two hcp (**H1**, **H2**) three-fold hollow sites by their proximity to $O_{oss}$ have been distinguished. Not surprisingly (Figure 5.11), the strongest effect of $O_{oss}$ on the adsorption of H was calculated for **F1** sites, located directly above the occupied oss site. Adsorption complexes of H at **F1** are strongly destabilized, by about 75 kJ $mol^{-1}$ compared to H adsorbed on the ideal Ag(111) surface without subsurface impurities, where $E_{ad}$ = -198 kJ $mol^{-1}$. At adsorption site **H1**, in nearest-neighbour position of $O_{oss}$, the calculated

destabilization of H with respect to the ideal Ag(111) surface is very small, only 5 kJ mol$^{-1}$. More importantly, at the somewhat more distant sites **F2** and **H2** adsorption of hydrogen becomes more stable than on the clean Ag(111) surface, by 12–13 kJ mol$^{-1}$. [Qualitatively, similar H adsorption energies were calculated at the lower content of subsurface oxygen, $\theta_{oss}$ = 1/9 ML (not shown).] Note that on Ag(111), with *all* octahedral interstitial positions beneath the top Ag layer occupied by O atoms ($\theta_{oss}$ = 1 ML), the adsorption interaction of H atoms strengthens by as much as 88 kJ mol$^{-1}$, compared to the clean Ag(111) surface [147].

## 5.9.2 Activation

With a coverage $\theta_{oss}$ = 1/4 ML and a $p(2\times2)$ unit cell, the most stable co-adsorption configuration of two H atoms at two neighbouring fcc sites **F2**, $\theta_H$ = 1/2 ML (Figure 5.12) was chosen as final state (FS) of the $H_2$ activation process in this model. $H_2$ dissociation on this surface was calculated endothermic by 15 kJ mol$^{-1}$ (Table 5.3), i.e. it is ~15 kJ mol$^{-1}$ more favourable than on the clean Ag(110) surface. The corresponding activation energy for $H_2$ dissociation is 98 kJ mol$^{-1}$; the activated complex with H-H = 142 pm represents a late TS (Table 5.3). The calculated activation energy of $H_2$ on $O_{oss}$/Ag(111) is ~30 kJ mol$^{-1}$ higher than on the $p(2\times1)$O/Ag(110) surface, but ~25 kJ mol$^{-1}$ lower than the lowest value on a clean Ag(110) surface. This latter finding agrees with other DF results according to which subsurface O reduces the barrier of $H_2$ activation compared to clean silver surface [147]. The calculated activation barrier for $H_2$ was shown to decrease from 107 kJ mol$^{-1}$ for the clean Ag(111) surface [or from 126 kJ mol$^{-1}$ on Ag(110)] to 71 kJ mol$^{-1}$ for subsurface oxygen at a coverage 1/2 ML [147]. The activation energy $E_a$ = 98 kJ mol$^{-1}$ for $\theta_{oss}$ = 1/4 ML is 27 kJ mol$^{-1}$ higher than that preceding result, because a higher coverage of subsurface O in the latter case resulted in a more stable final state. Note that the barrier of 71 kJ mol$^{-1}$ by Xu et al. [147] is very close to the $H_2$ activation energies of 69–76 kJ mol$^{-1}$ determined in the study for added-row modified $p(n\times1)$O/Ag(110) surfaces discussed above.

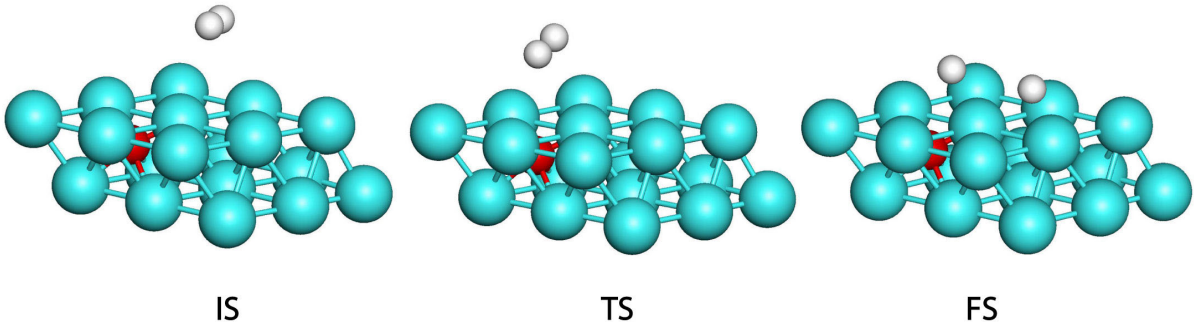


**Figure 5.12:** Hydrogen activation on OH/Ag(110) surface where OH is adsorbed at short bridge site. IS – initial state; TS – transition state; FS – final state.

These similar values of the activation barrier seem accidental in view of the fact that the corresponding mechanisms of $H_2$ activation on silver systems with oxygen at the surface and in the subsurface region are different. Whereas surface oxygen centres of added-row systems act directly as active centres for hydrogen adsorption, the effect of subsurface oxygen centres is indirect, via induction of an upward shift of the d-manifold of the Ag atoms in the surface [147].

## 5.10 Conclusions

Hydrogen dissociation was studied on different models of surface oxygen. For isolated oxygen centres adsorbed on Ag(110) surface a mechanism that involves successive activation of two $H_2$ molecules has been suggested. Interaction with a first $H_2$ molecule produces a hydroxyl group and an H atom on the metal surface; the OH group is able to react with another $H_2$ molecule to produce water (which desorbs) and one more H atom on the metal surface. Surprisingly, activation of $H_2$ on adsorbed hydroxyl groups exhibits the lowest activation barrier among the species considered. As a single surface oxygen centre can produce two atomic H species (that can further participate in hydrogenation) and afterwards desorbs as $H_2O$ molecule, the catalytic protocol in this model should

include an oxygen source. A similar mechanism was considered for the reconstructed *p*(2×1)O/Ag(110) surface with the difference that a single O centre gives rise to only one H atom on a metal terrace, ready to participate in hydrogenation of other molecules.

Oxygen adsorption on Ag(110) surface is almost iso-energetic at all the sites except for the top site and the diffusion barrier between the sites ranges from 1 kJ $mol^{-1}$ to 7 kJ $mol^{-1}$. The penetration of oxygen from surface to sub-surface sites has been studied; a local minimum under the short bridge site was found that is 81 kJ $mol^{-1}$ higher in energy compared to the short bridge. Subsurface incorporation of oxygen induces significant structural stress. Nearest-neighbour distances between Ag centres close to $O_{oss}$ are elongated to 340–350 pm, from 293 pm.

Subsurface oxygen species $O_{oss}$, located in interstitial octahedral positions, decrease the barrier for $H_2$ activation compared to clean Ag surfaces. However, they seem less efficient for $H_2$ activation than surface oxygen as the corresponding activation barrier was calculated higher. Moreover, in the absence of adsorbed oxygen, subsurface oxygen species are unstable and predicted to leave the subsurface sites with a low (or without any) activation barrier. Nevertheless, subsurface oxygen species can be regarded as sites promoting the formation of atomic hydrogen required for hydrogenation reactions on silver catalysts.

Also oxygen adsorption on long stepped surfaces like Ag(221) surface was studied, which are comprised of (111) planes, even though one can expect similar oxygen adsorption on these surface. However, because of the different freedom of motion of the surface atoms some differences was expected in the behaviour of oxygen atoms over this surface. Yet, calculations showed that the behaviour of oxygen on Ag(221) is rather similar to that on the Ag(111) surface. The adsorption energies of oxygen at different sites are similar to those of Ag(111) surface whereas the penetration barrier of oxygen to sub-surface sites is reduced at site 3 compared to site 1.

Various sources of oxygen come to mind. Oxygen may be supplied by the oxide support of the silver clusters, from the “bulk” region of large silver particles, or even

from decay products of the compound to be hydrogenated (e.g. in the case of unsaturated aldehydes). Clearly, further studies of this topic are highly desirable, in particular efforts to characterize the structure of the catalyst in more detail.

# Chapter 6

# Acrolein hydrogenation on clean and oxygen-modified surfaces of silver

Silver catalysts were experimentally demonstrated to exhibit notably higher selectivity of acrolein hydrogenation to the desired product propenol (allyl alcohol) compared to group VIII metal catalysts. In this chapter the results of DF calculations performed to quantify reaction and activation energies of acrolein hydrogenation on model silver substrates will be presented. The clean metallic Ag(110) surface is considered along with three different partially oxidized Ag surfaces with oxygen atoms present either *on the surface*, *p*(4×1)O/Ag(110) and O/Ag(110), or *subsurface*, $O_{oss}$/Ag(111). On clean Ag(110) these results revealed the selectivity of acrolein hydrogenation to allyl alcohol to be notably smaller than observed for silver particles as catalysts. The presence of atomic oxygen is shown to make Ag surfaces less active for acrolein hydrogenation compared to clean Ag, but it acts to considerably improve the selectivity. An elucidation of these findings consistent with experimental observations is proposed. At variance with group VIII metal catalysts, where the selectivity to allyl alcohol is greatly reduced by hindered desorption of the latter, both possible products of partial hydrogenation of acrolein are predicted to desorb easily from clean as well as O-modified silver surfaces.

## 6.1 Selectivity of partial hydrogenation of α,β-unsaturated aldehydes on silver catalysts: State of research

A detailed review of experiments on acrolein hydrogenation was given in Chapter 2. In the following, we will summarize pertinent results. Partial hydrogenation of α,β-unsaturated aldehydes is an industrially important source of unsaturated alcohols which, in turn, are valuable fine chemicals to produce perfumes, pharmaceuticals, and flavouring materials [14,15]. However, on conventional catalysts of group VIII metals, the selectivity to the desired unsaturated alcohols is low (e.g., ~2% on Pt); instead, saturated aldehydes and alcohols are observed to form preferentially [14,15]. The challenge of the selective synthesis of unsaturated alcohols is commonly attributed to the disfavoured hydrogenation of C=O bonds compared to C=C ones. The desired process can be somewhat facilitated for higher α,β-unsaturated aldehydes, $R_1R_2C$=CH-CH=O, where bulky $R_i$ groups may sterically hinder the generally assumed preferential activation of the C=C bond by the catalyst [14,15]. Therefore, for the lowest unsaturated aldehyde acrolein ($R_1$ = $R_2$ = H) the transformation to allyl alcohol (propenol) compared to the corresponding saturated aldehyde propenal appears to be particularly difficult.

Silver is a widely used oxidation catalyst [18,19]. Quite surprisingly [11], supported silver catalysts exhibited a rather high selectivity (up to 42%) in the hydrogenation of acrolein to propenol [20]. Further studies substantiated the crucial role of silver as active component in the selective hydrogenation [20,58,164]. Among the major experimentally ascertained features of this catalytic process are [58]: (*i*) there is a threshold pressure of ~100 mbar, below which no formation of unsaturated alcohols was observed; (*ii*) defect sites appear to be important and the desired selectivity over bulky silver is notably reduced (to below 10%); (*iii*) the activity depends on the number of sites able to activate $H_2$ that are probably electron deficient; (*iv*) oxygen incorporated in silver catalysts during the reaction promotes hydrogen activation and notably affects both activity and selectivity of the hydrogenation. The reaction conditions were found to strongly affect the state of the catalysts, which further complicates the challenge to uncover their performance/properties relations [58]. Thus, the hydrogenation mechanism

of acrolein (and its analogues) on silver catalysts remains basically unclear at the molecular level.

DF studies were carried out to contribute to clarifying activity and selectivity of partial hydrogenation of the lowest α,β-unsaturated aldehydes (exemplified by acrolein) over silver catalysts. In view of the complexity of the catalytic systems just outlined, the study focused on describing bulky catalysts which were represented by sites on extended silver surfaces: regular clean and oxygen-modified surfaces. Effects and complications associated with catalyst defects as well as catalyst restructuring due to interaction with the support or during the reaction have not been addressed in the present investigation.

## 6.2 Models

Four substrate models were used to explore the thermodynamics of acrolein hydrogenation over Ag catalysts. Adsorption of acrolein on clean planar silver surfaces was found to be very weak and hence not accompanied by any essential bond activation [97]. Therefore, anticipating more open Ag surfaces to be more reactive, hydrogenation of acrolein on the Ag(110) surface was considered as representative of clean ideal planes of silver catalysts. The Ag(110) substrate was modelled as five-layer slab with a (4×2) surface unit cell (Figure 6.1a). For this clean surface and in the corresponding adsorption studies, the atomic positions of the "top" two Ag layers and, if present, of all adsorbates were relaxed. The remaining three layers at the "bottom" of the metallic slab were kept fixed at the optimized geometry of the bulk material (Ag–Ag = 293 pm). As already mentioned in Chapters 4 and 5, Ag surfaces easily undergo interactions with oxygen and a subsequent reconstruction occurs [69-73]. The effect of atomic oxygen was described with the help of the following three models: (*i*) the added row surface *p*(4×1)O/Ag(110) (Figure 6.1b), (*ii*) the Ag(110) surface with oxygen atom adsorbed at long bridge sites, O/Ag(110) (Figure 6.1a), and (*iii*) the Ag(111) surface with O centres in subsurface interstitial octahedral positions between the first (upper) and second (beneath it) metal

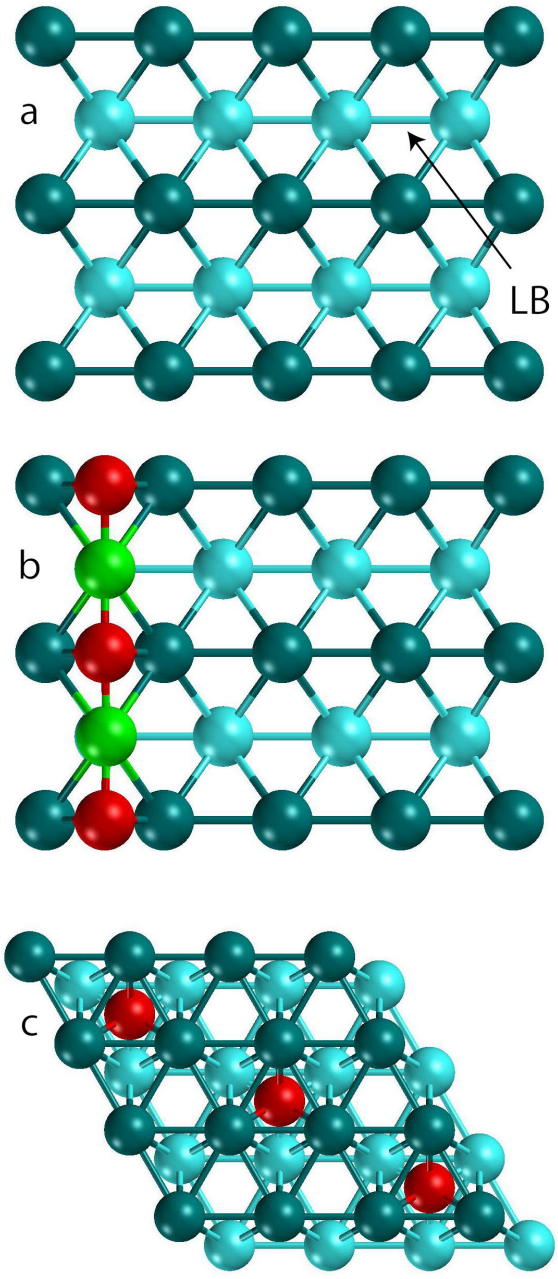


**Figure 6.1:** Top view of Ag substrate models studied: a) clean Ag(110) surface – (4×2) unit cell (LB – long bridge site), b) added row surface *p*(4×1)O/Ag(110) – (4×2) unit cell, c) Ag(111) surface with O atoms in octahedral subsurface (oss) positions, $O_{oss}$/Ag(111) – (3×3) unit cell. Colour coding of atomic centres: dark blue – surface-level Ag atoms, light blue – second-level Ag atoms, green – added row Ag atoms, red – O atoms.

layers, $O_{oss}$/Ag(111) (Figure 6.1c). Interstitial tetrahedral subsurface sites were not considered as they leave too little room for oxygen. In the *p*(4×1)O/Ag(110) model, a (4×2) unit cell with eight atoms per Ag layer was employed, enabling a surface coverage of 1/8 or higher. For the O/Ag(110) system a (3×2) surface unit cell was used, while subsurface O in $O_{oss}$/Ag(111) was studied using a (3×3) surface unit cell. These types of models have previously been discussed and justified for studies of surface processes [97,165]. For further technical details, see Chapter 3.

## 6.3 Reactants, intermediates and products in gas phase

In the gas phase, the trans isomer of acrolein has been calculated to be more stable than the cis isomer [97], in agreement with the 96% natural abundance of trans-acrolein. Thus, the trans-isomer (trans-C3=C2-C1=O, Figure 6.2a) was chosen as model of the reactant in the studies of thermodynamics and kinetics. The following four radicals could take part as intermediates in the first step of the partial hydrogenation of acrolein (Figure 6.2): hydroxyallyl ($CH_2$=CH-$CH^{\bullet}$-OH, panel b), allyloxy ($CH_2$=CH-$CH_2$-$O^{\bullet}$, panel c), 2-formylethyl ($CH_2^{\bullet}$-$CH_2$-CH=O, panel d), and 1-formylethyl ($CH_3$-$CH^{\bullet}$-CH=O, panel e). There intermediates are formed depending on whether the hydrogen atom is attached to atoms O, C1, C2 or C3 of acrolein, respectively. The products of partial hydrogenation of the C=O and C=C bonds of acrolein are propenol (propen-2-ol, Figure 6.2f) and propanal (Figure 6.2g), respectively.

The relative stabilities of intermediates and products of acrolein hydrogenation and the most characteristic interatomic distances of their optimized geometries, as calculated in the gas phase, can be found in Figure 6.2. Among the four intermediates, 1-formylethyl is the most stable one, followed by hydroxyallyl, which is only 20 kJ $mol^{-1}$ less stable; an important stabilizing contribution derives from opportunities for the unpaired electron of the radical intermediates to form resonance structures with C=O or C=C bonds. Consequently, allyloxy and 2-formylethyl are less stable than 1-formylethyl

by 132 and 66 kJ mol$^{-1}$, respectively, as sp$^3$-hybridized C1 (for allyloxy) and C2 (for 2-formylethyl) prevents any noticeably resonance stabilization. Of the two possible products of partial hydrogenation of acrolein, propanal is 61 kJ mol$^{-1}$ more stable than

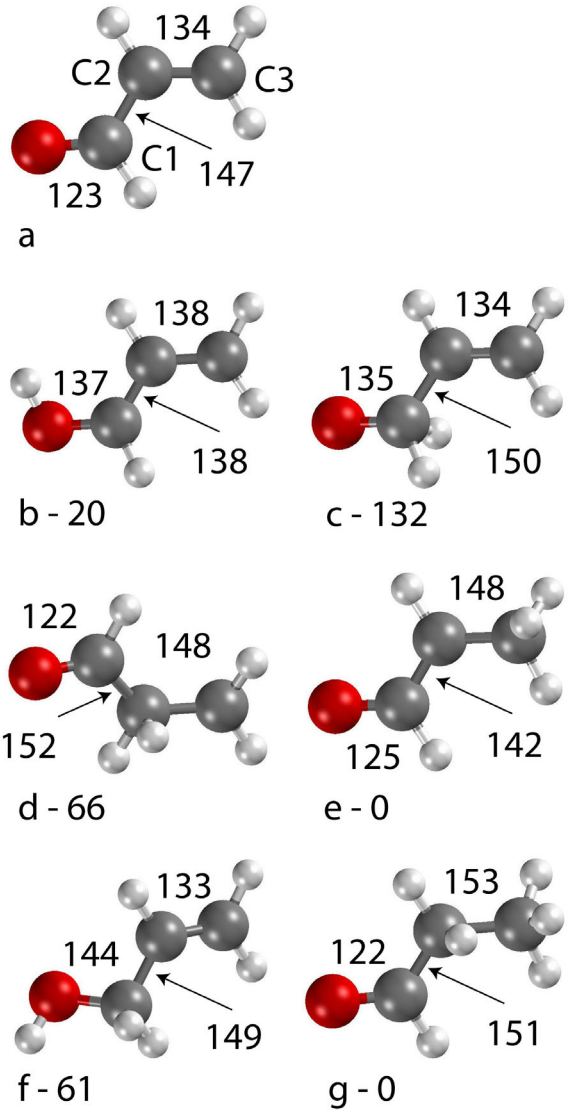


**Figure 6.2:** Sketches of structures, calculated in the gas phase, of various reactants, radical intermediates, and products: a) acrolein b) hydroxyallyl, c) allyloxy, d) 2-formylethyl, e) 1-formylethyl, f) propenol, g) propanal. Dark grey – C atoms, red – O atoms, small light grey – H atoms. Selected interatomic distances (pm) are displayed. Relative total energies (kJ mol$^{-1}$) of the isomers **b-d** with respect to **e** and of **f** vs. **g** are shown next to the labels **a-g**.

propenol, in agreement with experimental observation of gas phase partial hydrogenation of acrolein [13].

Calculated gas-phase thermodynamic characteristics of considered elementary reactions of partial acrolein hydrogenation are summarized in Figure 6.3. All routes of the first hydrogen atom attacking acrolein were calculated endothermic, with energy losses ranging from rather small values accompanying the formation of 1-formethyl and hydroxyallyl to notably endothermic effects of 80 kJ $mol^{-1}$ (2-formethyl) and even ~150 kJ $mol^{-1}$ (allyloxy). Nevertheless, attaching the second H atom to these intermediates is energetically so favourable that the overall energy balance for each of the partial hydrogenation processes becomes definitely positive, with a gain of 80 kJ $mol^{-1}$ when propenol is formed and as much as ~140 kJ $mol^{-1}$ in the case of propanal as product. In the gas phase, the latter reaction route can be classified as thermodynamically notably preferred over the formation of propenol, although this qualification did not carry over to the corresponding activation energies.

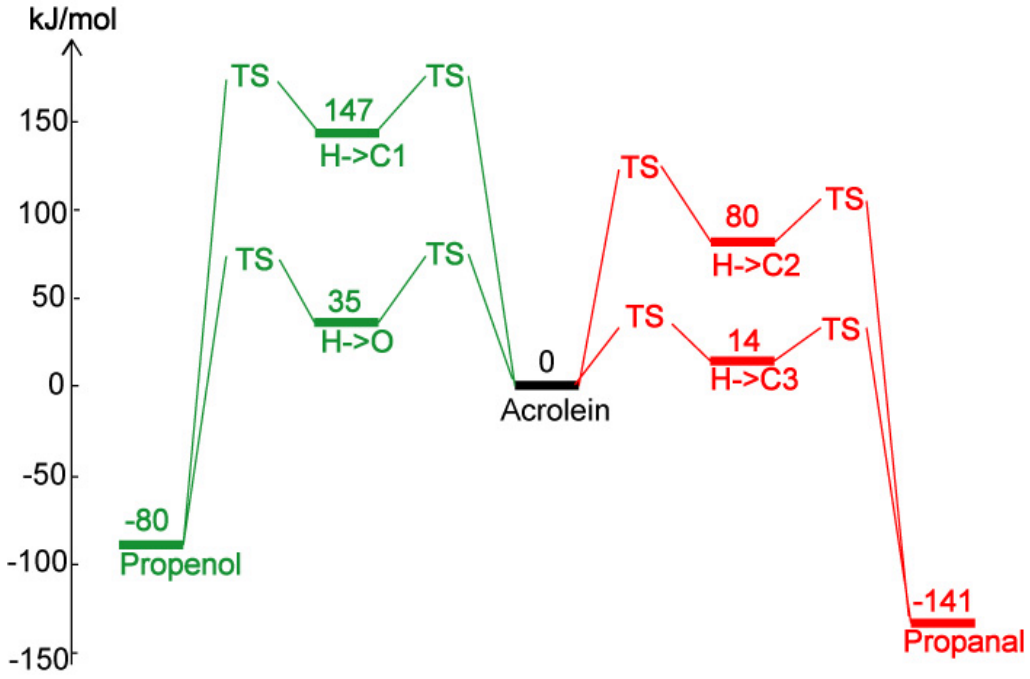


**Figure 6.3:** Reaction energy landscape for acrolein hydrogenation in the gas phase; energies are shown relative to the trans-isomer of acrolein and a $H_2$ molecule.

In the following, the discussion will be focused on the thermodynamics of the two routes of selective hydrogenation of acrolein on Ag surfaces. As has been done up to now, only the products of either C=C or C=O bond hydrogenation will be considered, in line with the fact that no other isomers, such as propen-1-ol, have been detected under experimental conditions. However, before exploring reaction thermodynamics, one needs to address structure and energetic of the various adsorption complexes involved.

## 6.4 Adsorption of reactants, intermediates and products of acrolein hydrogenation

**Acrolein.** Trans-acrolein interacts weakly with the clean Ag(110) surface, according to the calculated adsorption energy of -13 kJ $mol^{-1}$ at a low coverage of 1/6 ML [13]. Essentially the same result, $E_{ad}$ = -16 kJ $mol^{-1}$, was obtained in this study for 1/8 ML coverage. In the low-coverage regime, essentially vanishing adsorption interactions of

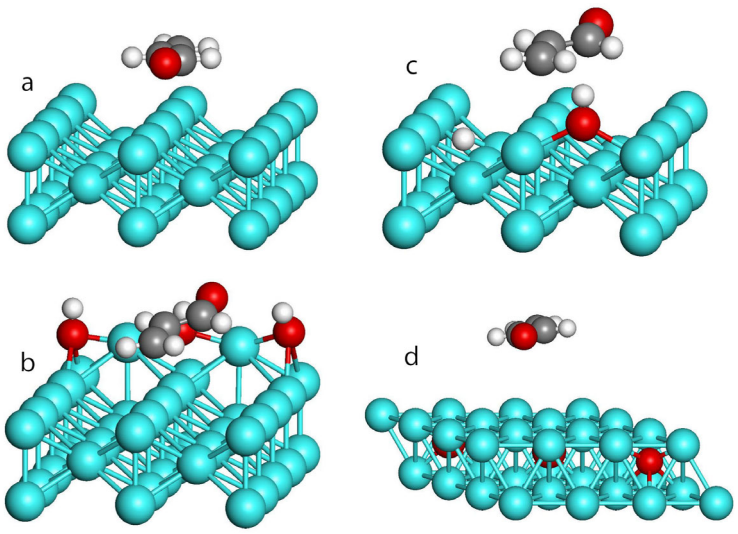


**Figure 6.4:** Sketches of calculated adsorption complexes of acrolein on a) Ag(110), b) *p*(4×1)OH/Ag(110), c) OH/Ag(110) and d) $O_{oss}$/Ag(111). Colour coding of atomic centres as in Figures 6.1 and 6.2.

acrolein molecules were calculated also on the clean surface Ag(111) and even on the stepped surface Ag(221) [13]. Similar to clean Ag, on *p*(4×1)O/Ag(110), O/Ag(110) and $O_{oss}$/Ag(111) surfaces, considered as models for silver modified by oxygen, acrolein was calculated to be very weakly bound, with adsorption energy of only ~ -10 kJ $mol^{-1}$ and adsorbate-substrate distances hardly indicative of noticeable interactions. However, when surface oxygen atoms are transformed into hydroxyl groups, like OH/Ag(110) and *p*(4×1)OH/Ag(110), acrolein binds somewhat stronger: with adsorption energies of ~ -30 kJ $mol^{-1}$ and ~ -60 kJ $mol^{-1}$, respectively.

This strengthening of the adsorption bonding of acrolein should be traced back to the formation of a hydrogen bond (bond length of 200 pm) between the H atom of the hydroxyl group and the oxygen atom of acrolein. But even in the latter most strongly bound adsorption complexes, acrolein is only weakly activated, as measured by the adsorption-induced elongations, 1 pm, of the C=C and C=O bonds. On all model silver substrates under scrutiny, the molecular plane of adsorbed acrolein was found to be oriented almost parallel to the surface planes (see Figure 6.4).

Adsorption complexes of the second reactant – hydrogen atoms – have already been discussed in Chapters 4 and 5, which deals with the activation of molecular hydrogen on silver catalysts. The calculated data on adsorption complexes of various intermediates and two product species of partial hydrogenation of acrolein on all four substrate models are summarized in Table 6.1 and will be outlined in the following.

**Hydroxyallyl.** This is the second most stable intermediate among those under discussion. The stabilization of hydroxyallyl by resonance effects reduces its reactivity and, thus, its ability to adsorb on silver surfaces. On all four substrate models under study this intermediate exhibits the weakest bonding; in all cases, its centre C3 is involved in the adsorbate-substrate interaction. The adsorption complex on Ag(110) is sketched in Figure 6.2. There, the C3-Ag bond length is 228 pm and the binding energy is calculated at -69 kJ $mol^{-1}$ (Table 6.1). Oxygen centres *on the surface* weaken the adsorption interaction, to -59 kJ $mol^{-1}$ on *p*(4×1)O/Ag(110) and -26 kJ $mol^{-1}$ on O/Ag(110), with only slightly elongated C3-Ag distances of 234 and 229 pm, respectively. When oxygen

acts in *subsurface* positions, the adsorption energy, -42 kJ $mol^{-1}$, of hydroxyallyl on $O_{oss}$/Ag(111) falls between of the two values just mentioned. Interestingly, the C3-Ag distance becomes the longest, 241 pm, among the adsorption complexes of hydroxyallyl studied.

**Table 6.1**: Calculated adsorption energies ($E_{ad}$, kJ $mol^{-1}$) and selected interatomic distances adsorbate-substrate (X-Ag, pm)[a] of intermediates and products of partial hydrogenation of acrolein on model surfaces representing silver catalysts.

| Adsorbate | X | Ag(110) | | *p*(4×1)O/Ag(110) | | O/Ag(110) | | $O_{oss}$/Ag(111) | |
|---|---|---|---|---|---|---|---|---|---|
| | | $E_{ad}$ | X-Ag | $E_{ad}$ | X-Ag | $E_{ad}$ | X-Ag | $E_{ad}$ | X-Ag |
| Hydroxyallyl | C3 | -69 | 228 | -59 | 234 | -26 | 229 | -42 | 241 |
| Allyloxy | O | -186 | 235 | -195 | 233 | -189 | 232 | -148 | 238 |
| 2-formylethyl | C3 | -115 | 220 | -112 | 221 | -83 | 222 | -95 | 224 |
| 1-formylethyl | C2 | -122 | 242 | -121 | 237 | -113 | 236 | -68 | 237 |
| Propenol | C3 | -19 | 273 | -37 | 284 | -18 | 272 | -20 | 380 |
| | C2 | | 304 | | 327 | | 315 | | 345 |
| Propanal | O | -20 | 253 | -3 | 393 | -8 | 380 | -13 | 458 |
| | C1 | | 350 | | 353 | | 341 | | 383 |

[a] X is the atomic centre the adsorbate closest to a surface atom Ag.

**Allyloxy.** This is the most strongly bound intermediate on all surfaces considered. As pointed out above, when discussing the stability of intermediates in the gas phase (Sect. 6.3), the unpaired electron on the O centre of an allyloxy radical cannot be noticeably stabilized by delocalization to a conjugated π-system, at variance with 1-formethyl and hydroxyallyl. Hence, the allyloxy radical is most active in interacting with the surface. It binds to the examined silver surfaces via the activated O atom, similar, e.g., to the adsorption complexes of methoxy species on metal surfaces [143,166,167]. On the Ag(110) surface, the binding energy of allyloxy was calculated at -186 kJ $mol^{-1}$ and the

oxygen atom of the adsorbate occupies the long bridge site with an Ag-O bond length of 235 pm (Figure 6.5b). On the *p*(4×1)O/Ag(110) and the O/Ag(110) surfaces, adsorption is slightly stronger, -195 and -189 kJ $mol^{-1}$, respectively, than on the clean Ag(110) surface; the corresponding Ag-O distances hardly change. On the $O_{oss}$/Ag(111) surface, allyloxy was calculated to adsorb notably weaker, with a binding energy of -148 kJ $mol^{-1}$, than on the other three surfaces considered. Here, the O atom of allyloxy occupies a fcc 3-fold hollow site, below which there is no $O_{oss}$ species located. However the surface Ag atoms forming this site are in close contact to with neighbouring $O_{oss}$ impurities and, hence, are partly electron-deficient. Thus, they interact less strongly than Ag atoms on clean metallic surface with the electronegative O atom of allyloxy. This mechanism of reducing the adsorption strength in the presence of an electronegative admixture subsurface of a metal is reminiscent to the effect that subsurface atomic C on Pd(111) has on CO adsorption in nearby positions [115].

**2-Formylethyl.** Similar to the allyloxy radical just discussed, the radical intermediate 2-formylethyl can hardly be stabilized by delocalizing the unpaired electron from the C3 atom. Therefore, this species binds to the surfaces via the C3 centre which features a high spin density in the gas phase; see Figure 6.5c for the adsorption complex on the Ag(110) surface. In line with the reactivity of the radical, 2-formylethyl binds to the surfaces under consideration rather strongly. The calculated adsorption energies are -115, -112, -83 and -95 kJ $mol^{-1}$ on Ag(110), *p*(4×1)O/Ag(110), O/Ag(110) and $O_{oss}$/Ag(111) surfaces, respectively; the Ag-C3 distances in this series vary by 4 pm only. This trend again indicates a slight destabilizing effect of oxygen on the adsorption of the intermediates, which however does not exceed ~30 kJ $mol^{-1}$. The difference between the adsorption energies of allyloxy and 2-formylethyl intermediates is partly due to the different affinities of C and O centres for surface Ag atoms, just like in cases of methyl and methoxy adsorption on the Cu(111) surface [143]. Indeed, according to the calculations, methyl species, $CH_3$, bind to Ag(111) with an energy of 103 kJ $mol^{-1}$; this value is very similar to those discussed above for 2-formylethyl adsorption on various silver substrates.

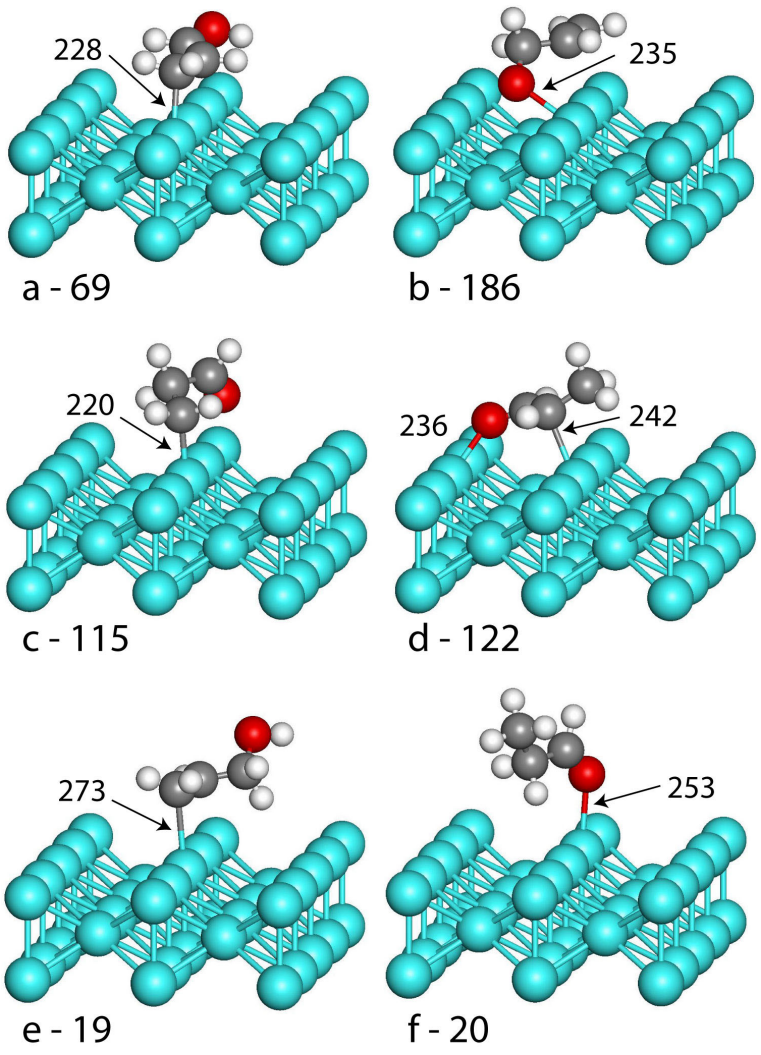


**Figure 6.5:** Sketches of calculated adsorption complexes of intermediates and products of partial hydrogenation of acrolein on the Ag(110) surface: a) hydroxyallyl, b) allyloxy, c) 2-formylethyl, d) 1-formylethyl, e) propenol and f) propanal. Arrows point to the shortest adsorbate-substrate interatomic distances (pm). Adsorption energies (kJ $mol^{-1}$, see Table 6.1) are shown next to the panel labels. Colour coding as in Figures 6.1 and 6.2.

**1-Formylethyl.** This intermediate is most stable in the gas phase (see above), partly due to resonance effects of the unpaired electron on the C2 centre with the nearby C=O double bond. Thus, despite the opportunity to interact with Ag surfaces beyond the C2 atom via its O atom, as exemplified for Ag(110) in Figure 6.5d, the overall adsorption interaction is not particularly strong, -122 to -113 kJ $mol^{-1}$ on clean Ag(110) and substrates with surface O admixtures. On the $O_{oss}$/Ag(111) model the interaction is

further notably weakened, to -68 kJ $mol^{-1}$. On this surface 1-formylethyl forms a C2-Ag bond of 237 pm and an O-Ag bond of 238 pm to Ag centers which belong to cages occupied by different subsurface oxygen centers.

**Propenol and propanal.** Like the reactant acrolein, both products of its partial hydrogenation, propenol and propanal, bind weakly to clean (see Figure 6.5e, 5.5f) and modified Ag surfaces. In all systems studied, the calculated adsorption energies do not exceed -20 kJ $mol^{-1}$ (in absolute values), except for propenol on the added row *p*(4×1)O/Ag(110) surface. Only there, the binding energy reaches the value of -37 kJ $mol^{-1}$ due to the hydrogen bond formed between an atom H attached to the C2 centre of propenol and an oxygen atom of the added row; that bond distance is 249 pm.

In general, these interactions should probably be qualified as physisorption, as indicated also by the nearest adsorbate-surface distances, which are longer (sometimes, significantly) than ~250 pm (see Table 6.1). Also, the adsorption-induced distortion of the two product molecules is very minor. Such weak adsorption of the products of partial hydrogenation of acrolein represents a crucial finding for understanding the selectivity of silver catalysts in this reaction (see below). In contrast, on Pt(111), propenol adsorbs with a binding energy of about -100 kJ $mol^{-1}$, much stronger than the alternative product propanal [168]. This large difference evidently is due to the strong coordination of the C=C π-bond of propenol to the Pt surface, while on Ag the contribution from this channel is very small. For instance, the adsorption energy of ethylene on Ag(111) is calculated to be only 10 kJ $mol^{-1}$.

## 6.5 Reaction energies of acrolein hydrogenation

Scheme 6.1 summarizes possible adsorption or desorption processes as well as surface reactions involved in partial hydrogenation of acrolein; the corresponding calculated reaction energies are presented in Figure 6.6. In the initial state (IS) structures chosen for

attacks of acrolein as reactant by the first hydrogen atom, acrolein is physisorbed on the surface whereas atomic H is considered to be adsorbed at the most stable sites on the surface under discussion: short bridge sites on Ag(110) and hollow sites on the surface model $O_{oss}$/Ag(111).

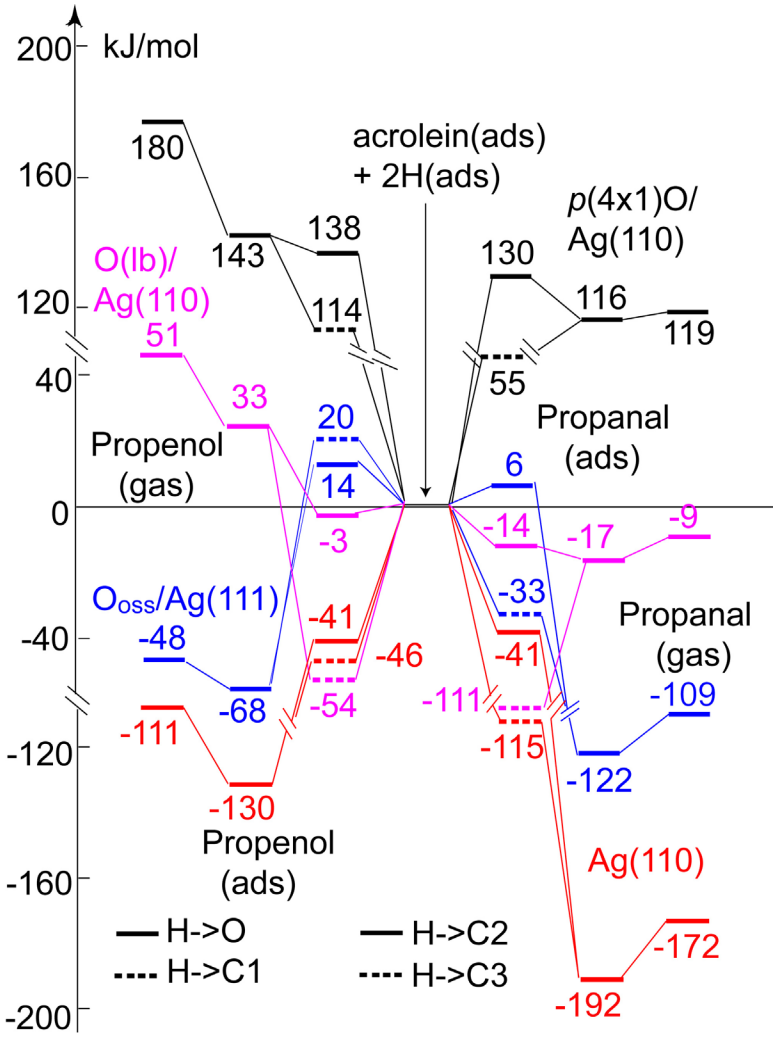


**Figure 6.6:** Reaction energies of partial hydrogenation of acrolein on four model Ag substrates with respect to the total energies of adsorbed acrolein molecule and $H_2$ molecules in the gas phase. On the left-hand side, stepwise interaction of H atoms with atoms O (solid line bars) and C1 (dashed line bars), resulting in the hydrogenation of the C1=O bond. On the right-hand side, stepwise interaction of H atoms with atoms C2 (solid bars) and C3 (dashed bars), resulting in the hydrogenation of the C2=C3 bond.

As discussed in Section 6.4, acrolein binds very weakly both on clean and oxygen-modified silver surfaces. Therefore, the contribution of the adsorption energy of acrolein to the overall energy profile of the hydrogenation processes is minor. Furthermore, it appears to be a sufficiently accurate approximation if one treats acrolein hydrogenation on model silver catalysts as starting with the reactant in the gas phase, in particular when the focus is on comparing competing reaction channels of the reactant acrolein. Hydrogen atoms bind rather strongly to the silver surfaces under consideration; therefore, the energy contribution due to hydrogen adsorption seems very important, if not crucial in some cases, for the overall reaction energetic. Indeed, on the Ag surfaces O/Ag(110) and *p*(4×1)O/Ag(110) with exposed O, the adsorption of atomic H can be as strong as ~ -330 kJ $mol^{-1}$ [165]. Such a strong binding of one reaction partner renders acrolein hydrogenation towards the desired product propenol considerably endothermic, in particular on *p*(4×1)O/Ag(110) (Figure 6.6). This finding prompted us to exclude O/Ag(110) and *p*(4×1)O/Ag(110) as possible models of oxygen-modified Ag catalysts from subsequent studies of activated complexes.

In contrast, on the clean Ag(110) surface, due to the endothermic nature of $H_2$ dissociative adsorption, 33 kJ $mol^{-1}$, all further steps of acrolein hydrogenation are exothermic; see Figure 6.6 and Table 6.2. Action of the $O_{oss}$/Ag(111) surface in the catalytic processes under consideration appears to be somehow intermediate between that of clean Ag(110) surface and two others just discussed ones, directly exposing surface oxygen. On $O_{oss}$/Ag(111), $H_2$ dissociation is slightly thermodynamically favourable, the reaction energy is -22 kJ $mol^{-1}$. As a consequence, the elementary reactions **c1**, **c2** and **c3** on this surface are characterized by a small positive enthalpy change of up to 20 kJ $mol^{-1}$ and the reaction **c4** is exothermic, $E_r$ = -33 kJ $mol^{-1}$ (see Table 6.2 and Figure 6.6). Subsequent hydrogenation steps **f** and **g** of the intermediates on Ag(110) and $O_{oss}$/Ag(111) surfaces are definitely exothermic (Table 6.2, Figure 6.6). To conclude, results of this section demonstrate that the model surfaces Ag(110) and $O_{oss}$/Ag(111) provide thermodynamically feasible conditions for the partial hydrogenation of acrolein molecules by means of adsorbed H atoms. Thus, in these systems, at variance with thermodynamically notably less favourable situations of directly exposed O centres on Ag surfaces, solely kinetic factors will define activity and selectivity of the model

catalysts in the reactions of partial hydrogenation of acrolein. Some of these kinetic aspects will be addressed in the following section.

## 6.6 Transition states and activation energies of acrolein hydrogenation on Ag(110) and $O_{oss}$/Ag(111) surfaces

We start by presenting an analysis of activation energies and transition states (TS) of the partial hydrogenation of acrolein (reaction steps **c1** – **g**, Scheme 6.1, Table 6.2, Figure 6.7) on Ag(110) model, representative for clean defect-free silver surfaces. All activation energies $E_a$ calculated for the hydrogenation steps **c1** – **g** are smaller than 80 kJ $mol^{-1}$, indicating rather rapid transformations. Both routes **c1**→**d** and **c2**→**e** from acrolein to the desired product propenol exhibit notably higher barriers for attaching the first hydrogen atom H1, compared to the second one H2, thus rendering the initial steps

**Scheme 6.1:** Elementary reaction steps of acrolein hydrogenation. A* and * denote adsorbed species A and empty surface site, respectively.

| | | | | |
|---|---|---|---|---|
| **a** | $CH_2CHCHO$ + * | ↔ | $CH_2CHCHO$* | |
| **b** | $H_2$ + 2* | ↔ | 2H* | |
| **c1** | $CH_2CHCHO$* + H* | ↔ | $CH_2CHCHOH$* | + * |
| **c2** | $CH_2CHCHO$* + H* | ↔ | $CH_2CHCH_2O$* | + * |
| **c3** | $CH_2CHCHO$* + H* | ↔ | $CH_2CH_2CHO$* | + * |
| **c4** | $CH_2CHCHO$* + H* | ↔ | $CH_3CHCHOH$* | + * |
| **d** | $CH_2CHCHOH$* + H* | ↔ | $CH_2CHCH_2OH$* | + * |
| **e** | $CH_2CHCH_2O$* + H* | ↔ | $CH_2CHCH_2OH$* | + * |
| **f** | $CH_2CH_2CHO$* + H* | ↔ | $CH_3CH_2CHO$* | + * |
| **g** | $CH_3CHCHO$* + H* | ↔ | $CH_3CH_2CHO$* | + * |
| **h** | $CH_2CHCH_2OH$* | ↔ | $CH_2CHCH_2OH$ | + * |
| **i** | $CH_3CH_2CHO$* | ↔ | $CH_3CH_2CHO$ | + * |

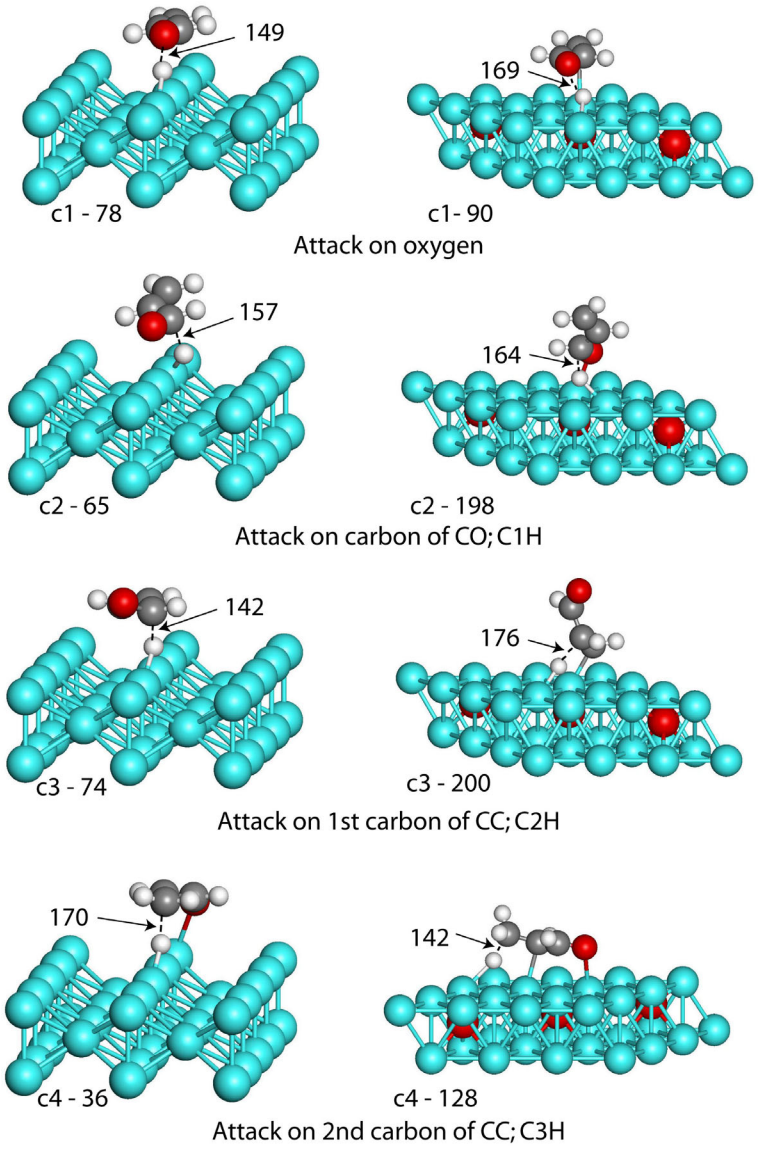


**Figure 6.7:** Transition state (TS) structures for reactions **c1** to **c4** (see Scheme 6.1 and Table 6.2) of partial acrolein hydrogenation on Ag(110): left column - Ag(110) model; right column - $O_{oss}$/Ag(111) model. Arrows point to the forming bonds and indicate the corresponding interatomic distances (pm). Activation energies (kJ $mol^{-1}$, see Table 6.2) are shown next to the reaction labels. Colour coding as in Figures 6.1 and 6.2.

**c1** and **c2** rate-limiting. The barrier $E_a$(**c2**) is 13 kJ $mol^{-1}$ lower than $E_a$(**c1**). Therefore, the kinetics of the acrolein→propenol transformations under study can be roughly approximated by the **c2→e** route alone. At variance with the formation of propenol, the routes **c3→f** and **c4→g**, leading to the undesired product propanal, are characterized by

somewhat higher barriers $E_a$(**f**) = 79 kJ mol$^{-1}$ and $E_a$(**g**) = 57 kJ mol$^{-1}$ of the attachment of the second hydrogen atom H2, compared to the initial processes **c3** (74 kJ mol$^{-1}$) and **c4** (36 kJ mol$^{-1}$) of H1 attachment. Here again the kinetics can be described to first approximation by the more favourable chain **c4**→**g**. The barrier $E_a$(**c2**) = 65 kJ mol$^{-1}$, calculated higher than $E_a$(**g**) = 57 kJ mol$^{-1}$, implies that on the Ag(110) surface the hydrogenation of acrolein (**c4**→**g**) to the undesired product propanal is faster than the competing reaction (**c2**→**e**) to the desired product propenol.

Let us have closer look at geometries of the TSs on the Ag(110) surface just mentioned; their structure is displayed in the left columns of Figures 6.7 and 6.8. During the formation of hydroxyallyl (reaction **c1**), acrolein moves toward adsorbed hydrogen, $H_a$, to reach a distance $H_a$-O of 149 pm in the TS (Figure 6.7c1). With the formation of this O-$H_a$ bond, the C1-O distance is elongated by 6 pm, indicating a weakening of the C=O bond. Concomitantly the centre C3 starts to form a bond with the surface, Ag-C3 = 250 pm, while the C1-C2 distance is shortened by 4 pm, indicative of a bond strengthening due to resonance effects. On the way to the TS for the formation of allyloxy (reaction **c2**), acrolein moves toward $H_a$ and the C1-$H_a$ contact shortens to 157 pm in the TS (Figure 6.7c2). With the formation of the C1-$H_a$ bond, the C1-O bond is weakened, as indicated by its elongation by ~5 pm, and the O atom becomes available for stronger interaction with the Ag surface. The formation of 2-formylethyl (reaction **c3**), occurs in a similar way: acrolein moves toward the adsorbed $H_a$ with the C2-$H_a$ distance shortened to 142 pm in the TS (Figure 6.7c3). Likewise, during the formation of 1-formylethyl (reaction **c4**), the C3-$H_a$ contact is shortened to 170 pm (Figure 6.7c4) and the distance C2-C3 one is elongated to 140 pm. On the way to in the hydrogenation TS of hydroxyallyl (reaction **d**), $H_a$ moves toward the hydroxyallyl species (Figure 6.8d), the C1-$H_a$ contact reaches 189 pm and C3-Ag = 234 pm. Similarly, in the hydrogenation of allyloxy (reaction **e**), $H_a$ moves towards allyloxy; in the TS (Figure 6.8e) O-$H_a$ = 182 pm. During hydrogenation of 2-formylethyl (reaction **f**), $H_a$ moves towards C3, resulting in a TS with C3-$H_a$ = 193 pm (Figure 6.8f). Finally, hydrogenation of 1-formylethyl (reaction **g**) takes place by moving $H_a$ towards C2, so that in the TS C2-$H_a$ = 201 pm (Figure 6.8g).

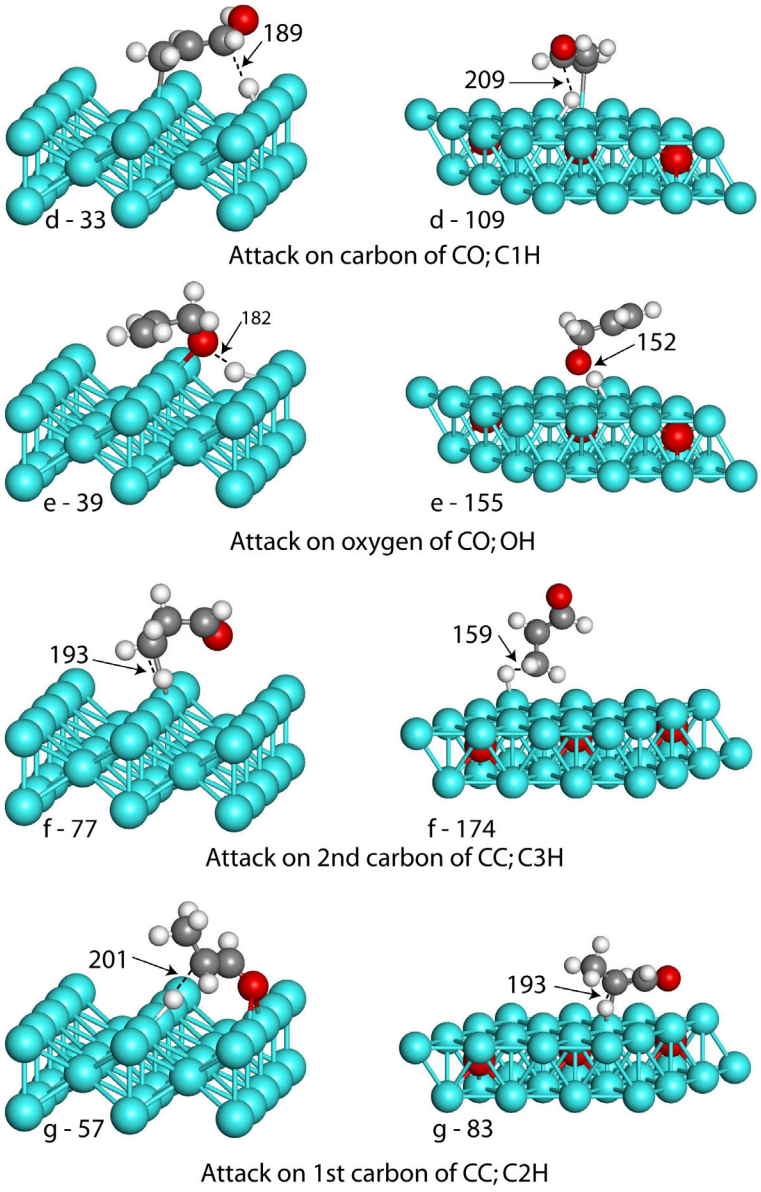


**Figure 6.8:** The same as in Figure 6.7, but for reactions **d** – **g** (see Scheme 6.1 and Table 6.2).

The presence of oxygen in silver catalysts, either due to a special pre-treatment or generated in during the course of the reaction, was recently found to notably increase both activity and selectivity of acrolein hydrogenation: on supported Ag catalysts the selectivity to propenol reached ~50% [58]. The observed two- to three-fold increase of the activity was mainly assigned to a noticeably enhanced dissociation rates of $H_2$ to produce adsorbed atomic H, the likely hydrogenation reactant of acrolein. Recall, that $H_2$

**Table 6.2:** Activation ($E_a$) and reaction ($E_r$) energies (kJ mol$^{-1}$) calculated for elementary reactions taking place during partial hydrogenation of acrolein (see Scheme 6.1) on Ag(110) and $O_{oss}$/Ag(111) surfaces.

| Reaction | Ag(110) | | $O_{oss}$/Ag(111) | |
|---|---|---|---|---|
| | $E_a$ | $E_r$ | $E_a$ | $E_r$ |
| **c1** | 78 | -41 | 90 | 14 |
| **c2** | 65 | -46 | 198 | 20 |
| **c3** | 74 | -41 | 200 | 6 |
| **c4** | 36 | -115 | 128 | -33 |
| **d** | 33 | -89 | 101 | -82 |
| **e** | 39 | -84 | 147 | -88 |
| **f** | 79 | -151 | 180 | -128 |
| **g** | 57 | -77 | 89 | -89 |

dissociation on clean silver surfaces under common experimental conditions requires to overcome prohibitively high activation barriers [165]. These barriers, however, can be notably reduced in the presence of oxygen, which thus enables the dissociation of hydrogen. According to the DF calculations (see Chap. 5), this effect should be similar for atomic oxygen species adsorbed on the silver surface [165] and those located subsurface, at interstitial positions between the first and the second layers of Ag atoms [147]. Here, effects of oxygen in silver catalysts as exemplified by subsurface atomic species $O_{oss}$ on Ag(111) on the activity and the selectivity of acrolein hydrogenation have been addressed, assuming that sufficient atomic H is available on the surface. For instance, these two scenarios are compatible if patches free of oxygen on the Ag surface co-exist with nearby oxygen-modified patches.

The calculated reaction and activation energies of the elementary steps of acrolein hydrogenation on the model $O_{oss}$/Ag(111) are given in Table 6.2 (see Figures 6.7 and 6.8, right columns). As already mentioned, the processes are overall favourable thermodynamically: only the individual reactions **c1**, **c2** and **c3** are slightly endothermic.

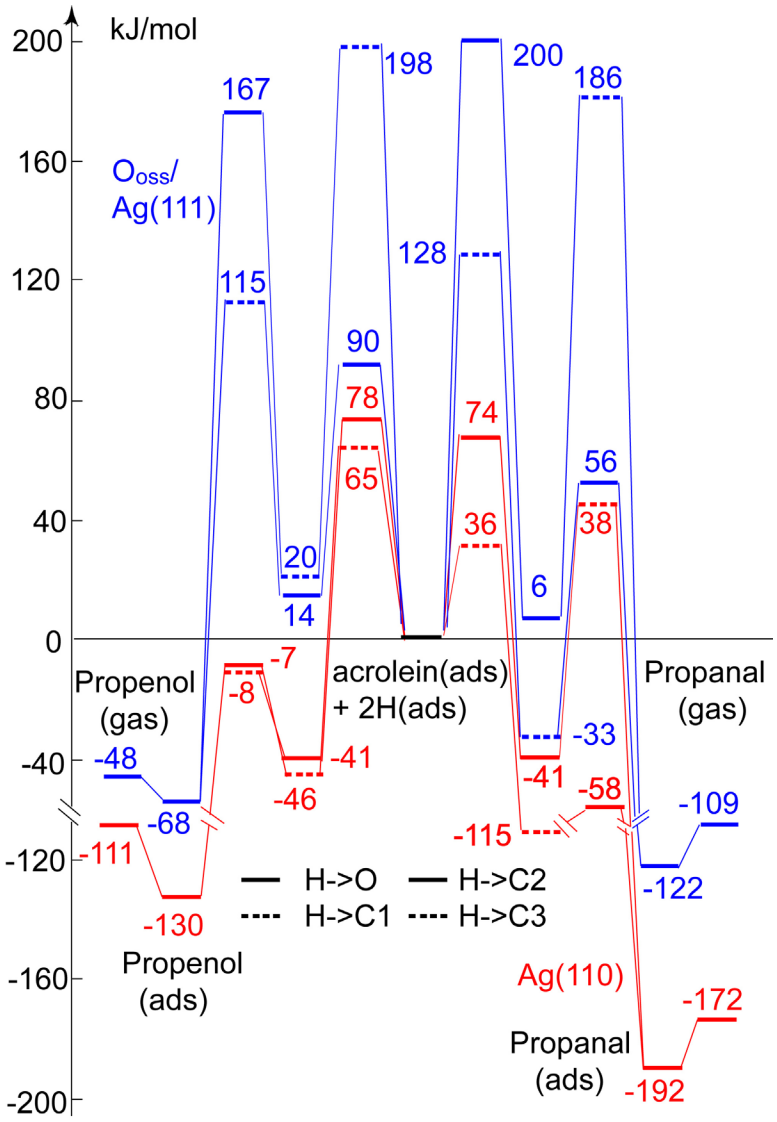


**Figure 6.9:** Reaction and activation energies (kJ $mol^{-1}$) of partial hydrogenation of acrolein on model Ag substrates Ag(110) and $O_{oss}$/Ag(111) with respect to the system of adsorbed acrolein molecule and two single hydrogen atoms.

One notices that on $O_{oss}$/Ag(111) the activation barriers for both processes, acrolein → propenol and acrolein → propanal, are considerably increased compared to clean Ag(110) (Table 6.2). Correspondingly, one expects the overall activity to be substantially lower.

The lowest barriers, that determine the selectivity acrolein → propenol on $O_{oss}$/Ag(111), are those of the channel **c1→d**, 90 and 101 kJ $mol^{-1}$, respectively; for the route acrolein → propanal, it is the channel **c4→g**, with barriers of 128 and 89 kJ $mol^{-1}$. From the values of the activation barriers **d** and **c4**, which differ by ~20 kJ $mol^{-1}$, the route acrolein → propenol can be classified as kinetically dominant over the route acrolein → propanal, with the concomitant selectivity to propenol close to 100%. As on Ag(110), the desorption of the products propenol and propanal from $O_{oss}$/Ag(111) is very slightly activated, by 18 and 8 kJ $mol^{-1}$, respectively (Table 6.1). This implies similar relative concentrations of the products under typical conditions on the surface and in the gas phase, namely ~100% of propenol. Figure 6.9 summarizes the reaction and activation energies of all calculated elementary steps of acrolein hydrogenation on the two models Ag(110) and $O_{oss}$/Ag(111).

Finally, a few words about the structures of the TSs involved in the model $O_{oss}$/Ag(111) (Figures 6.7 and 6.8, right-hand columns). The formation of hydroxyallyl (reaction **c1**) is accompanied by a displacement of acrolein towards adsorbed hydrogen, $H_a$, until the distance $H_a$-O becomes 169 pm in the TS (Figure 6.7c1); concomitantly, the adsorption interaction via the atom C3 strengthens, Ag-C3 = 284 pm. To form allyloxy (reaction **c2**), acrolein moves in the TS toward $H_a$ and the C1-$H_a$ contact decreases to 164 pm (Figure 6.7c2). The formation of the C1-$H_a$ bond weakens the C1-O bond, which is elongated by 4 pm, thus enabling a stronger interaction of the O atom with the surface. The reaction **c3** occurs in a similar way: acrolein moves toward the adsorbed $H_a$ with a concomitant shortening of the C2-$H_a$ distance to 176 pm in the TS (Figure 6.7c3). Likewise, during reaction **c4** (formation of 1-formylethyl), the C3-$H_a$ contact shortens to 142 pm (Figure 6.7c4) and the distance C2-C3 elongates to 150 pm.

In reaction **d**, $H_a$ moves toward hydroxyallyl until it reaches the TS (Figure 6.8d) with a C1-$H_a$ contact of 209 pm and a C3-Ag distance of 293 pm. In the hydrogenation of allyloxy (reaction **e**) $H_a$ moves towards allyloxy; in the TS, O-$H_a$ = 152 pm (Figure 6.8e). During the of hydrogenation of 2-formylethyl (reaction **f**), $H_a$ approaches centre C3, resulting in a TS with C3-$H_a$ = 159 pm (Figure 6.8f). The formation of propanal from 1-

formylethyl (reaction **g**) involves a displacement of $H_a$ towards C2, resulting in a TS structure with C2-$H_a$ = 193 pm (Figure 6.8g).

The present calculated results for $O_{oss}$/Ag(111) may explain the observed selectivity enhancement of acrolein hydrogenation to propenol on silver catalysts in the presence of oxygen [58], provided that seemingly *more active parts of silver catalysts, free of oxygen* [see the data for Ag(110)] in effect do not mediate the hydrogenation, e.g., due to insufficient supply of atomic hydrogen. This assumption is in line with the above-mentioned DF results that the unfavourable $H_2$ dissociation on silver can be strongly facilitated by oxygen [165,147].

## 6.7 Summary and conclusions

The intriguing problem of rationalizing the selectivity of silver catalysts in the hydrogenation of α,β-unsaturated aldehydes to unsaturated alcohols has been addressed. For this purpose, DF calculations of acrolein hydrogenation by adsorbed atoms H were carried out: structure and energies of essential intermediates and transition states on model silver surfaces were determined. The experimentally explored hydrogenation catalysts based on supported Ag particles are quite complex [11,20,58,164]. Their properties are noticeably altered under reaction conditions and reliable experimental information on active sites is still lacking [58]. Therefore, to deepen the understanding of the catalytic action of the silver component, the present work focused on two limiting situations of extended clean and oxygen-modified silver surfaces, represented by Ag(110) and $O_{oss}$/Ag(111) models.

On Ag(110), the computational results reveal a small selectivity of acrolein hydrogenation, in line with observed data for bulky silver catalysts [58]. The $O_{oss}$/Ag(111) system is shown to be less active with respect to hydrogenation of acrolein by adsorbed H atoms than clean Ag surface. However, the selectivity of $O_{oss}$/Ag(111) to

propenol becomes very high. At variance with the model catalyst surface Pt(111) [168], where the selectivity to propenol is strongly reduced by hindered desorption of the latter, at common reaction temperatures both products, propanal and propenol, are predicted to be easily desorbed from both Ag(110) and $O_{oss}$/Ag(111) surfaces.

These conclusions are conceptually important to design more efficient catalysts for selective partial hydrogenation of unsaturated aldehydes of the industrial demand. Nevertheless, more work is required to build a sufficiently complete microscopic picture of the hydrogenation action of silver catalysts. To this end, it is necessary to detect and characterize sites that are responsible for the formation of atomic hydrogen as a reactant and to determine the reactivity of various defects on the catalysts.

# Chapter 7
# Summary

Selective hydrogenation of unsaturated aldehydes with conjugated double bonds is an important route to unsaturated alcohols. However, on conventional catalysts of group VIII metals, α,β-unsaturated aldehydes preferentially undergo hydrogenation of the C=C bond to yield saturated aldehydes while the selectivity to allylic alcohols is very low. In the gas phase, hydrogenation of the C=O bond is disfavoured with respect to hydrogenation of the adjacent C=C bond, both thermodynamically and kinetically. Thus, the selective hydrogenation of the C=O bond represents a challenge which is somewhat facilitated for higher aldehydes $R_1R_2C$=CH-CH=O, where bulky substituents $R_i$, interacting with the catalyst, may sterically hinder the activation of the C=C bond. The lowest α,β-unsaturated aldehyde, acrolein, does not exhibit such steric hindrance and the transformation to unsaturated alcohols is even more difficult.

Quite unexpectedly, silver being a widely used oxidation catalyst, when supported on silica, $Ag/SiO_2$, exhibits a rather high selectivity (~40 %) for allylic alcohol during acrolein hydrogenation, in comparison to group VIII metals such as Pt. Recent experimental studies substantiated the crucial role of Ag as an active component in the selective hydrogenation. However, the detailed catalytic mechanism at the molecular level was unclear. The whole chain of transformations on a clean silver surface appears to be surprising in the light of the weak adsorption of acrolein, coupled with a low probability of $H_2$ activation on silver surfaces.

Molecular hydrogen binds to silver surfaces very weakly, with a binding energy of about 10 kJ $mol^{-1}$. On platinum surfaces hydrogen is readily available. Moreover silver is known to be an oxidizing agent. Beneficial effects of oxygen pretreatment of $Ag/SiO_2$ catalysts with respect to acrolein hydrogenation have been recently demonstrated by Claus et al. [60]. The overall hydrogenation activity increased two- to three-fold after oxidative pretreatment of the catalyst. Oxygen pretreatment also increased the selectivity towards the desired product allyl alcohol, to more than 50%. Regenerative oxygen pretreatment of a deactivated $Ag/SiO_2$ catalysts not only restored the initial conversion level, but significantly increased the hydrogenation activity and improved the selectivity.

To address the mechanism of acrolein hydrogenation at a silver catalyst and especially the origin of atomically adsorbed hydrogen as a prerequisite of this reaction, accurate density functional calculations using the plane-wave program VASP (Vienna ab initio simulation) with the GGA exchange-correlation functional PW91 were performed. The interaction between atomic cores and electrons was described by the projector augmented wave (PAW) method. For adsorption and reaction studies, the silver substrates were represented by five-layer slabs with unit cells containing four to nine atoms per layer for the (111) and (110) Ag surfaces and eight to twelve atoms per layer for the (221) surface; these models enable one to consider surface coverages as low as ¼ for the (111) and (110) surfaces and 1/8 for the (221) surface.

For acrolein hydrogenation, hydrogen has to be available on the surface of the catalyst. From the experimental work of Claus et al. it is clear that silver as a catalyst plays a crucial role to achieve a selectivity of ~ 40% to alcohol. Thus, as a first step dissociative adsorption of hydrogen on silver surfaces was examined. It is well known that stepped surfaces may facilitate the activation of adsorbed species. Thus, (110) and (221) surfaces have been considered. The planar surface (111) surface was investigated for comparison. Before studying hydrogen activation, hydrogen adsorption was examined on these surfaces and it is found that all these surfaces have similar binding energies of ~ 200 kJ $mol^{-1}$ for atomic hydrogen. Hydrogen diffusion happens easily on silver surfaces with a diffusion barrier of ~ 10 kJ $mol^{-1}$. Hydrogen activation on Ag(110) surface has been studied extensively, considering different combinations of possible final states. Out

of all the activation barriers calculated, the lowest one of 122 kJ $mol^{-1}$ corresponds to a final state where one hydrogen atom sits at a long bridge and the other occupies a short bridge site.

Inspired by the studies of this thesis, Claus et al. showed that oxygen pretreatment of $Ag/SiO_2$ catalysts increases the selectivity to allyl alcohol. Thus oxygen impurities may be decisive in hydrogen activation. To inspect possible species, oxygen adsorption on the (111), (110) and (221) silver surfaces was considered. Oxygen binds very strongly on the Ag(110) surface with ~ 350 kJ $mol^{-1}$ at long bridge sites. At 3-fold and 4-fold hollow sites it has a similar binding energy. The diffusion barrier between these sites is very low, about 5 kJ $mol^{-1}$. Experimentally and theoretically, the added row *p*(nx1)O/Ag(110) surface is a well studied structure of adsorbed oxygen, hence the possibility of hydrogen dissociative adsorption on this surface was inspected. It was found that when the molecular axis of $H_2$ is kept in parallel to the added O-Ag row a transition state exists above an O-Ag pair. The barrier for this activation of hydrogen is 71 kJ $mol^{-1}$. As a final state one hydrogen atom adsorbs on oxygen and the other on the neighbouring silver atom. As the adsorption energy for both the hydrogen atoms attached to oxygen atoms of the added row is highly exothermic, the hydrogen atom moves from silver to the neighbouring free oxygen with a barrier of 12 kJ $mol^{-1}$. Hydrogen preferentially diffuses to the free oxygen centres of the added row as the binding to Ag terrace sites is less exothermic. When the molecular axis of hydrogen is perpendicular to the added row direction, activation of the $H_2$ bond leads to adsorbed water; removal of water is quiet facile as it binds to the surface with energy of ~ 20 kJ $mol^{-1}$. Since all of the oxygen atoms of the added row surface phase may be covered by hydrogen atoms forming hydroxyl, in the course of hydrogen activation also hydrogen activation on hydroxyl groups has been taken into account. Here the lowest barrier was calculated at 22 kJ $mol^{-1}$. The result of this reaction is the formation of one water molecule and a free hydrogen atom on a silver terrace. Thus, on the oxygen covered Ag(110) surface hydrogen activation is considerably facilitated, fulfilling a prerequisite of acrolein hydrogenation.

In addition hydrogen activation on isolated oxygen atoms adsorbed on Ag(110) surface was studied in detail. For hydrogen activation on oxygen adsorbed at a long bridge site of the Ag(110) surface, a barrier of 47 kJ $mol^{-1}$ was calculated which is about 30% lower than on the added row surface. The adsorption reaction of $H_2$ is exothermic and resulted in the formation of a hydroxyl group and a hydrogen atom bound to Ag. Similar to the process considered for the hydrogen activation on surface hydroxyl groups of the added row, hydrogen activation via hydroxyl adsorbed on the clean Ag(110) surface was examined. The corresponding barrier of hydrogen activation, calculated at 10 kJ $mol^{-1}$, is much lower than on all other oxygen species considered. In summary the most efficient mechanism for hydrogen activation found is dissociative adsorption near an isolated O atom at the Ag(110) surface where each oxygen produces two adsorbed hydrogen atoms and the oxygen is removed in the form of water, which is easily desorbs from the surface.

It is well known that oxygen adsorption leads to a reconstruction of silver surfaces. For the Ag(111) surface experimentalists have observed the formation of a silver oxide over-layer, but the structure of this phase remains unclear till today. Different subsurface oxygen species were suggested. On Ag(111), formation of sub-surface oxygen centers is endothermic compared to adsorption on the surface. Oxygen penetrating from a 3-fold fcc hollow sites on the surface to a sub-surface octahedral site experiences a barrier calculated at ~ 80 kJ $mol^{-1}$. The barrier for hydrogen activation above oxygen adsorbed at octahedral sub-surface sites of Ag(111) surface, $O_{oss}$/Ag(111) is 98 kJ $mol^{-1}$, which is less than the barrier of 122 kJ $mol^{-1}$ on clean Ag(110) surface. On the Ag(221) surface, the effect of oxygen centres is similar to that on the Ag(111) surface.

To investigate the mechanism of acrolein hydrogenation to propenol or propanal on Ag surfaces a thermodynamic study on acrolein adsorption, intermediates and final states was undertaken. Connecting to the studies on hydrogen activation, Ag(110), O/Ag(110), *p*(4x1)O/Ag(110) and $O_{oss}$/Ag(111) surfaces as substrates were examined. As a primary step, relative energies of the four possible intermediates – hydroxyallyl, allyloxy, 1-formylethyl and 2-formylethyl – were determined in the gas phase. It was found that hydroxyallyl formed by hydrogen attack on oxygen of acrolein and 1-

formylethyl formed by hydrogen attack on the last carbon of acrolein, are most stable. The binding energy of acrolein on a clean Ag(110) surface is 20 kJ $mol^{-1}$, but on oxygen-modified surfaces like O/Ag(110) and *p*(4x1)O/Ag(110) acrolein binds notably stronger due to a hydrogen bond between its carbonyl group and a hydroxyl group on the surface, formed during the dissociative adsorption of hydrogen. Both products of hydrogenation, propenol and propanal, are weakly adsorbed with ~ 20 kJ $mol^{-1}$, allowing easy desorption as a final step. Out of the four intermediates allyloxy shows the strongest binding energy and hydroxyallyl the weakest. The reaction energies for acrolein hydrogenation to propenol and propanal on all substrates are endothermic with the exception of the Ag(110) surface where all reactions are exothermic. On $O_{oss}$/Ag(110) surface some reactions are exothermic.

For more detailed studies including kinetic aspects, the Ag(110) and $O_{oss}$/Ag(110) surfaces were selected because the reaction energies on the latter ones are less endothermic compared to the other two surfaces, O/Ag(110) and *p*(4x1)O/Ag(110). The barriers for the formation of all the four intermediates during hydrogen attack on acrolein, hydroxyallyl, allyloxy, 1-formyethyl and 2-formylethyl, were calculated on both these substrates. Barriers on clean Ag(110) are smaller compared to the barriers on the $O_{oss}$/Ag(111) surface. A small barrier of about 36 kJ $mol^{-1}$ was calculated for the formation of the intermediate 1- formylethyl on Ag(110) surface, which is formed by hydrogen attack on the last carbon of the C=C bond of acrolein. A higher barriers of 57 kJ $mol^{-1}$ were obtained for the second hydrogen attack on the C=C bond. For the alternative hydrogen attack on the C=O bond, a barrier of about 65 kJ $mol^{-1}$ was determined when hydrogen attacks a carbon centre. The second hydrogen attack on either centre of the carbonyl group has a small barrier (39 or 33 kJ $mol^{-1}$, respectively) which leads to the desired product propenol. The rate determining step for hydrogenation of C=C is the formation of 2-formyethyl and the rate determining step for the hydrogenation of C=O is the attack of the first hydrogen. On the Ag(110) surface, as the activation barrier for the first hydrogen attack on C=C is low; the computational results seem to indicate a relatively high preference for propanal, at variance with experiment. Investigations of further models seem advisable; also, this result may indicate a limit of the accuracy of the computational approach employed.

On $O_{oss}$/Ag(111) surface sites the barriers are high and the reaction prefers to go in the direction of hydrogenation of C=O resulting in propenol as the product. The lowest barrier among the first hydrogen attacks on either of the groups is 90 kJ $mol^{-1}$. As the barriers are high the overall reaction is slow. However it shows a higher selectivity to propenol, in agreement with experiment. Therefore, based on these calculations, one can conclude that oxygen species like $O_{oss}$/Ag(111) represent the active sites responsible for higher selectivity to allyl alcohols.

In comparison to a computational study of Sautet et al. for the Pt(111) surface [168], where hydrogen is readily available for the hydrogenation of acrolein, the selectivity to allyl alcohol seems to be much higher on the $O_{oss}$/Ag(111) surface. On Pt(111) propenol binds very strongly with almost 200 kJ $mol^{-1}$, while on $O_{oss}$/Ag(111), propenol has only a binding energy of 20 kJ $mol^{-1}$. Because of the strong binding of propenol on Pt(111) the selectivity is only 1%.

In conclusion, in this thesis the following main results were obtained. Various paths to hydrogen dissociative adsorption on silver surfaces mediated by oxygen species were suggested which reduce the barrier of hydrogen activation. Acrolein hydrogenation on the surface Ag(110) and the oxygen reconstructed silver surface was successfully characterized computationally. The calculated barriers suggest that the $O_{oss}$/Ag(111) surface yields a high selectivity to allyl alcohol even though the reaction may be slow due to high hydrogenation barriers of acrolein and the intermediates.

This thesis has answered a series of pertinent questions. However, open problems remain because acrolein hydrogenation is a complex process. The most interesting ones for further studies are (i) the identification of other oxygen species promoting hydrogen activation as an exothermic reaction together with a high selectivity to allyl alcohol, (ii) examination of a concerted attack of two hydrogen atoms on acrolein as an alternative hydrogenation path, (iii) the modelling of the side reactions of propanal and propenol to propanol as second hydrogenation step, and (iv) establishing a comprehensive kinetic model that is compatible with all known experimental and computational results..

## References:


[1] R. A. van Santen, M. Neurock. Molecular heterogeneous catalysis. Wiley-VCH, Weinheim, 2006.

[2] G. A. Somorjai. Introduction to surface chemistry and catalysis. Wiley, New York, 1994.

[3] P. Hohenberg, W. Kohn. Phys. Rev. B 136 (1964) 864.

[4] W. Kohn, L. J. Sham. Phys. Rev. A 140 (1965) 1133.

[5] J. Grolig, in: Ullmann's encyclopedia of industrial chemistry, 7th ed., Wiley-VCH, Weinheim, Electronic Release 2003.

[6] T. Eiichiro, S. Toshiaki, H.Toshiaki. Curable resinous composition comprising combination of polymerizable cycloacetal compound with unsaturated polyester. United States Patent 3978155.

[7] T. V. Andrushkevich, G. Ya Popova. Russian Chem. Rev. 60 (1991) 1023.

[8] W. Masaru, I. Toru, A. Yuichi, A. Taku, I. Hiroshi. Bioresource technology 98 (2007) 1285

[9] Emergency and continuous exposure limits for selected airborne contaminants. Volume 1. Prepared by the committee on toxicology, Board on toxicology and environmental health hazards, Commission on life sciences national research council national academy press Washington, D.C. April 1984

[10] U.S. Department of health and human services. Hazardous substances data bank National toxicology information program, National library of medicine, Bethesda, MD, 1993, http://www.cdc.gov/niosh/.

[11] P. Claus. Topics Catal. 5 (1998) 51.

[12] C. Mohr, H. Hofmeister, M. Lucas, P. Claus. Chem. Eng. Technol. 23 (2000) 324.

[13] T. B. L. W. Marinelli, S. Nabuurs, V. Ponec. J. Catal. 151 (1995) 431.

[14] V. Ponec. Appl. Catal. A 149 (1997) 27.

[15] P. Gallezot, D. Richard. Catal. Rev. Sci. Eng. 40 (1998) 81.

[16] T. Birchem, C. M. Pradier, Y. Berthier, G. Cordier. J. Catal. 146 (1994) 503.

[17] T. B. L. W. Marinelli, V. Ponec. J. Catal. 156 (1995) 51.

[18] R. B. Grant, R. M. Lambert. J. Catal. 92 (1985) 364.

[19] R. M. Lambert, F. J. Williams, R. L. Cropley, A. Palermo. J. Mol. Catal. A: Chemical 228 (2005) 27.

[20] M. Bron, D. Teschner, A. Knop-Gericke, B. Steinhauer, A. Scheybal, M. Hävecker, D. Wang, R. Födisch, D. Hönicke, A. Wootsch, R. Schlögl, P. Claus. J. Catal. 234 (2005) 37.

[21] M. Bron, E. Kondratenko, A. Trunschke, P. Claus. Z. Phys. Chem. 218 (2004) 1.

[22] M. Bron, D. Teschner, A. Knop-Gericke, A. Scheybal, B. Steinhauer, M. Hävecker, R. Födisch, D. Hönicke, R. Schlögl, P. Claus. Catal. Commun. 6 (2005) 371.

[23] D. Loffreda, F. Delbecq, F. Vigne, P. Sautet. Angew. Chem. Int. Ed. 44 (2005) 5279.

[24] P. Claus. in: Catalysis of organic reactions (Ed. R. E. Malz, Jr.), Chemical industries series, Vol. 68, Marcel Dekker, New York, 1996, p. 419.

[25] R. N. Cartner, A. B. Anton, G. Apai. Surf. Sci. 290 (1993) 319.

[26] M. Lucas, P. Claus. Chem. Eng. Technol. 28 (2005) 867.

[27] M. Lucas, P. Claus. Chem.-Ing.-Techn. 67 (1995) 773.

[28] C. J. Brinker, G. W. Scherer. Sol-Gel science: The physics and chemistry of sol-gel processing. Elsevier science, USA. 1989; J. D. Wright, N.A.J.M. Sommerdijk. Sol-Gel Materials: Chemistry and applications. Taylor & Francis books ltd., 11 New fetter lane, London. 2001; M. A. Aegerter, M. Mennig. Sol-Gel technologies for glass producers and users. Kluwer academic publishers, 101 Philip drive, Massachusetts 02061 USA. 2004.

[29] L. Chunqing, K. Santi, W. Stephen. High flux mixed matrix membranes for separations. United States patent 20070209505.

[30] T. Maschmeyer, F. Rey, G. Sankar, J. M. Thomas. Nature 378 (1995) 159.

[31] P. Claus, P. A. Crozier, P. Druska, Fresenius. J. Anal. Chem. 361 (1998) 677.

[32] W. Grunert, A. Bruckner, H. Hofmeister, P. Claus. J. Phys. Chem. B. 108 (2004) 5709.

[33] P. Claus, H. Hofmeister. J. Phys. Chem. B 103 (1999) 2766.

[34] W. Grunert, A. Bruckner, H. Hofmeister, P. Claus. J. Phys. Chem. B. 108 (2004) 5709.

[35] L. Schlapbach, A. Züttel. Nature. 414 (2001) 353.

[36] Ph. Avouris, D. Schmeisser, J. E. Demuth. Phys. Rev. Lett. 48 (1982) 199.

[37] P. T. Sprunger, E. W. Plummer. Phys. Rev. B. 48 (1993) 14436.

[38] K. Christmann. Surf. Sci. Rep. 9 (1988) 1.

[39] X. Zhou, J. M. White, B. E. Koel. Surf. Sci. 218 (1989) 201.

[40] G. Lee, E. W. Plummer. Phys. Rev. B. 51 (1995) 7250.

[41] C. Mijoule, V. Russier, Surf. Sci. 254 (1991) 329.

[42] A. Eichler, G. Kresse, J. Hafner. Surf. Sci. 397 (1998) 116.

[43] J. Greeley, M. Mavrikakis. J. Phys. Chem. B. 109 (2005) 3460.

[44] R. A. Van Santen, H. P. C. E. Kuipers. Adv. Catal. 35 (1987) 265.

[45] M. Bron, P. Claus. Personal communication to K.M. Neyman.

[46] P. Claus. Appl. Catal. A. 291 (2005) 222.

[47] V. Zhukov, K. D. Rendulic, A. Winkler. Vacuum 47 (1996) 5.

[48] L. Stobinski, R. Dus. Appl. Surf. Sci. 62 (1992) 77.

[49] S. Giorgio, C. R. Henry, B. Pauwels, G. van Tendeloo. Mater. Sci. Eng. A 297 (2001) 107,

[50] A. C. Gluhoi, H. S. Vreeburg, J. W. Bakker, B. E. Nieuwenhuys. App. Cat. A: General 291 (2005) 145

[51] R. J. Mikovksy, M. Boudart, H. S. Taylor. J. Am. Chem. Soc. 76 (1954) 3814.

[52] M. A. Vennice, B. Sen. J. Catal. 115 (1989) 65.

[53] J. E. Bailie, C. H. Rochester, G. J. Hutchings. J. Chem. Soc. Faraday Trans. 93 (1997) 4389.

[54] S. Fuji, N. Osaka, M. Akita, K. Itoh. J. Phys. Chem. 99 (1995) 6994.

[55] J. L. Solomon, R. J. Madix, J. Stohr. J. Chem. Phys. 89 (1988) 5316.

[56] J. L. Solomon, R. J. Madix. J. Phys. Chem. 91 (1987) 6241.

[57] J. C. de Jesús, F. Zaera. Surf. Sci. 430 (1999) 99.

[58] M. Bron, D. Teschner, A. Knop-Gericke, F. C. Jentoft, J. Kröhnert, J. Hohmeyer, C. Volckmar, B. Steinhauer, R. Schlögl, P. Claus. Phys. Chem. Chem. Phys. 9 (2007) 3559.

[59] C. Mohr, H. Hofmeister, M. Lucas, J. Radnik, P. Claus. J. Am. Chem. Soc, 125 (1905) 2003.

[60] M. Bron, D. Teschner, U. Wild, B. Steinhauer, A. Knop-Gericke, C. Volckmar, BA. Wootsch, R. Schlögl, P. Claus. In preparation.

[61] S. Linic and M. A. Barteau. J. Catal. 214 (2003) 200.

[62] C. Stegelmann, N. C. Schiodt, C. T. Campbell, P. Stoltze. J. Catal. 221 (2004) 630.

[63] V. I. Bukhtiyarov, M. Havecker, V. V. Kaichev, A. Knop-Gericke, R. W. Mayer, R. Schlögl. Phys. Rev. B 67 (2003) 235422.

[64] S. A. Tan, R. B. Grant, R. M. Lambert. Appl. Catal. 31 (1987) 159.

[65] J. Schnadt, A. Michaelides, J. Knudsen, R. T. Vang, K. Reuter, M. Lægsgaard, M. Scheffler, F. Besenbacher. Phys. Rev. Lett. 96 (2006) 146101.

[66] M. Schmid, A. Reicho, A. Stierle, I. Costina, J. Klikovits, P. Kostelnik, O. Dubay, G. Kresse, J. Gustafson, E. Lungren, J. N. Andersen, H. Dosch, P. Varga. Phys. Rev. Lett. 96 (2006) 146102.

[67] C. T. Campbell, M. T. Paffett. Surf. Sci. 143 (1984) 517.

[68] C. T. Campbell. Surf. Sci. 157 (1985) 43.

[69] M. Pascal, C. L. A. Lamont, P. Baumgärtel, R. Terborg, J. T. Hoeft, O. Schaff, M. Polcik, A. M. Bradshaw, R. L. Toomes, D. P. Woodruff. Surf. Sci. 464 (2000) 83.

[70] M. Canepa, P. Cantini, F. Fossa, L. Mattera, S. Terreni. Phys. Rev. B 47 (1993) 15823.

[71] L. Becker, S. Aminpirooz, A. Schmalz, B. Hillert, M. Pedio, J. Haase. Phys. Rev. B. 44 (1991) 13655.

[72] K. Berge, A. Goldmann. Surf. Sci. 540 (2003) 343.

[73] O. Nakagoe, K. Watanabe, N. Takagi, Y. Matsumoto. J. Phys. Chem. B. 109 (2005) 14536.

[74] V. I. Bukhtiyarov, V. V. Kaichev, I. P. Prosvirin. J. Chem. Phys. 111 (1999) 2169.

[75] C. I. Carlisle, D. A. King, M.-L. Bocquet, J. Cerda, P. Sautet. Phys. Rev. Lett. 84 (2000) 3899.

[76] Ch. A. Wert. Trapping of hydrogen in metals. Hydrogen in metals II: G. Alefeld, J. Völkl, Eds.; Springer-Verlag (Top in Appl Phys): Berlin, Vol. 29 (1978) p. 305

[77] M. K. Rose, A. Borg, T. Mitsui, D. F. Ogletree, M. Slameron. J. Chem. Phys. 115 (2001) 10927.

[78] S. T. Ceyer. Acc. Chem. Res. 34 (2001) 737.

[79] J. Greeley, M. Mavrikakis. Surf. Sci. 540 (2003) 215.

[80] J. Greeley, W. P. Krekelberg, M. Mavrikakis. Angew. Chem. Int. Ed. 43 (2004) 4296.

[81] H. Over, A. P. Seitsonen. Science. 297 (2002) 2003.

[82] D. Herein, A. Nagy, H. Schubert, G. Weinberg, E. Kitzelmann, R. Schlögl, Z. Phys. Chem. 197 (1996) 67.

[83] C. I. Carlisle, T. Fujimoto, W. S. Sim, and D. A. King. Surf. Sci., 470 (2000) 15 and references therein.

[84] W.-X. Li, C. Stampfl, M. Scheffler. Phys. Rev. B. 67 (2003) 045408.

[85] A. B. Mohammad, I. V. Yudanov, K. H. Lim, K. M. Neyman, N. Rösch. J. Phys. Chem. C (2008) in press.

[86] G. J. Hutchings, F. King, I. P. Okoye, M. B. Bradley, C. H. Rochester. J. Cat. 148 (1994) 453.

[87] P. Claus, H. Hofmeister. J. Phys. Chem. B 103 (1999) 2766.

[88] J. P. Perdew, J. A. Chevary, S. H. Vosko, K. A. Jackson, M. R. Pederson, D. J. Singh, C. Fiolhais. Phys. Rev. B. 46 (1992) 6671.

[89] B. Hammer, L. B. Hansen, J. K. Nørskov. Phys. Rev. B. 59 (1999) 7413.

[90] D. R. Lide, Ed., CRC Handbook of Chemistry and Physics, 77th Ed., CRC Press, London, 1996.

[91] J. P. Perdew, K. Burke, M. Ernzerhof. Phys. Rev. Lett. 77 (1996) 3865.

[92] T. Schimizu, M. Tsukada.. Surf. Sci. 295 (1993) L1017.

[93] H. Katagiri, T. Uda, K. Terakura. Surf. Sci. 424 (1999) 322.

[94] B. Hammer, L. B. Hansen, J. K. Nørskov. J. Phys. Rev. B. 59 (1999) 7413.

[95] J. Greeley, J. K. Nørskov, M. Mavrikakis. Annu. Rev. Phys. Chem. 53 (2002) 319.

[96] B. C. Khanra, Y. Jugnet, J. C. Bertolini. J. Mol. Cat. A: Chemical 208 (2004) 167.

[97] K. H. Lim, Z.-X Chen, K. M. Neyman, N. Rösch. Chem. Phys. Lett. 420 (2006) 60.

[98] G. Kresse, J. Furthmüller. Phys. Rev. B 54 (1996) 11169.

[99] G. Kresse, J. Hafner. Phys. Rev. B 47 (1993) 558.

[100] G. Kresse, J. Furthmüller. Comp. Mat. Sci. 6 (1999) 15.

[101] J. P. Perdew, Y. Wang. Phys. Rev. B 45 (1992) 13244.

[102] C.E. Blom, G. Grassi, A. Bauder. J. Am. Chem. Soc. 106 (1984) 7427.

[103] F. Delbecq, P. Sautet. J. Catalysis. 211 (2002) 398.

[104] W. Koch, M. C. Holthaussen. A chemist's guide to density functional theory. 2nd Ed. Wiley-VCH, Weinheim, (2001) p.65-91.

[105] P. E. Blöchl. Phys. Rev. B 50 (1994) 17953.

[106] G. Kresse, D. Joubert. Phys. Rev. B 59 (1999) 1758.

[107] J. J. Monkhorst, J. D. Pack. Phys. Rev. B 13 (1976) 5188.

[108] M. Methfessel, A. T. Paxton. Phys. Rev. B 40 (1989) 3616.

[109] C. Kittel. Introduction to solid state physics, Wiley, New York, 1971; J. Donohue, The structures of the elements, Wiley, New York, 1974.

[110] N.H. de Leeuw, C. J. Nelson, C. R. A. Catlow, P. Sautet, W. Dong. Phys. Rev. B 69 (2004) 45419.

[111] R. Alfoonso, A. V. Cugini, D. S. Sholl. Surf. Sci. 546 (2003) 12.

[112] W. X. Li, C. Stampfl, M. Scheffler. Phys. Rev. B 65 (2002) 75407.

[113] M. Lindroos, C. J. Barnes, M. Valden, D. A. King. Surf. Sci. 218 (1989) 269

[114] Y. Y. Sun, H. Xu, Y. P. Feng, A. C. H. Huan, A. T. S. Wee. Phys. Rev. Let. 93 (2004) 136102.

[115] K. H. Lim, K. M. Neyman, N. Rösch. Chem. Phys. Lett. 432 (2006) 184.

[116] Z.-X. Chen, K. H. Lim, K. M. Neyman, N. Rösch. J. Phys. Chem. B 109 (2005) 4568.

[117] G. Mills, H.Jónsson, G. K. Schenter. Surf. Sci. 324 (1995) 305.

[118] CRC Handbook of chemistry and physics 1913-1995, edited by D. R. Lide (CRC Press, Boca Raton, Florida, 1995), 75th ed.

[119] G. Lee, E. W. Plummer, Phys. Rev. B 51 (1995)7250.

[120] F. Bartolucci, R. Franchy, J. C. Barnard, R. R. Palmer. Phys. Rev. Lett. 80 (1998) 5224.

[121] H. A. Engelhardt, D. Menzel. Surf. Sci. 57 (1976) 591.

[122] W. Heiland, F. Iberl, E. Taglauer, D. Menzel. 53 (1975) 383.

[123] H. Dürr, Th. Fauster, R. Schneider. Surf. Sci. 244 (1991) 237

[124] S. R. Parkin, H. C. Zeng, M. Y. Zhou, K. A. R. Mitchell. Phys. Rev. B 41 (1990) 5432.

[125] D. J. Coulman, J. Wintterlin, R. J. Behm, G. Ertl. Phys. Rev. Lett. 64 (1990) 1761

[126] Y. Kuk, F. M. Chua, P. J. Silverman, J. A. Meyer. Phys. Rev. B 41 (1990) 12393

[127] H. Bu, C. D. Roux, J. W. Rabalais. J. Chem. Phys. 97 (1992) 1465

[128] G. Kleinle, J. Wintterlin, G. Ertl, R. J. Behm, F. Jona, W. Moritz. Surf. Sci. 225 (1990) 171

[129] F. Besenbacher, I. Stensgaard, L. Ruan, J. K. Nørskov, K. W. Jacobsen. Surf. Sci. 272 (1992) 334

[130] L. Yang, T. S. Rahman, G. Biracco, R. Tattarek. Phys. Rev. B 40 (1989) 12271

[131] T. Hashizume, M. Taniguchi, H. Lu, K. Tanaka, T. Sakurai. Jpn. J. Appl. Phys. 30 (1991) L1529

[132] F. Jensen, F. Besenbacher, E. Laegsgaard, I. Stensgaard. Phys. Rev. B 41 (1990) 10233.

[133] M. Taniguchi, K. Tanaka, T. Hashizume, T. Sakurai. Surf. Sci. 262 (1992) L123.

[134] W. W. Pai, N. C. Bartelt, M. R. Peng, J. E. Reutt-Robey. Surf. Sci. 330 (1995) L679.

[135] J. Perdew, A. Zunger. Phys. Rev. B 23 (1981) 5048.

[136] G. Rovida, F. Pratesi, M. Maglietta, E. Ferroni, Surf. Sci. 43 (1974) 230.

[137] R.B. Grant, R.M. Lambert, Surf. Sci. 146 (1984) 256.

[138] I. V. Yudanov, K. M. Neyman, N. Rösch. Phys. Chem. Chem. Phys. 6 (2004) 116.

[139] Q. Sun, Y. Wang, K. Fan, J. Deng. Surf. Sci. 459 (2000) 213.

[140] V. I. Pazzi, P. Herman, T. Philipsen, E. J. Baerends, G. F. Tantardini. Surf. Sci. 443 (1999) 1.

[141] F. E. Olsson, N. Lorente, M. Persson. Surf. Sci. 522 (2003) L27.

[142] A. Puschmann, J. Haase. Surf. Sci. 144 (1984) 559.

[143] Z.-X. Chen, K. M. Neyman, K. H. Lim, N. Rösch. Langmuir 20 (2004) 8068.

[144] A. Michaelides, M.-L. Bocquet, P. Sautet, A. Alavi, D. A. King. Chem. Phys. Lett. 367 (2003) 344.

[145] W.-X. Li, C. Stampfl, M. Scheffler. Phys. Rev. Lett. 90 (2003) 256102.

[146] A. Michaelides, K. Reuter, M. Scheffler. J. Vac. Sci. Technol. A 23 (2005) 1487.

[147] Y. Xu, J. Greeley, M. Mavrikakis. J. Am. Chem. Soc. 127 (2005) 12823.

[148] L. Guillemot, K. Bobrov. Surf. Sci. 601 (2007) 871.

[149] M. Canepa, P. Cantini, L. Mattera, E. Narducci, M. Salvietti, S. Terreni. Surf. Sci. 322 (1995) 271.

[150] A. Montoya, B. S. Haynes. J. Phys. Chem. C 111 (2007) 1333.

[151] A. Michaelides, V. A. Ranea, P. L. de Andres, D. A. King. Phys. Rev. Let. 90 (2003) 216102.

[152] Anna Ignaczak, J. A. N. F. Gommes. J. Elec. Analyt. Chem. 420 (1997) 209.

[153] P. Vassilve, R. A. van Santen, M. T. M. Koper. J. Chem. Phys. 122 (2005) 54701.

[154] S. Meng, E. G. Wang, S. Gao, Phys. Rev. B, 69 (2004) 195404.

[155] D. Sebastian, L. D. Site. J. Chem. Theory Comput. 1 (2005) 78.

[156] F. Sim, A. St-Amant, I. Papai, D. R. Salahub. J. Am. Chem. Soc. 114 (1992) 4391.

[157] R. N. Barnett, U. Landman. Phys. Rev. B, 48 (1993) 2081.

[158] M. A. Henderson. Sur. Sci. Reports 46 (2002) 1.

[159] D. M. Camaioni, C. A. Schwerdtfeger. J. Phys. Chem. A 109 (2005) 10795.

[160] M. W. Ribarsky, W. D. Luedtke, U. Landman. Phys. Rev. B, 32 (1985) 1430.

[161] A. J. Nagy, G. Mestl, D. Herein, G. Weinberg, E. Kitzelmann, R. Schlögl. J. Catal. 182 (1999) 417.

[162] A. J. Nagy, G. Mestl, R. Schlögl. J. Catal. 188 (1999) 58.

[163] Q. Sun, A. B. Mohammad, L. Moskaleva, Z. –X. Chen, N. Rösch. In preparation

[164] M. Bron, E. Kondratenko, A. Trunschke, P. Claus. Z. Phys. Chem. 218 (2004) 405.

[165] A. B. Mohammad, K. H. Lim, I. V. Yudanov, K. M. Neyman, N. Rösch. Phys. Chem. Chem. Phys. 9 (2007) 1247.

[166] K. M. Neyman, K. H. Lim, Z.-X. Chen, L. V. Moskaleva, A. Bayer, A. Reindl, D. Borgmann, R. Denecke, H.-P. Steinrück, N. Rösch. Phys. Chem. Chem. Phys. 9 (2007) 3470.

[167] A. Montoya, B. S. Haynes, J. Phys. Chem. C 111 (2007) 9867.

[168] D. Loffreda, F. Delbecq, F. Vigne, P. Sautet. Angew. Chem. Int. Ed. 44 (2005) 5279.

# Appendix A

# Common Supplementary Material for all the calculations

**Table A1S.** Unit cell parameters of Ag(110)

| | Ag(110) | | | Ag(111) | | Ag(221) | |
|---|---|---|---|---|---|---|---|
| | 2x2 | 3x2 | 4x2 | 2x2 | 3x3 | 4x2 | 4x3 |
| a, Å | 5.855 | 8.782 | 11.710 | 5.855 | 8.782 | 8.782 | 8.782 |
| b, Å | 8.280 | 8.280 | 8.280 | 5.855 | 8.782 | 5.855 | 8.782 |
| c, Å | 17.565 | 17.565 | 21.594 | 16.732 | 23.902 | 20.700 | 23.460 |
| | $\alpha = \beta = \gamma = 90°$ | | | $\alpha = \beta = 90°; \gamma = 60°$ | | $\alpha = \beta = \gamma = 90°$ | |

**Table A2S**. Total energy (eV) of atoms in the gas phase

| Species | O | H | OH | $H_2O$ | $H_2$ |
|---|---|---|---|---|---|
| Total energy | -1.810 | -1.119 | -7.550 | -14.272 | -6.783 |

TE – Total energy; IS – Initial state; TS – Transition state; FS – Final state

**Table A3S.** Cartesian coordinates (Å) of Ag(110) substrate atoms and the total energy, TE (eV)

| | 2x2 | | | 3x2 | | | 4x2 | | |
|---|---|---|---|---|---|---|---|---|---|
| | x | y | z | x | y | z | x | y | z |
| Ag | 0.000 | 0.000 | 8.830 | 0.000 | 0.000 | 8.830 | 0.000 | 0.000 | 8.830 |
| Ag | 2.927 | 0.000 | 8.830 | 2.927 | 0.000 | 8.830 | 2.927 | 0.000 | 8.830 |
| Ag | 0.000 | 4.140 | 8.830 | 5.855 | 0.000 | 8.830 | 5.855 | 0.000 | 8.830 |
| Ag | 2.927 | 4.140 | 8.830 | 0.000 | 4.140 | 8.830 | 8.782 | 0.000 | 8.830 |
| Ag | 1.464 | 2.070 | 10.178 | 2.927 | 4.140 | 8.830 | 0.000 | 4.140 | 8.830 |
| Ag | 4.391 | 2.070 | 10.178 | 5.855 | 4.140 | 8.830 | 2.927 | 4.140 | 8.830 |
| Ag | 1.464 | 6.210 | 10.178 | 1.464 | 2.070 | 10.178 | 5.855 | 4.140 | 8.830 |
| Ag | 4.391 | 6.210 | 10.178 | 4.391 | 2.070 | 10.178 | 8.782 | 4.140 | 8.830 |
| Ag | 0.000 | 0.000 | 11.710 | 7.319 | 2.070 | 10.178 | 1.464 | 2.070 | 10.178 |
| Ag | 2.927 | 0.000 | 11.710 | 1.464 | 6.210 | 10.178 | 4.391 | 2.070 | 10.178 |
| Ag | 0.000 | 4.140 | 11.710 | 4.391 | 6.210 | 10.178 | 7.319 | 2.070 | 10.178 |
| Ag | 2.927 | 4.140 | 11.710 | 7.319 | 6.210 | 10.178 | 10.246 | 2.070 | 10.178 |
| Ag | 1.464 | 2.070 | 13.173 | 0.000 | 0.000 | 11.710 | 1.464 | 6.210 | 10.178 |
| Ag | 4.391 | 2.070 | 13.173 | 2.927 | 0.000 | 11.710 | 4.391 | 6.210 | 10.178 |
| Ag | 1.464 | 6.210 | 13.173 | 5.855 | 0.000 | 11.710 | 7.319 | 6.210 | 10.178 |
| Ag | 4.391 | 6.210 | 13.173 | 0.000 | 4.140 | 11.710 | 10.246 | 6.210 | 10.178 |
| Ag | 0.000 | 0.000 | 14.637 | 2.927 | 4.140 | 11.710 | 0.000 | 0.000 | 11.526 |
| Ag | 2.927 | 0.000 | 14.637 | 5.855 | 4.140 | 11.710 | 2.927 | 0.000 | 11.526 |
| Ag | 0.000 | 4.140 | 14.637 | 1.464 | 2.070 | 13.173 | 5.855 | 0.000 | 11.526 |
| Ag | 2.927 | 4.140 | 14.637 | 4.391 | 2.070 | 13.173 | 8.782 | 0.000 | 11.526 |
| Ag | | | | 7.319 | 2.070 | 13.173 | 0.000 | 4.140 | 11.526 |
| Ag | | | | 1.464 | 6.210 | 13.173 | 2.927 | 4.140 | 11.526 |
| Ag | | | | 4.391 | 6.210 | 13.173 | 5.855 | 4.140 | 11.526 |
| Ag | | | | 7.319 | 6.210 | 13.173 | 8.782 | 4.140 | 11.526 |
| Ag | | | | 0.000 | 0.000 | 14.637 | 1.464 | 2.070 | 12.874 |
| Ag | | | | 2.927 | 0.000 | 14.637 | 4.391 | 2.070 | 12.874 |
| Ag | | | | 5.855 | 0.000 | 14.637 | 7.319 | 2.070 | 12.874 |
| Ag | | | | 0.000 | 4.140 | 14.637 | 10.246 | 2.070 | 12.874 |
| Ag | | | | 2.927 | 4.140 | 14.637 | 1.464 | 6.210 | 12.874 |
| Ag | | | | 5.855 | 4.140 | 14.637 | 4.391 | 6.210 | 12.874 |
| Ag | | | | | | | 7.319 | 6.210 | 12.874 |
| Ag | | | | | | | 10.246 | 6.210 | 12.874 |
| Ag | | | | | | | 0.000 | 0.000 | 14.222 |
| Ag | | | | | | | 2.927 | 0.000 | 14.222 |
| Ag | | | | | | | 5.855 | 0.000 | 14.222 |
| Ag | | | | | | | 8.782 | 0.000 | 14.222 |
| Ag | | | | | | | 0.000 | 4.140 | 14.222 |
| Ag | | | | | | | 2.927 | 4.140 | 14.222 |
| Ag | | | | | | | 5.855 | 4.140 | 14.222 |
| Ag | | | | | | | 8.782 | 4.140 | 14.222 |
| TE | | -49.100 | | | -73.875 | | | -96.80 | |

**Table A4S.** Cartesian coordinates (Å) of Ag(111) substrate atoms and the total energy, TE (eV)

| | 2x2 | | | 3x3 | | |
|---|---|---|---|---|---|---|
| | x | y | z | x | y | z |
| Ag | 0.000 | 0.000 | 4.770 | 0.000 | 0.000 | 11.946 |
| Ag | 2.927 | 0.000 | 4.770 | 2.927 | 0.000 | 11.946 |
| Ag | 4.391 | 2.535 | 4.770 | 5.855 | 0.000 | 11.946 |
| Ag | 1.464 | 2.535 | 4.770 | 1.464 | 2.535 | 11.946 |
| Ag | 1.464 | 0.845 | 7.181 | 2.927 | 5.070 | 11.946 |
| Ag | 4.391 | 0.845 | 7.181 | 4.391 | 2.535 | 11.946 |
| Ag | 5.855 | 3.380 | 7.181 | 5.855 | 5.070 | 11.946 |
| Ag | 2.927 | 3.380 | 7.181 | 7.319 | 2.535 | 11.946 |
| Ag | 2.927 | 1.690 | 9.561 | 8.782 | 5.070 | 11.946 |
| Ag | 5.855 | 1.690 | 9.561 | 1.464 | 0.845 | 14.333 |
| Ag | 7.318 | 4.225 | 9.561 | 4.391 | 0.845 | 14.333 |
| Ag | 4.391 | 4.225 | 9.561 | 7.319 | 0.845 | 14.333 |
| Ag | 4.391 | 2.535 | 11.951 | 2.927 | 3.380 | 14.333 |
| Ag | 1.464 | 2.535 | 11.951 | 4.391 | 5.916 | 14.333 |
| Ag | 0.000 | 0.000 | 11.951 | 5.855 | 3.380 | 14.333 |
| Ag | 2.927 | 0.000 | 11.951 | 7.319 | 5.916 | 14.333 |
| Ag | 5.855 | 3.380 | 14.341 | 8.782 | 3.380 | 14.333 |
| Ag | 2.927 | 3.380 | 14.341 | 10.246 | 5.916 | 14.333 |
| Ag | 1.464 | 0.845 | 14.341 | 2.927 | 1.690 | 16.732 |
| Ag | 4.391 | 0.845 | 14.341 | 5.855 | 1.690 | 16.732 |
| Ag | | | | 8.782 | 1.690 | 16.732 |
| Ag | | | | 4.391 | 4.225 | 16.732 |
| Ag | | | | 5.855 | 6.761 | 16.732 |
| Ag | | | | 7.319 | 4.225 | 16.732 |
| Ag | | | | 8.782 | 6.761 | 16.732 |
| Ag | | | | 10.246 | 4.225 | 16.732 |
| Ag | | | | 11.710 | 6.761 | 16.732 |
| Ag | | | | 0.000 | 0.000 | 19.122 |
| Ag | | | | 2.927 | 0.000 | 19.122 |
| Ag | | | | 5.855 | 0.000 | 19.122 |
| Ag | | | | 1.464 | 2.535 | 19.122 |
| Ag | | | | 2.927 | 5.070 | 19.122 |
| Ag | | | | 4.391 | 2.535 | 19.122 |
| Ag | | | | 5.855 | 5.070 | 19.122 |
| Ag | | | | 7.319 | 2.535 | 19.122 |
| Ag | | | | 8.782 | 5.070 | 19.122 |
| Ag | | | | | | |
| Ag | | | | | | |
| Ag | | | | | | |
| Ag | | | | | | |
| TE | | -49.100 | | | -91.868 | |

**Table A5S.** Cartesian coordinates (Å) of Ag(221) substrate atoms and the energy (eV)

| | 4x2 | | | 4x3 | | | | | |
|---|---|---|---|---|---|---|---|---|---|
| | x | y | z | x | y | z | x | y | z |
| Ag | 0.000 | 0.000 | 8.280 | 0.039 | 0.000 | 8.352 | 1.464 | 4.391 | 18.630 |
| Ag | 0.000 | 2.927 | 8.280 | 0.039 | 2.927 | 8.352 | 1.464 | 7.319 | 18.630 |
| Ag | 2.439 | 1.464 | 8.970 | 0.039 | 5.855 | 8.352 | 3.903 | 0.000 | 19.320 |
| Ag | 2.439 | 4.391 | 8.970 | 2.454 | 1.464 | 8.948 | 3.903 | 2.927 | 19.320 |
| Ag | 4.879 | 0.000 | 9.660 | 2.454 | 4.391 | 8.948 | 3.903 | 5.855 | 19.320 |
| Ag | 4.879 | 2.927 | 9.660 | 2.454 | 7.319 | 8.948 | 6.343 | 1.464 | 20.010 |
| Ag | 7.318 | 1.464 | 10.350 | 4.857 | 0.000 | 9.610 | 6.343 | 4.391 | 20.010 |
| Ag | 7.318 | 4.391 | 10.350 | 4.857 | 2.927 | 9.610 | 6.343 | 7.319 | 20.010 |
| Ag | 0.976 | 0.000 | 11.040 | 4.857 | 5.855 | 9.610 | 8.782 | 0.000 | 20.700 |
| Ag | 0.976 | 2.927 | 11.040 | 7.257 | 1.464 | 10.272 | 8.782 | 2.927 | 20.700 |
| Ag | 3.415 | 1.464 | 11.730 | 7.257 | 4.391 | 10.272 | 8.782 | 5.855 | 20.700 |
| Ag | 3.415 | 4.391 | 11.730 | 7.257 | 7.319 | 10.272 | 2.439 | 1.464 | 21.390 |
| Ag | 5.855 | 0.000 | 12.420 | 0.955 | 0.000 | 11.050 | 2.439 | 4.391 | 21.390 |
| Ag | 5.855 | 2.927 | 12.420 | 0.955 | 2.927 | 11.050 | 2.439 | 7.319 | 21.390 |
| Ag | 8.294 | 1.464 | 13.110 | 0.955 | 5.855 | 11.050 | | | |
| Ag | 8.294 | 4.391 | 13.110 | 3.416 | 1.464 | 11.715 | | | |
| Ag | 1.952 | 0.000 | 13.800 | 3.416 | 4.391 | 11.715 | | | |
| Ag | 1.952 | 2.927 | 13.800 | 3.416 | 7.319 | 11.715 | | | |
| Ag | 4.391 | 1.464 | 14.490 | 5.857 | 0.000 | 12.406 | | | |
| Ag | 4.391 | 4.391 | 14.490 | 5.857 | 2.927 | 12.406 | | | |
| Ag | 6.831 | 0.000 | 15.180 | 5.857 | 5.855 | 12.406 | | | |
| Ag | 6.831 | 2.927 | 15.180 | 8.283 | 1.464 | 13.103 | | | |
| Ag | 0.488 | 1.464 | 15.870 | 8.283 | 4.391 | 13.103 | | | |
| Ag | 0.488 | 4.391 | 15.870 | 8.283 | 7.319 | 13.103 | | | |
| Ag | 2.927 | 0.000 | 16.560 | 1.952 | 0.000 | 13.800 | | | |
| Ag | 2.927 | 2.927 | 16.560 | 1.952 | 2.927 | 13.800 | | | |
| Ag | 5.367 | 1.464 | 17.250 | 1.952 | 5.855 | 13.800 | | | |
| Ag | 5.367 | 4.391 | 17.250 | 4.391 | 1.464 | 14.490 | | | |
| Ag | 7.806 | 0.000 | 17.940 | 4.391 | 4.391 | 14.490 | | | |
| Ag | 7.806 | 2.927 | 17.940 | 4.391 | 7.319 | 14.490 | | | |
| Ag | 1.464 | 1.464 | 18.630 | 6.831 | 0.000 | 15.180 | | | |
| Ag | 1.464 | 4.391 | 18.630 | 6.831 | 2.927 | 15.180 | | | |
| Ag | 3.903 | 0.000 | 19.320 | 6.831 | 5.855 | 15.180 | | | |
| Ag | 3.903 | 2.927 | 19.320 | 0.488 | 1.464 | 15.870 | | | |
| Ag | 6.343 | 1.464 | 20.010 | 0.488 | 4.391 | 15.870 | | | |
| Ag | 6.343 | 4.391 | 20.010 | 0.488 | 7.319 | 15.870 | | | |
| Ag | 8.782 | 0.000 | 0.000 | 2.927 | 0.000 | 16.560 | | | |
| Ag | 8.782 | 2.927 | 0.000 | 2.927 | 2.927 | 16.560 | | | |
| Ag | 2.683 | 1.464 | 0.690 | 2.927 | 5.855 | 16.560 | | | |
| Ag | 2.683 | 4.391 | 0.690 | 5.367 | 1.464 | 17.250 | | | |
| Ag | | | | 5.367 | 4.391 | 17.250 | | | |
| | | | | 5.367 | 7.319 | 17.250 | | | |
| | | | | 7.806 | 0.000 | 17.940 | | | |
| | | | | 7.806 | 2.927 | 17.940 | | | |
| | | | | 7.806 | 5.855 | 17.940 | | | |
| | | | | 1.464 | 1.464 | 18.630 | | | |
| TE | | -103.2905 | | | | -155.49 | | | |

# Appendix B

# Supplementary Material for Hydrogen adsorption on Ag Surfaces

**Table B1S.** The Cartesian coordinates (Å) of hydrogen adsorbed on Ag(110), Ag(111) and Ag(221) slabs and the corresponding total energies (eV).

**Ag(110)**

| Top Ag | | | Short bridge | | |
|---|---|---|---|---|---|
| x | y | z | x | y | z |
| 0.000 | 0.000 | 7.1734 | 1.4637 | 0.000 | 7.7687 |
| | | -51.738 | | | -52.252 |

| Long bridge | | | 4-fold hollow | | |
|---|---|---|---|---|---|
| 0.000 | 2.070 | 8.8139 | 1.4637 | 2.07 | 8.4299 |
| Total energy | | -52.222 | | | -51.968 |

**Ag(111)**

| | top | | | bridge | | |
|---|---|---|---|---|---|---|
| | x | y | z | x | y | z |
| H | 0.000 | 0.000 | 3.108 | 1.464 | 0.000 | 3.676 |
| Total energy | | | -54.416 | | | -54.803 |

| | fcc | | | hcp | | |
|---|---|---|---|---|---|---|
| H | 2.927 | 1.690 | 3.860 | 1.464 | 0.845 | 3.866 |
| Total energy | | | -54.917 | | | -54.908 |

**Ag(221)**

| | Edge bridge | | | Terrace 3-fold hollow | | |
|---|---|---|---|---|---|---|
| | x | y | z | x | Y | z |
| H | 0.044 | 1.464 | 7.267 | 5.845 | 1.464 | 8.912 |
| Total energy | | | -106.538 | | | -106.478 |

| | edge 3-fold hollow-2 | | | edge 3-fold hollow-1 | | |
|---|---|---|---|---|---|---|
| H | 1.899 | 2.927 | 7.797 | 0.990 | 1.464 | 7.580 |
| Total energy | | -106.582 | | | -106.530 | |

**Table B2S.** Structural (Å) and energetic (eV) characteristics of complexes relevant to hydrogen dissociation on Ag(110) surface

| **IS** | $H_2$ at 300 pm height | | |
|---|---|---|---|
| | x | y | z |
| H | 2.5614 | 0.0000 | 5.8303 |
| H | 3.3042 | 0.0000 | 5.8303 |
| Total Energy | | -55.901 | |

| | FS | | | TS | | |
|---|---|---|---|---|---|---|
| **SB/SB** | x | y | z | x | y | z |
| H | 1.4637 | 0.0000 | 7.7570 | 2.1588 | 0.0000 | 7.3400 |
| H | 4.3911 | 0.0000 | 7.7570 | 3.7094 | 0.0000 | 7.3400 |
| | Total energy | | -55.308 | | -54.529 | |
| **3f/3f** | | | | | | |
| H | 1.4637 | 1.0607 | 8.4544 | 0.8089 | 8.1484 | 7.3706 |
| H | 4.3911 | 7.2193 | 8.4544 | 5.0458 | 0.1316 | 7.3706 |
| | Total energy | | -55.556 | | -54.521 | |
| **LB/LB**[a] | | | | | | |
| H | 0.0000 | 2.0700 | 8.8015 | 0.6125 | 1.4000 | 7.8305 |
| H | 2.9274 | 2.0700 | 8.8015 | 2.3244 | 1.4000 | 7.8305 |
| | Total energy | | -55.201 | | -54.223 | |
| **SB/LB** | | | | | | |
| H | 0.0000 | 2.0700 | 8.8139 | 0.4976 | 1.6916 | 8.3263 |
| H | 1.4637 | 0.0000 | 7.7687 | 1.2430 | 0.7038 | 7.7614 |
| | Total energy | | -55.336 | | -54.636 | |
| **SB/3-f** | | | | | | |
| H | 1.4637 | 4.1111 | 7.7799 | 0.3610 | 7.8460 | 7.2509 |
| H | 4.3911 | 5.2595 | 8.4563 | 4.7322 | 7.8572 | 7.6228 |
| | Total energy | | -55.449 | | -54.561 | |
| **LB/3-f** | | | | | | |
| H | 2.9355 | 2.1015 | 8.8122 | 0.8565 | 0.7547 | 7.5741 |
| H | 1.4787 | 5.2188 | 8.4005 | 5.1476 | 0.9244 | 7.6142 |
| | Total energy | | -55.359 | | -54.471 | |

[a] Complex oriented along the troughs.

**Table B3S.** Frequencies ($cm^{-1}$) of final state (FS) and transition state (TS) complexes for H-H bond breaking on Ag(110) surface

| **SB/SB** | $\nu_1$ | $\nu_2$ | $\nu_3$ | $\nu_4$ | $\nu_5$ | $\nu_6$ |
|---|---|---|---|---|---|---|
| FS | 1149 | 1132 | 1111 | 1061 | 449 | 389 |
| TS | 1608 | 1538 | 481 | 263 | 138 | 1113 *i* |
| **3f/3f** | | | | | | |
| FS | 1012 | 1002 | 930 | 919 | 687 | 582 |
| TS | 1264 | 963 | 565 | 469 | 376 | 1228 *i* |
| **LB/LB**[a] | | | | | | |
| FS | 861 | 746 | 722 | 653 | 547 | 382 |
| TS | 1094 | 1004 | 352 | 323 | 38 | 889 *i* |
| **SB/LB** | | | | | | |
| FS | 1146 | 1027 | 725 | 595 | 455 | 246 |
| TS | 1623 | 1584 | 548 | 398 | 157 | 996 *i* |
| **SB/3-f** | | | | | | |
| FS | 1168 | 1027 | 1022 | 904 | 571 | 223 |
| TS | 1583 | 1453 | 424 | 174 | 157 | 1123 *i* |
| **LB/3-f** | | | | | | |
| FS | 990 | 930 | 712 | 588 | 541 | 443 |
| TS | 1585 | 1522 | 533 | 440 | 238 | 1058 *i* |

[a] Complex oriented along the troughs.

**Table B4S.** Cartesian coordinates (Å) of added row atoms on Ag (110) and the resulting total energy (eV)

| | clean | | | TS | | |
|---|---|---|---|---|---|---|
| | x | y | z | x | y | z |
| H | | | | 1.4637 | 0.4309 | 5.8769 |
| H | | | | 1.4637 | 1.4865 | 5.2675 |
| O | 1.4637 | 0.0000 | 7.0744 | 1.4637 | 8.2489 | 6.8624 |
| O | 1.4637 | 4.1400 | 7.0744 | 1.4637 | 4.2023 | 7.1131 |
| Ag | 1.4637 | 2.0700 | 7.1650 | 1.4637 | 2.1639 | 7.0268 |
| Ag | 1.4637 | 6.2100 | 7.1650 | 1.4637 | 6.2251 | 7.1972 |
| Total Energy | | -65.991 | | Total Energy | | -72.049 |
| | **InterState** | | | | **DS** | |
| H | 1.4637 | -0.090 | 5.4548 | 1.4637 | 8.4002 | 5.2362 |
| H | 1.4637 | 2.2042 | 5.1795 | 1.4637 | 3.3737 | 5.2999 |
| O | 1.4637 | -0.037 | 6.4275 | 1.4637 | 0.2577 | 6.2013 |
| O | 1.4637 | 4.0549 | 7.1168 | 1.4637 | 4.3454 | 7.0913 |
| Ag | 1.4637 | 2.0374 | 6.8199 | 1.4637 | 2.3358 | 6.5971 |
| Ag | 1.4637 | 6.2327 | 7.3527 | 1.4637 | 6.5126 | 7.2047 |
| Total Energy | | -72.466 | | Total Energy | | -72.335 |
| | **FS** | | | | | |
| H | 1.4637 | 0.0364 | 5.4328 | | | |
| H | 1.4637 | 4.1036 | 5.4328 | | | |
| O | 1.4637 | 0.0103 | 6.4088 | | | |
| O | 1.4637 | 4.12972 | 6.4088 | | | |
| Ag | 1.4637 | 2.0700 | 7.3389 | | | |
| Ag | 1.4637 | 6.2100 | 7.3389 | | | |
| Total Energy | | -75.115 | | | | |

**Table B5S.** Frequencies ($cm^{-1}$) of final state (FS), intermediate stable state(Inter), diffusion state (DS) and transition state (TS) for H-H bond breaking on Ag(110) surface

| | TS | Inter | DS | FS |
|---|---|---|---|---|
| $\nu_1$ | 1914 | 3608 | 3603 | 3576 |
| $\nu_2$ | 1192 | 1586 | 1526 | 3573 |
| $\nu_3$ | 855 | 824 | 830 | 690 |
| $\nu_4$ | 843 | 481 | 243 | 683 |
| $\nu_5$ | 213 | 240 | 205 | 191 |
| $\nu_6$ | 654*i* | 135 | 380*i* | 170 |

# Appendix C

# Supplementary Material for Oxygen adsorption on Ag Surfaces.

**Table C1S.** (a) Cartesian coordinates (Å) of oxygen adsorbed on Ag(110) and the corresponding total energies (eV) and (b) frequencies

| **Long bridge** | x | y | z | **Top** | x | y | z |
|---|---|---|---|---|---|---|---|
| O | 0.000 | 2.070 | 8.406 | O | 0.000 | 0.000 | 6.976 |
| Ag | 0.000 | 8.161 | 8.731 | Ag | 0.000 | 0.000 | 8.909 |
| Ag | 2.927 | 8.219 | 8.824 | Ag | 2.927 | 0.000 | 8.716 |
| Ag | 0.000 | 4.259 | 8.731 | Ag | 0.000 | 4.140 | 8.814 |
| Ag | 2.927 | 4.201 | 8.824 | Ag | 2.927 | 4.140 | 8.814 |
| Ag | 1.484 | 2.070 | 10.191 | Ag | 1.474 | 2.076 | 10.212 |
| Ag | 4.371 | 2.070 | 10.191 | Ag | 4.381 | 2.076 | 10.212 |
| Ag | 1.449 | 6.210 | 10.182 | Ag | 1.474 | 6.204 | 10.212 |
| Ag | 4.406 | 6.210 | 10.182 | Ag | 4.381 | 6.204 | 10.212 |
| TE | | -54.55 | | TE | | -53.05 | |
| **Short bridge** | | | | | | | |
| O | 1.464 | 0.000 | 7.441 | | | | |
| Ag | 5.775 | 0.000 | 8.780 | | | | |
| Ag | 3.007 | 0.000 | 8.780 | | | | |
| Ag | 0.003 | 4.140 | 8.823 | | | | |
| Ag | 2.924 | 4.140 | 8.823 | | | | |
| Ag | 1.464 | 2.084 | 10.207 | | | | |
| Ag | 4.391 | 2.058 | 10.207 | | | | |
| Ag | 1.464 | 6.196 | 10.207 | | | | |
| Ag | 4.391 | 6.222 | 10.207 | | | | |
| TE | | -54.11 | | | | TE | |
| **4-fold hollow** | | -54.56 | | **3-fold hollow** | | -54.63 | |
| O | 1.464 | 2.070 | 8.207 | O | 1.464 | 1.333 | 8.159 |
| Ag | 0.006 | 0.151 | 8.752 | Ag | -0.070 | -0.052 | 8.764 |
| Ag | 2.922 | 0.151 | 8.752 | Ag | 2.997 | -0.052 | 8.764 |
| Ag | 0.006 | 3.989 | 8.752 | Ag | -0.008 | 4.153 | 8.809 |
| Ag | 2.922 | 3.989 | 8.752 | Ag | 2.935 | 4.153 | 8.809 |
| Ag | 1.464 | 2.070 | 10.414 | Ag | 1.464 | 2.112 | 10.241 |
| Ag | 4.391 | 2.070 | 10.280 | Ag | 4.391 | 2.070 | 10.233 |
| Ag | 1.464 | 6.210 | 10.099 | Ag | 1.464 | 6.198 | 10.190 |
| Ag | 4.391 | 6.210 | 9.978 | Ag | 4.391 | 6.215 | 10.152 |

(b) Frequencies ($cm^{-1}$)

| | $\nu_1$ | $\nu_2$ | $\nu_3$ |
|---|---|---|---|
| Long bridge | 334 | 266 | 130 |
| Short bridge | 411 | 396 | 72i |
| 4-fold hollow | 338 | 68 | 74i |
| 3-fold hollow | 334 | 278 | 255 |
| Top | 539 | 61 | 132i |

**Table C2S(a).** Structural changes (Å) for the top two layers of the four layer model of Ag(111) surface upon oxygen adsorption at fcc and Octa sites and the corresponding total energies (eV). Fcc – fcc hollow site, Octa – octahedral subsurface site

| Fcc | x | y | z | Octa | x | y | z |
|---|---|---|---|---|---|---|---|
| O | 2.927 | 1.690 | 10.695 | O | 2.927 | 1.690 | 12.780 |
| Ag | -0.019 | -0.011 | 11.963 | Ag | -0.016 | -0.009 | 11.907 |
| Ag | 2.927 | -0.104 | 11.875 | Ag | 2.927 | -0.241 | 11.748 |
| Ag | 5.874 | -0.011 | 11.963 | Ag | 5.871 | -0.009 | 11.907 |
| Ag | 1.373 | 2.587 | 11.875 | Ag | 1.255 | 2.656 | 11.748 |
| Ag | 2.927 | 5.093 | 11.963 | Ag | 2.927 | 5.089 | 11.907 |
| Ag | 4.482 | 2.587 | 11.875 | Ag | 4.600 | 2.656 | 11.748 |
| Ag | 5.859 | 5.068 | 11.967 | Ag | 5.859 | 5.068 | 11.860 |
| Ag | 7.319 | 2.540 | 11.967 | Ag | 7.319 | 2.540 | 11.860 |
| Ag | 8.778 | 5.068 | 11.967 | Ag | 8.778 | 5.068 | 11.860 |
| Ag | 1.469 | 0.848 | 14.315 | Ag | 1.409 | 0.813 | 14.385 |
| Ag | 4.386 | 0.848 | 14.315 | Ag | 4.446 | 0.813 | 14.385 |
| Ag | 7.319 | 0.852 | 14.343 | Ag | 7.319 | 0.849 | 14.312 |
| Ag | 2.927 | 3.374 | 14.315 | Ag | 2.927 | 3.444 | 14.385 |
| Ag | 4.397 | 5.912 | 14.343 | Ag | 4.395 | 5.913 | 14.312 |
| Ag | 5.831 | 3.367 | 14.327 | Ag | 5.853 | 3.380 | 14.311 |
| Ag | 7.319 | 5.943 | 14.327 | Ag | 7.319 | 5.917 | 14.311 |
| Ag | 8.806 | 3.367 | 14.327 | Ag | 8.784 | 3.380 | 14.311 |
| Ag | 10.240 | 5.912 | 14.343 | Ag | 10.242 | 5.913 | 14.312 |
| Ag | 2.927 | 1.690 | 10.695 | Ag | 2.927 | 1.690 | 12.780 |
| TE | | -97.39 | | TE | | -96.71 | |

**Table C2S(b).** Transition state for the diffusion of oxygen from Fcc site to Octahedral site and the corresponding frequencies ($cm^{-1}$)

| Fcc to Octa | x | y | z |
|---|---|---|---|
| O | 2.927 | 1.690 | 11.975 |
| Ag | 13.151 | 7.593 | 11.955 |
| Ag | 7.319 | 7.259 | 11.780 |
| Ag | 10.269 | 7.593 | 11.955 |
| Ag | 9.946 | 2.708 | 11.780 |
| Ag | 11.710 | 5.096 | 11.955 |
| Ag | 4.691 | 2.708 | 11.780 |
| Ag | 5.861 | 5.067 | 11.955 |
| Ag | 7.319 | 2.543 | 11.955 |
| Ag | 8.776 | 5.067 | 11.955 |
| Ag | 1.463 | 0.845 | 14.322 |
| Ag | 4.392 | 0.845 | 14.322 |
| Ag | 7.319 | 0.849 | 14.342 |
| Ag | 2.927 | 3.381 | 14.322 |
| Ag | 4.395 | 5.914 | 14.342 |
| Ag | 5.838 | 3.370 | 14.360 |
| Ag | 7.319 | 5.935 | 14.360 |
| Ag | 8.799 | 3.370 | 14.360 |
| Ag | 10.243 | 5.914 | 14.342 |
| Ag | 2.927 | 1.690 | 11.975 |
| TE | | -96.50 | |

| | $\nu_1$ | $\nu_2$ | $\nu_3$ |
|---|---|---|---|
| Frequencies | 507 | 491 | 211i |

**Table C3S(a).** Cartesian coordinates (Å) of the relaxed top two layers of substrate along with oxygen adsorbed at surface and sub-surface sites of Ag(221), and the corresponding total energies (eV). Fcc – fcc hollow site, Octa – octahedral subsurface site

| Fcc-1[a] | x | y | z | Octa-1[a] | x | y | z |
|---|---|---|---|---|---|---|---|
| O | 1.031 | 1.464 | 7.310 | O | 0.425 | 1.464 | 9.157 |
| Ag | 8.778 | 8.675 | 8.319 | Ag | -0.083 | 8.449 | 8.119 |
| Ag | 8.778 | 3.034 | 8.319 | Ag | -0.083 | 3.261 | 8.119 |
| Ag | 0.030 | 5.855 | 8.374 | Ag | -0.005 | 5.855 | 8.263 |
| Ag | 2.554 | 1.464 | 8.875 | Ag | 2.656 | 1.464 | 8.919 |
| Ag | 2.476 | 4.410 | 9.005 | Ag | 2.461 | 4.405 | 8.927 |
| Ag | 2.476 | 7.299 | 9.005 | Ag | 2.461 | 7.305 | 8.927 |
| Ag | 4.889 | 8.778 | 9.650 | Ag | 4.897 | 8.753 | 9.598 |
| Ag | 4.889 | 2.932 | 9.650 | Ag | 4.897 | 2.957 | 9.598 |
| Ag | 4.878 | 5.855 | 9.639 | Ag | 4.866 | 5.855 | 9.587 |
| Ag | 7.297 | 1.464 | 10.293 | Ag | 7.208 | 1.464 | 10.359 |
| Ag | 7.279 | 4.385 | 10.290 | Ag | 7.265 | 4.404 | 10.292 |
| Ag | 7.279 | 7.325 | 10.290 | Ag | 7.265 | 7.305 | 10.292 |
| Ag | 0.965 | 0.006 | 11.040 | Ag | 0.973 | 8.741 | 11.066 |
| Ag | 0.965 | 2.922 | 11.040 | Ag | 0.973 | 2.969 | 11.066 |
| Ag | 0.955 | 5.855 | 11.065 | Ag | 0.953 | 5.855 | 11.008 |
| Ag | 3.405 | 1.464 | 11.687 | Ag | 3.417 | 1.464 | 11.709 |
| Ag | 3.421 | 4.386 | 11.742 | Ag | 3.415 | 4.397 | 11.702 |
| Ag | 3.421 | 7.323 | 11.742 | Ag | 3.415 | 7.313 | 11.702 |
| Ag | 5.865 | 0.001 | 12.429 | Ag | 5.851 | 8.775 | 12.412 |
| Ag | 5.865 | 2.926 | 12.429 | Ag | 5.851 | 2.935 | 12.412 |
| Ag | 5.869 | 5.855 | 12.414 | Ag | 5.853 | 5.855 | 12.405 |
| Ag | 8.291 | 1.464 | 13.116 | Ag | 8.286 | 1.464 | 13.103 |
| Ag | 8.287 | 4.395 | 13.121 | Ag | 8.285 | 4.396 | 13.093 |
| Ag | 8.287 | 7.315 | 13.121 | Ag | 8.285 | 7.314 | 13.093 |
| TE | | -161.06 | | TE | | -160.33 | |

a – for notations of Fcc-1 and Octa-1 please see the figure 5.4 of chapter 5

**Table C3S(b).** Cartesian coordinates (Å) of the relaxed top two layers of substrate along with oxygen adsorbed at surface and sub-surface sites of Ag(221), and the corresponding total energies (eV). Fcc – fcc hollow site, Octa – octahedral subsurface site

| Fcc-2 [a] | x | y | z | Octa-2 [a] | x | y | z |
|---|---|---|---|---|---|---|---|
| O | 3.571 | 2.927 | 7.908 | O | 3.121 | 2.927 | 9.832 |
| Ag | 8.765 | 8.768 | 8.343 | Ag | 8.634 | 8.746 | 8.273 |
| Ag | 8.753 | 2.927 | 8.373 | Ag | 8.602 | 2.927 | 8.329 |
| Ag | 8.765 | 5.869 | 8.343 | Ag | 8.634 | 5.891 | 8.273 |
| Ag | 2.415 | 1.371 | 8.827 | Ag | 2.223 | 1.271 | 8.718 |
| Ag | 2.415 | 4.484 | 8.827 | Ag | 2.223 | 4.584 | 8.718 |
| Ag | 2.419 | 7.319 | 8.967 | Ag | 2.369 | 7.319 | 8.842 |
| Ag | 4.859 | 8.759 | 9.635 | Ag | 4.819 | 8.773 | 9.575 |
| Ag | 4.987 | 2.927 | 9.526 | Ag | 5.259 | 2.927 | 9.381 |
| Ag | 4.859 | 5.878 | 9.635 | Ag | 4.819 | 5.864 | 9.575 |
| Ag | 7.278 | 1.451 | 10.303 | Ag | 7.314 | 1.401 | 10.335 |
| Ag | 7.278 | 4.403 | 10.303 | Ag | 7.314 | 4.454 | 10.335 |
| Ag | 7.257 | 7.319 | 10.298 | Ag | 7.202 | 7.319 | 10.297 |
| Ag | 0.976 | 0.028 | 11.019 | Ag | 0.959 | 8.773 | 11.018 |
| Ag | 0.981 | 2.927 | 11.028 | Ag | 0.922 | 2.927 | 11.060 |
| Ag | 0.976 | 5.827 | 11.019 | Ag | 0.959 | 5.864 | 11.018 |
| Ag | 3.418 | 1.471 | 11.681 | Ag | 3.412 | 1.428 | 11.735 |
| Ag | 3.418 | 4.384 | 11.681 | Ag | 3.412 | 4.427 | 11.735 |
| Ag | 3.403 | 7.319 | 11.719 | Ag | 3.401 | 7.319 | 11.676 |
| Ag | 5.855 | 0.004 | 12.411 | Ag | 5.838 | 8.786 | 12.411 |
| Ag | 5.840 | 2.927 | 12.360 | Ag | 5.846 | 2.927 | 12.378 |
| Ag | 5.855 | 5.851 | 12.411 | Ag | 5.838 | 5.851 | 12.411 |
| Ag | 8.285 | 1.466 | 13.102 | Ag | 8.285 | 1.461 | 13.106 |
| Ag | 8.285 | 4.388 | 13.102 | Ag | 8.285 | 4.394 | 13.106 |
| Ag | 8.302 | 7.319 | 13.070 | Ag | 8.283 | 7.319 | 13.076 |
| TE | | -160.91 | | TE | | -160.40 | |

a – for notations of Fcc-1 and Octa-1 please see the figure 5.4 of chapter 5

**Table C3S(c).** Cartesian coordinates (Å) of the relaxed top two layers of substrate along with oxygen adsorbed at surface and sub-surface sites of Ag(221), and the corresponding total energies (eV). Fcc – fcc hollow site, Octa – octahedral subsurface site

| Fcc-3 [a] | x | y | z | Octa-3 [a] | x | y | z |
|---|---|---|---|---|---|---|---|
| O | 1.031 | 1.464 | 7.310 | O | 0.425 | 1.464 | 9.157 |
| Ag | 8.778 | 8.675 | 8.319 | Ag | -0.083 | 8.449 | 8.119 |
| Ag | 8.778 | 3.034 | 8.319 | Ag | -0.083 | 3.261 | 8.119 |
| Ag | 0.030 | 5.855 | 8.374 | Ag | -0.005 | 5.855 | 8.263 |
| Ag | 2.554 | 1.464 | 8.875 | Ag | 2.656 | 1.464 | 8.919 |
| Ag | 2.476 | 4.410 | 9.005 | Ag | 2.461 | 4.405 | 8.927 |
| Ag | 2.476 | 7.299 | 9.005 | Ag | 2.461 | 7.305 | 8.927 |
| Ag | 4.889 | 8.778 | 9.650 | Ag | 4.897 | 8.753 | 9.598 |
| Ag | 4.889 | 2.932 | 9.650 | Ag | 4.897 | 2.957 | 9.598 |
| Ag | 4.878 | 5.855 | 9.639 | Ag | 4.866 | 5.855 | 9.587 |
| Ag | 7.297 | 1.464 | 10.293 | Ag | 7.208 | 1.464 | 10.359 |
| Ag | 7.279 | 4.385 | 10.290 | Ag | 7.265 | 4.404 | 10.292 |
| Ag | 7.279 | 7.325 | 10.290 | Ag | 7.265 | 7.305 | 10.292 |
| Ag | 0.965 | 0.006 | 11.040 | Ag | 0.973 | 8.741 | 11.066 |
| Ag | 0.965 | 2.922 | 11.040 | Ag | 0.973 | 2.969 | 11.066 |
| Ag | 0.955 | 5.855 | 11.065 | Ag | 0.953 | 5.855 | 11.008 |
| Ag | 3.405 | 1.464 | 11.687 | Ag | 3.417 | 1.464 | 11.709 |
| Ag | 3.421 | 4.386 | 11.742 | Ag | 3.415 | 4.397 | 11.702 |
| Ag | 3.421 | 7.323 | 11.742 | Ag | 3.415 | 7.313 | 11.702 |
| Ag | 5.865 | 0.001 | 12.429 | Ag | 5.851 | 8.775 | 12.412 |
| Ag | 5.865 | 2.926 | 12.429 | Ag | 5.851 | 2.935 | 12.412 |
| Ag | 5.869 | 5.855 | 12.414 | Ag | 5.853 | 5.855 | 12.405 |
| Ag | 8.291 | 1.464 | 13.116 | Ag | 8.286 | 1.464 | 13.103 |
| Ag | 8.287 | 4.395 | 13.121 | Ag | 8.285 | 4.396 | 13.093 |
| Ag | 8.287 | 7.315 | 13.121 | Ag | 8.285 | 7.314 | 13.093 |
| TE | | -160.84 | | TE | | -160.21 | |

a – for notations of Fcc-1 and Octa-1 please see the figure 5.4 of chapter 5

**Table C4S(a).** Structural changes (Å) of the top two layers for the transition state of the oxygen diffusion from surface Fcc-1 to sub-surface Octa-1 of Ag(221) and the corresponding total energies (eV), frequencies ($cm^{-1}$).

| Fcc-1 to Octa-1 | x | y | z |
|---|---|---|---|
| O | 0.900 | 1.464 | 8.650 |
| Ag | 8.482 | 8.518 | 8.255 |
| Ag | 8.482 | 3.191 | 8.255 |
| Ag | 0.033 | 5.855 | 8.371 |
| Ag | 2.982 | 1.464 | 8.845 |
| Ag | 2.489 | 4.385 | 8.963 |
| Ag | 2.489 | 7.324 | 8.963 |
| Ag | 5.064 | 8.711 | 9.619 |
| Ag | 5.064 | 2.999 | 9.619 |
| Ag | 4.887 | 5.855 | 9.631 |
| Ag | 7.333 | 1.464 | 10.340 |
| Ag | 7.317 | 4.440 | 10.413 |
| Ag | 7.317 | 7.269 | 10.413 |
| Ag | 1.004 | 0.006 | 11.007 |
| Ag | 1.004 | 2.921 | 11.007 |
| Ag | 1.028 | 5.855 | 11.049 |
| Ag | 3.447 | 1.464 | 11.685 |
| Ag | 3.447 | 4.369 | 11.709 |
| Ag | 3.447 | 7.341 | 11.709 |
| Ag | 5.879 | 0.007 | 12.443 |
| Ag | 5.879 | 2.920 | 12.443 |
| Ag | 5.845 | 5.855 | 12.454 |
| Ag | 8.315 | 1.464 | 13.094 |
| Ag | 8.313 | 4.392 | 13.122 |
| Ag | 8.313 | 7.317 | 13.122 |
| TE | | -160.33 | |

| | $\nu_1$ | $\nu_2$ | $\nu_3$ |
|---|---|---|---|
| Frequencies | 437 | 354 | 176i |

**Table C4S(b).** Structural changes (Å) of the top two layers for the transition state of the oxygen diffusion from surface Fcc-2 to sub-surface Octa-2 of Ag(221) and the corresponding total energies (eV), frequencies ($cm^{-1}$).

| Fcc-2 to Octa-2 | x | y | z |
|---|---|---|---|
| O | 3.300 | 2.927 | 9.279 |
| Ag | 8.520 | 8.725 | 8.296 |
| Ag | 8.447 | 2.927 | 8.369 |
| Ag | 8.520 | 5.912 | 8.296 |
| Ag | 2.068 | 1.283 | 8.735 |
| Ag | 2.068 | 4.572 | 8.735 |
| Ag | 2.327 | 7.319 | 8.908 |
| Ag | 4.808 | 8.780 | 9.595 |
| Ag | 5.401 | 2.927 | 9.406 |
| Ag | 4.808 | 5.858 | 9.595 |
| Ag | 7.351 | 1.367 | 10.430 |
| Ag | 7.351 | 4.488 | 10.430 |
| Ag | 7.164 | 7.319 | 10.346 |
| Ag | 0.970 | 8.767 | 11.054 |
| Ag | 0.955 | 2.927 | 11.051 |
| Ag | 0.970 | 5.870 | 11.054 |
| Ag | 3.407 | 1.473 | 11.665 |
| Ag | 3.407 | 4.381 | 11.665 |
| Ag | 3.407 | 7.319 | 11.683 |
| Ag | 5.813 | 0.009 | 12.435 |
| Ag | 5.833 | 2.927 | 12.394 |
| Ag | 5.813 | 5.846 | 12.435 |
| Ag | 8.290 | 1.464 | 13.141 |
| Ag | 8.290 | 4.391 | 13.141 |
| Ag | 8.269 | 7.319 | 13.093 |
| TE | | -160.38 | |

| | $\nu_1$ | $\nu_2$ | $\nu_3$ |
|---|---|---|---|
| Frequencies | 459 | 346 | 133i |

**Table C4S(c).** Structural changes (Å) of the top two layers for the transition state of the oxygen diffusion from surface Fcc-3 to sub-surface Octa-3 of Ag(221) and the corresponding total energies (eV), frequencies ($cm^{-1}$).

| Fcc-3 to Octa-3 | x | y | z |
|---|---|---|---|
| O | 5.600 | 4.391 | 9.881 |
| Ag | 8.618 | 0.000 | 8.288 |
| Ag | 8.768 | 2.895 | 8.278 |
| Ag | 8.768 | 5.888 | 8.278 |
| Ag | 2.258 | 1.388 | 8.866 |
| Ag | 2.312 | 4.391 | 8.924 |
| Ag | 2.258 | 7.395 | 8.866 |
| Ag | 4.788 | 0.000 | 9.589 |
| Ag | 4.574 | 2.659 | 9.365 |
| Ag | 4.574 | 6.124 | 9.365 |
| Ag | 7.213 | 1.471 | 10.275 |
| Ag | 7.639 | 4.391 | 10.394 |
| Ag | 7.213 | 7.312 | 10.275 |
| Ag | 0.891 | 0.000 | 11.056 |
| Ag | 1.044 | 2.876 | 11.060 |
| Ag | 1.044 | 5.906 | 11.060 |
| Ag | 3.416 | 1.454 | 11.713 |
| Ag | 3.447 | 4.391 | 11.687 |
| Ag | 3.416 | 7.328 | 11.713 |
| Ag | 5.854 | 0.000 | 12.396 |
| Ag | 5.858 | 2.924 | 12.398 |
| Ag | 5.858 | 5.858 | 12.398 |
| Ag | 8.271 | 1.474 | 13.098 |
| Ag | 8.301 | 4.391 | 13.140 |
| Ag | 8.271 | 7.308 | 13.098 |
| TE | | -160.05 | |

| | $\nu_1$ | $\nu_2$ | $\nu_3$ |
|---|---|---|---|
| Frequencies | 466 | 432 | 127i |

**Table C5S.** Structural (Å) and energetic (eV) of water adsorbed on Ag(110) surface

| **Top of Ag** | x | y | z |
|---|---|---|---|
| H | 2.165 | 0.773 | 6.267 |
| H | 2.165 | 7.506 | 6.267 |
| O | 2.759 | 0.000 | 6.316 |
| TE | | -63.59 | |
| **Bridge** | | | |
| H | 2.208 | 2.832 | 6.841 |
| H | 2.208 | 1.308 | 6.841 |
| O | 2.664 | 2.070 | 6.423 |
| TE | | -63.41 | |
| **4-fold hollow** | | | |
| H | 1.015 | 2.834 | 6.839 |
| H | 1.015 | 1.306 | 6.839 |
| O | 1.463 | 2.070 | 6.417 |
| TE | | -63.43 | |

**Table C6S.** Structural (Å) and energetic (eV) changes of hydrogen dissociative adsorption over oxygen adsorbed at long bridge site of Ag(110) surface; (b) Vibrational frequencies of the transition state

| | x | y | z |
|---|---|---|---|
| **TS** | | | |
| H | 5.840 | 3.772 | 6.796 |
| H | 5.847 | 2.909 | 7.134 |
| O | 0.000 | 1.941 | 8.054 |
| TE | | -60.84 | |
| **FS** | | | |
| H | 0.000 | 6.065 | 8.873 |
| H | 0.000 | 2.058 | 6.750 |
| O | 0.000 | 2.070 | 7.729 |
| TE | | -62.36 | |

(b) Vibrational frequencies ($cm^{-1}$) of the transition state

| | $\nu_1$ | $\nu_2$ | $\nu_3$ | $\nu_4$ | $\nu_5$ | $\nu_6$ |
|---|---|---|---|---|---|---|
| TS | 1945 | 1235 | 993 | 526 | 25 | 951i |

**Table C7S.** Structural (Å) and energetic (eV) changes of hydrogen adsorption over oxygen adsorbed at sub-surface site of Ag(111) surface with O coverage of ¼.

| | x | y | z |
|---|---|---|---|
| Fcc1 | 2.927 | 1.690 | 10.525 |
| TE | | -58.88 | |
| Fcc2 | 7.616 | 4.397 | 10.588 |
| TE | | -59.80 | |
| Hcp1 | 4.657 | 0.691 | 10.775 |
| TE | | -59.59 | |
| Hcp2 | 5.855 | 3.380 | 10.574 |
| TE | | -59.77 | |

**Table C8S(a).** Structural (Å) and energetic (eV) changes of hydrogen dissociative adsorption over oxygen adsorbed at sub-surface site of Ag(111) surface (b) Vibrational frequency of the transition state

| | x | y | z |
|---|---|---|---|
| **IS** | | | |
| H | 4.948 | 3.420 | 8.171 |
| H | 5.597 | 3.047 | 8.176 |
| TE | | -63.28 | |
| **TS** | | | |
| H | 4.501 | 4.214 | 10.150 |
| H | 5.639 | 3.384 | 10.007 |
| TE | | -62.26 | |
| **FS** | | | |
| H | 4.385 | 5.919 | 10.440 |
| H | 0.367 | 3.168 | 10.708 |
| TE | | -63.06 | |

**Table C8S(b).** Vibrational frequencies ($cm^{-1}$) of the transition state of the above table.

| | $\nu_1$ | $\nu_2$ | $\nu_3$ | $\nu_4$ | $\nu_5$ | $\nu_6$ |
|---|---|---|---|---|---|---|
| TS | 1460 | 1073 | 893 | 300 | 161 | 784i |

**Table C9S.** Structural (Å) and energetic (eV) changes of hydrogen dissociative adsorption on hydroxyl adsorbed at long bridge site of Ag(110) surface (b) Vibrational frequencies ($cm^{-1}$) of the transition state

| | x | y | z |
|---|---|---|---|
| **TS** | | | |
| H | 1.464 | 2.461 | 7.243 |
| H | 1.483 | 3.343 | 7.328 |
| H | 1.375 | 0.595 | 6.403 |
| O | 1.437 | 0.992 | 7.293 |
| TE | | -66.08 | |
| **FS** | | | |
| H | 2.156 | 0.776 | 6.232 |
| H | 2.152 | 7.507 | 6.219 |
| H | -0.003 | 6.151 | 8.793 |
| O | 2.744 | -0.001 | 6.308 |
| TE | | -66.71 | |

(b) Vibrational frequencies ($cm^{-1}$) of the transition state

| | $\nu_1$ | $\nu_2$ | $\nu_3$ | $\nu_4$ | $\nu_5$ | $\nu_6$ |
|---|---|---|---|---|---|---|
| TS | 2235 | 1139 | 1055 | 607 | 12 | 461i |

**Table C10S.** Structural (Å) and energetic (eV) changes of hydrogen dissociation in perpendicular to the added row and on oxygen atom of *p*(2x1)O/Ag(110) surface. (b) Vibrational frequencies ($cm^{-1}$) of the transition state

| | x | y | z |
|---|---|---|---|
| **TS** | | | |
| H | 1.732 | 4.140 | 4.499 |
| H | 2.355 | 4.140 | 5.510 |
| O | 1.444 | 0.000 | 7.134 |
| O | 1.646 | 4.140 | 6.266 |
| Ag | 1.498 | 2.151 | 7.224 |
| Ag | 1.498 | 6.129 | 7.224 |
| TE | | -71.32 | |
| **FS** | | | |
| H | 4.391 | 4.140 | 7.768 |
| H | 1.464 | 4.140 | 5.431 |
| O | 1.464 | 0.000 | 7.142 |
| O | 1.464 | 4.140 | 6.405 |
| Ag | 1.464 | 2.120 | 7.187 |
| Ag | 1.464 | 6.159 | 7.187 |
| TE | | -73.53 | |

(b) Vibrational frequencies ($cm^{-1}$) of the transition state

| | $\nu_1$ | $\nu_2$ | $\nu_3$ | $\nu_4$ | $\nu_5$ | $\nu_6$ |
|---|---|---|---|---|---|---|
| TS | 2673 | 992 | 712 | 332 | 162 | 850i |

**Table C11S.** Structural (Å) and energetic (eV) changes of hydrogen diffusion from terrace short bridge to the added row hydroxyl resulting in water formation over *p*(2x1)O/Ag(110) surface. (b) Vibrational frequencies ($cm^{-1}$) of the transition state

| **IS** | x | y | z |
|---|---|---|---|
| H | 4.391 | 4.140 | 7.768 |
| H | 1.464 | 4.140 | 5.431 |
| O | 1.464 | 0.000 | 7.142 |
| O | 1.464 | 4.140 | 6.405 |
| Ag | 1.464 | 2.120 | 7.187 |
| Ag | 1.464 | 6.159 | 7.187 |
| TE | | -73.53 | |
| **TS** | | | |
| H | 2.359 | 4.140 | 5.180 |
| H | 3.473 | 4.140 | 7.210 |
| O | 1.425 | 0.000 | 7.136 |
| O | 2.121 | 4.140 | 6.132 |
| Ag | 1.602 | 2.161 | 7.124 |
| Ag | 1.602 | 6.119 | 7.124 |
| TE | | -72.66 | |
| **FS** | | | |
| H | 0.539 | 4.140 | 4.564 |
| H | 1.028 | 4.140 | 6.045 |
| O | 1.447 | 0.000 | 7.072 |
| O | 0.216 | 4.140 | 5.484 |
| Ag | 1.537 | 2.165 | 7.398 |
| Ag | 1.537 | 6.115 | 7.398 |
| TE | | -74.22 | |

(b) Vibrational frequencies ($cm^{-1}$) of the transition state

| | $\nu_1$ | $\nu_2$ | $\nu_3$ | $\nu_4$ | $\nu_5$ | $\nu_6$ |
|---|---|---|---|---|---|---|
| TS | 3513 | 1356 | 667 | 414 | 269 | 832i |

**Table C12S.** Structural (Å) and energetic (eV) changes of hydrogen diffusion from terrace short bridge to the added row hydroxyl resulting in water formation over *p*(2x1)O/Ag(110) surface. (b) Vibrational frequencies ($cm^{-1}$) of the transition state

| **IS**[a] | x | y | z |
|---|---|---|---|
| H | 1.464 | 0.003 | 5.466 |
| H | 1.464 | 4.137 | 5.466 |
| H | 1.464 | 8.280 | 5.458 |
| O | 1.464 | 12.418 | 6.441 |
| O | 1.464 | 4.142 | 6.441 |
| O | 1.464 | 8.280 | 6.434 |
| Ag | 1.464 | 2.070 | 7.344 |
| Ag | 1.464 | 6.213 | 7.342 |
| Ag | 1.464 | 10.347 | 7.342 |
| TE | | -112.70 | |
| **TS** | | | |
| H | 2.182 | 3.083 | 5.763 |
| H | 1.465 | 3.594 | 5.912 |
| H | 1.545 | 12.416 | 5.531 |
| H | 5.498 | 4.613 | 5.772 |
| H | 1.557 | 8.286 | 5.485 |
| O | 1.427 | 12.410 | 6.499 |
| O | 0.398 | 4.450 | 6.370 |
| O | 1.550 | 8.287 | 6.459 |
| Ag | 1.792 | 2.064 | 7.341 |
| Ag | 1.378 | 6.232 | 7.364 |
| Ag | 1.433 | 10.340 | 7.355 |
| TE | | -119.25 | |
| **FS** | | | |
| H | 1.512 | 4.140 | 7.275 |
| H | 0.493 | 4.140 | 4.065 |
| H | 1.301 | 0.097 | 5.503 |
| H | 0.392 | 4.140 | 5.604 |
| H | 1.301 | 8.183 | 5.503 |
| O | 1.419 | 0.096 | 6.473 |
| O | 5.699 | 4.140 | 4.791 |
| O | 1.419 | 8.184 | 6.473 |
| Ag | 1.487 | 2.174 | 7.304 |
| Ag | 1.487 | 6.106 | 7.304 |
| Ag | 1.480 | 10.350 | 7.345 |
| TE | | -120.00 | |

a – Only substrate TE and the structural parameters are shown. Hydrogen gas phase energy has to be added while calculating the rest of energetic

(b) Vibrational frequencies ($cm^{-1}$) of the transition state

| | $\nu_1$ | $\nu_2$ | $\nu_3$ | $\nu_4$ | $\nu_5$ | $\nu_6$ |
|---|---|---|---|---|---|---|
| TS | 2283 | 1269 | 1071 | 770 | 246 | 493i |

**Table C13S.** Structural (Å) and energetic (eV) changes of hydrogen diffusion from added row Ag of *p*(2x1)O/Ag(110) surface to the neighbouring terrace site, long bridge. (b) Vibrational frequencies ($cm^{-1}$) of the transition state

| **IS** | x | y | z |
|---|---|---|---|
| H | 1.464 | 8.176 | 5.455 |
| H | 1.464 | 2.330 | 5.180 |
| O | 1.464 | 8.243 | 6.427 |
| O | 1.464 | 4.055 | 7.117 |
| Ag | 1.464 | 2.037 | 6.820 |
| Ag | 1.464 | 6.233 | 7.353 |
| TE | | -72.47 | |
| **TS** | | | |
| H | 2.352 | 1.185 | 5.747 |
| H | 1.382 | 4.063 | 5.316 |
| O | 1.443 | 8.154 | 7.102 |
| O | 1.220 | 4.036 | 6.277 |
| Ag | 1.565 | 2.007 | 6.949 |
| Ag | 1.383 | 6.041 | 7.056 |
| TE | | -72.29 | |
| **FS** | | | |
| H | 4.391 | 2.985 | 8.550 |
| H | 1.464 | 4.212 | 5.256 |
| O | 1.464 | 0.003 | 7.160 |
| O | 1.464 | 4.110 | 6.224 |
| Ag | 1.464 | 2.071 | 6.829 |
| Ag | 1.464 | 6.071 | 7.342 |
| TE | | -73.60 | |

(b) Vibrational frequencies ($cm^{-1}$) of the transition state

| | $\nu_1$ | $\nu_2$ | $\nu_3$ |
|---|---|---|---|
| TS | 1586 | 226 | 279i |

**Table C14S.** Structural (Å) and energetic (eV) changes of hydrogen diffusion from added row Ag of *p*(2x1)O/Ag(110) surface to the neighbouring terrace site, short bridge. (b) Vibrational frequencies ($cm^{-1}$) of the transition state

| **IS** | x | y | z |
|---|---|---|---|
| H | 1.464 | 8.176 | 5.455 |
| H | 1.464 | 2.330 | 5.180 |
| O | 1.464 | 8.243 | 6.427 |
| O | 1.464 | 4.055 | 7.117 |
| Ag | 1.464 | 2.037 | 6.820 |
| Ag | 1.464 | 6.233 | 7.353 |
| TE | | -72.47 | |
| **TS** | | | |
| H | 2.501 | 2.114 | 5.709 |
| H | 1.233 | 4.079 | 5.461 |
| O | 1.449 | 8.183 | 7.142 |
| O | 0.765 | 4.099 | 6.317 |
| Ag | 1.382 | 2.023 | 6.923 |
| Ag | 1.204 | 6.082 | 7.056 |
| TE | | -72.33 | |
| **FS** | | | |
| H | 0.539 | 4.140 | 4.564 |
| H | 1.028 | 4.140 | 6.045 |
| O | 1.447 | 0.000 | 7.072 |
| O | 0.216 | 4.140 | 5.484 |
| Ag | 1.537 | 2.165 | 7.398 |
| Ag | 1.537 | 6.115 | 7.398 |
| TE | | -74.22 | |

(b) Vibrational frequencies ($cm^{-1}$) of the transition state

| | $\nu_1$ | $\nu_2$ | $\nu_3$ |
|---|---|---|---|
| TS | 1585 | 386 | 124i |

# Appendix D

# Supplementary Material for Acrolein adsorption on Ag Surfaces

**Table D1S.** Cartesian coordinates (Å) of $O_{oss}$/Ag(111) surface and the total energy (eV)

| | | | | Ag(111)_sub(O) | | | |
|---|---|---|---|---|---|---|---|
| | x | y | z | | x | y | z |
| O | 2.927 | 1.690 | 12.899 | Ag | 4.391 | 0.845 | 21.512 |
| O | 7.319 | 4.225 | 12.899 | Ag | 7.319 | 0.845 | 21.512 |
| O | 11.710 | 6.761 | 12.899 | Ag | 2.927 | 3.380 | 21.512 |
| Ag | 0.107 | 0.062 | 11.466 | Ag | 4.391 | 5.916 | 21.512 |
| Ag | 7.319 | 7.482 | 11.466 | Ag | 5.855 | 3.380 | 21.512 |
| Ag | 5.748 | 0.062 | 11.466 | Ag | 7.319 | 5.916 | 21.512 |
| Ag | 10.139 | 2.597 | 11.466 | | | | |
| Ag | 2.927 | 4.947 | 11.466 | | | | |
| Ag | 4.498 | 2.597 | 11.466 | | | | |
| Ag | 5.748 | 5.132 | 11.466 | | | | |
| Ag | 7.319 | 2.412 | 11.466 | | | | |
| Ag | 8.889 | 5.132 | 11.466 | | | | |
| Ag | 1.389 | 0.802 | 14.336 | | | | |
| Ag | 4.465 | 0.802 | 14.336 | | | | |
| Ag | 7.319 | 0.931 | 14.336 | | | | |
| Ag | 2.927 | 3.466 | 14.336 | | | | |
| Ag | 4.465 | 5.873 | 14.336 | | | | |
| Ag | 5.781 | 3.337 | 14.336 | | | | |
| Ag | 7.319 | 6.001 | 14.336 | | | | |
| Ag | 8.857 | 3.337 | 14.336 | | | | |
| Ag | 10.172 | 5.873 | 14.336 | | | | |
| Ag | 2.927 | 1.690 | 16.732 | | | | |
| Ag | 5.855 | 1.690 | 16.732 | | | | |
| Ag | 8.782 | 1.690 | 16.732 | | | | |
| Ag | 4.391 | 4.225 | 16.732 | | | | |
| Ag | 5.855 | 6.761 | 16.732 | | | | |
| Ag | 7.319 | 4.225 | 16.732 | | | | |
| Ag | 8.782 | 6.761 | 16.732 | | | | |
| Ag | 10.246 | 4.225 | 16.732 | | | | |
| Ag | 11.710 | 6.761 | 16.732 | | | | |
| Ag | 0.000 | 0.000 | 19.122 | | | | |
| Ag | 2.927 | 0.000 | 19.122 | | | | |
| Ag | 5.855 | 0.000 | 19.122 | | | | |
| Ag | 1.464 | 2.535 | 19.122 | | | | |
| Ag | 2.927 | 5.070 | 19.122 | | | | |
| Ag | 4.391 | 2.535 | 19.122 | | | | |
| Ag | 5.855 | 5.070 | 19.122 | | | | |
| Ag | 7.319 | 2.535 | 19.122 | | | | |
| Ag | 8.782 | 5.070 | 19.122 | | | | |
| Ag | 1.464 | 0.845 | 21.512 | | | | |
| | | | | | | -130.527 | |

**Note:** Five-layer Ag(111) surface with top 2-layer relaxed along with subsurface oxygen with a oxygen coverage of 1/3

**Table D2S.** Cartesian coordinates (Å) of substrate atoms of *p*(4x1)O/Ag(110), O(LB)/Ag(110) surfaces and the resulting total energies (eV)

| | *p*(4x1)O/Ag(110) | | | O(lb)/Ag(110) | | |
|---|---|---|---|---|---|---|
| | x | y | z | x | y | z |
| H | 1.412 | 4.142 | 5.435 | 0.003 | 6.206 | 8.681 |
| H | 1.690 | 0.003 | 5.424 | 0.496 | 2.071 | 6.895 |
| O | 1.595 | 0.002 | 6.397 | 8.782 | 2.071 | 7.739 |
| O | 1.423 | 4.142 | 6.412 | | | |
| Ag | 1.474 | 2.067 | 7.315 | | | |
| Ag | 1.474 | 6.217 | 7.315 | | | |
| TE | | -122.82 eV | | | -86.25 eV | |
| | | | | | | |
| H | 1.673 | 0.003 | 5.462 | 0.443 | 2.073 | 6.866 |
| O | 1.589 | 0.003 | 6.434 | 8.805 | 2.074 | 7.751 |
| O | 1.418 | 4.143 | 7.092 | | | |
| Ag | 1.488 | 2.035 | 7.179 | | | |
| Ag | 1.488 | 6.250 | 7.178 | | | |
| TE | | -118.11 eV | | | -83.15 eV | |
| | | | | | | |
| O | 1.440 | 8.278 | 7.044 | 8.694 | 2.071 | 8.317 |
| O | 1.458 | 4.138 | 7.057 | | | |
| Ag | 1.478 | 2.066 | 7.175 | | | |
| Ag | 1.513 | 6.209 | 7.170 | | | |
| TE | | -113.70 eV | | | -78.27 eV | |

**Note:** The substrate for added row surface remains the same as of the clean Ag(110) surface, and for O(LB)/Ag(110) surface the substrate is designed for (3x2) unit cell

**Table D3S.** Energies (eV) and frequencies ($cm^{-1}$) of acrolein, its intermediates and products formed during hydrogenation.

| | H→O | H→C1 | H→C2 | H→C3 | acrolein | propenol | propanal |
|---|---|---|---|---|---|---|---|
| 1 | 3569 | 3159 | 3168 | 3569 | 3165 | 3733 | 3060 |
| 2 | 3156 | 3090 | 3068 | 3156 | 3110 | 3159 | 3045 |
| 3 | 3106 | 3064 | 3006 | 3106 | 3078 | 3089 | 3023 |
| 4 | 3060 | 2802 | 2923 | 3061 | 2808 | 3078 | 2957 |
| 5 | 3007 | 2682 | 2798 | 3006 | 1708 | 2944 | 2932 |
| 6 | 1552 | 1632 | 1678 | 1553 | 1630 | 2911 | 2776 |
| 7 | 1454 | 1409 | 1422 | 1454 | 1417 | 1663 | 1746 |
| 8 | 1358 | 1278 | 1396 | 1358 | 1347 | 1456 | 1462 |
| 9 | 1274 | 1226 | 1332 | 1273 | 1272 | 1426 | 1458 |
| 10 | 1253 | 1211 | 1216 | 1254 | 1153 | 1375 | 1407 |
| 11 | 1228 | 1102 | 1173 | 1231 | 1012 | 1287 | 1384 |
| 12 | 1081 | 1042 | 1093 | 1084 | 993 | 1240 | 1368 |
| 13 | 914 | 1011 | 1067 | 915 | 971 | 1201 | 1278 |
| 14 | 911 | 944 | 963 | 912 | 910 | 1128 | 1231 |
| 15 | 733 | 928 | 841 | 735 | 604 | 1019 | 1120 |
| 16 | 697 | 860 | 749 | 701 | 555 | 1004 | 1087 |
| 17 | 543 | 622 | 620 | 539 | 305 | 949 | 1025 |
| 18 | 515 | 535 | 489 | 524 | 186 | 926 | 906 |
| 19 | 442 | 414 | 315 | 457 | 134 | 905 | 870 |
| 20 | 282 | 300 | 190 | 279 | 74 | 637 | 684 |
| 21 | 238 | 129 | 106 | 243 | 23 | 443 | 505 |
| 22 | 159 | 122 | 58 | 158 | | 324 | 313 |
| 23 | 67 | 74 | 26 | 98 | | 272 | 179 |
| 24 | 61 | 52 | 3 | 5 | | 144 | 96 |
| 25 | | | | | | 101 | 86 |
| 26 | | | | | | 45 | 29 |
| 27 | | | | | | 15 | 1 |
| TE | -50.56 | -49.40 | -50.09 | -50.77 | -47.53 | -55.15 | -55.78 |

**Table D4S.** Cartesian coordinates (Å) of acrolein, its intermediates and the products adsorbed on Ag(110) surface

| H→O | x | y | z | H→C1 | x | y | z |
|---|---|---|---|---|---|---|---|
| H | 3.557 | 3.083 | 6.396 | | 9.834 | 3.000 | 6.372 |
| H | 2.842 | 4.756 | 6.260 | | 9.510 | 4.821 | 6.149 |
| H | 6.187 | 2.965 | 6.112 | | 7.947 | 1.473 | 6.669 |
| H | 5.026 | 5.815 | 6.495 | | 7.084 | 4.420 | 6.271 |
| H | 7.295 | 5.596 | 6.087 | | 6.657 | 1.995 | 5.554 |
| C | 4.966 | 4.719 | 6.489 | | 7.782 | 3.583 | 6.393 |
| C | 6.141 | 4.046 | 6.243 | | 7.141 | 2.233 | 6.529 |
| C | 3.649 | 4.139 | 6.664 | | 9.118 | 3.824 | 6.356 |
| O | 7.342 | 4.634 | 5.917 | | 6.195 | 2.185 | 7.573 |
| TE | | -148.08 | | | | -148.13 | |
| H→C2 | | | | H→C3 | | | |
| H | 6.352 | 3.267 | 6.292 | | 7.151 | 4.836 | 5.777 |
| H | 6.936 | 4.941 | 6.454 | | 5.445 | 5.233 | 6.028 |
| H | 3.996 | 3.055 | 4.855 | | 8.088 | 2.783 | 6.556 |
| H | 5.134 | 5.168 | 4.886 | | 5.010 | 2.708 | 6.614 |
| H | 4.387 | 5.670 | 6.434 | | 5.914 | 4.195 | 4.675 |
| C | 4.841 | 4.825 | 5.896 | | 5.993 | 3.192 | 6.599 |
| C | 3.847 | 3.733 | 5.727 | | 7.090 | 2.335 | 6.778 |
| C | 6.082 | 4.275 | 6.639 | | 6.131 | 4.427 | 5.732 |
| O | 2.921 | 3.488 | 6.503 | | 7.091 | 1.098 | 7.138 |
| TE | | -148.08 | | | | -148.84 | |
| Propenol | | | | Propanal | | | |
| H | 6.960 | 3.729 | 5.952 | | 6.386 | 4.872 | 4.296 |
| H | 6.222 | 5.406 | 6.275 | | 5.182 | 5.993 | 3.623 |
| H | 5.459 | 1.839 | 5.435 | | 3.809 | 3.914 | 4.421 |
| H | 3.956 | 4.464 | 6.077 | | 4.226 | 6.327 | 5.989 |
| H | 3.116 | 1.435 | 4.732 | | 6.407 | 6.581 | 4.763 |
| H | 4.156 | 1.913 | 6.653 | | 5.383 | 5.188 | 6.625 |
| C | 4.835 | 3.817 | 5.986 | | 4.818 | 5.440 | 5.701 |
| C | 4.538 | 2.378 | 5.720 | | 3.846 | 4.323 | 5.460 |
| C | 6.069 | 4.340 | 6.108 | | 5.748 | 5.736 | 4.529 |
| O | 3.546 | 2.307 | 4.685 | | 3.106 | 3.836 | 6.310 |
| TE | | -152.15 eV | | | | -152.79 eV | |
| Acrolein | | | | | | | |
| H | 1.421 | 4.774 | 6.325 | | | | |
| H | 2.030 | 3.018 | 6.314 | | | | |
| H | 3.778 | 5.600 | 6.451 | | | | |
| H | 4.459 | 2.550 | 6.304 | | | | |
| C | 4.698 | 3.637 | 6.364 | | | | |
| C | 3.556 | 4.531 | 6.456 | | | | |
| C | 2.251 | 4.079 | 6.437 | | | | |
| O | 5.889 | 4.022 | 6.309 | | | | |
| TE | | -144.50 | | | | | |

**Table D5S.** Cartesian coordinates (Å) of TS's, acrolein hydrogenation on Ag(110) surface

| H→O | x | y | z | H→C1 | x | y | z |
|---|---|---|---|---|---|---|---|
| H | 2.854 | 3.414 | 6.086 | | 2.172 | 3.298 | 5.304 |
| H | 2.376 | 5.200 | 6.266 | | 1.495 | 5.022 | 5.494 |
| H | 5.299 | 2.799 | 6.011 | | 4.523 | 2.800 | 5.933 |
| H | 4.774 | 5.827 | 6.532 | | 3.672 | 5.771 | 6.431 |
| H | 7.501 | 4.162 | 7.499 | | 4.258 | 3.323 | 7.759 |
| C | 4.485 | 4.780 | 6.388 | | 3.505 | 4.731 | 6.134 |
| C | 5.557 | 3.862 | 6.179 | | 4.675 | 3.829 | 6.327 |
| C | 3.140 | 4.431 | 6.359 | | 2.330 | 4.333 | 5.617 |
| O | 6.795 | 4.214 | 6.186 | | 5.865 | 4.300 | 6.411 |
| TE | | -146.84 | | | | -146.98 | |
| H→C2 | | | | H→C3 | | | |
| H | 6.288 | 2.845 | 5.946 | | 4.443 | 2.814 | 5.650 |
| H | 6.769 | 4.646 | 5.903 | | 4.816 | 4.617 | 5.480 |
| H | 4.003 | 2.172 | 5.594 | | 2.171 | 2.030 | 5.895 |
| H | 4.332 | 5.271 | 5.849 | | 2.364 | 5.151 | 5.801 |
| H | 4.153 | 4.386 | 7.429 | | 4.655 | 3.928 | 7.400 |
| C | 4.622 | 4.242 | 6.096 | | 2.726 | 4.114 | 5.783 |
| C | 3.616 | 3.220 | 5.662 | | 1.780 | 3.079 | 6.036 |
| C | 5.992 | 3.893 | 6.004 | | 4.103 | 3.849 | 5.799 |
| O | 2.450 | 3.474 | 5.404 | | 0.586 | 3.232 | 6.424 |
| TE | | -146.88 | | | | -147.28 | |
| HC1; H→O | | | | HO;H→C1 | | | |
| H | 7.187 | 3.632 | 6.242 | | 6.800 | 3.431 | 6.331 |
| H | 6.919 | 5.458 | 6.489 | | 5.726 | 4.945 | 6.390 |
| H | 5.223 | 2.141 | 6.108 | | 5.532 | 1.126 | 5.836 |
| H | 4.485 | 5.135 | 6.424 | | 3.696 | 3.617 | 6.226 |
| H | 3.947 | 2.959 | 5.176 | | 2.789 | 1.766 | 5.405 |
| H | 4.138 | 1.325 | 8.257 | | 4.536 | 0.809 | 7.696 |
| C | 5.149 | 4.267 | 6.344 | | 4.664 | 3.082 | 6.261 |
| C | 4.461 | 2.947 | 6.162 | | 4.617 | 1.694 | 6.026 |
| C | 6.491 | 4.458 | 6.402 | | 5.808 | 3.857 | 6.510 |
| O | 3.543 | 2.677 | 7.202 | | 3.523 | 1.125 | 5.396 |
| TE | | -150.88 | | | | -150.89 | |
| HC3; H→C2 | -151.40 | | | HC2; H→C3 | -150.43 | | |
| H | 9.681 | 1.794 | 4.111 | | 3.615 | 4.584 | 5.830 |
| H | 8.038 | 2.458 | 4.066 | | 2.798 | 5.836 | 6.810 |
| H | 6.642 | 1.131 | 5.461 | | 1.471 | 2.266 | 5.363 |
| H | 9.493 | 1.416 | 6.620 | | 0.635 | 5.090 | 6.305 |
| H | 9.362 | 3.385 | 4.821 | | 1.477 | 4.679 | 4.776 |
| H | 8.359 | 2.994 | 7.482 | | 4.176 | 4.093 | 7.641 |
| C | 8.648 | 1.688 | 5.980 | | 1.419 | 4.454 | 5.861 |
| C | 7.492 | 0.947 | 6.141 | | 0.926 | 3.041 | 5.948 |
| C | 8.943 | 2.380 | 4.686 | | 2.776 | 4.785 | 6.502 |
| O | 7.309 | 0.041 | 7.057 | | 11.660 | 2.708 | 6.617 |

**Table D6S.** Cartesian coordinates (Å) of acrolein, its intermediates and the products adsorbed on O(lb)/Ag(110) surface

| H→O | x | y | z | H→C1 | x | y | z |
|---|---|---|---|---|---|---|---|
| H | 1.425 | 7.396 | 6.388 | | 0.884 | 3.363 | 5.897 |
| H | 8.687 | 0.087 | 6.135 | | 0.405 | 5.156 | 5.893 |
| H | 1.228 | 4.862 | 5.907 | | 7.874 | 1.646 | 6.224 |
| H | 7.298 | 6.332 | 6.210 | | 6.844 | 4.569 | 6.275 |
| H | 7.280 | 4.055 | 5.748 | | 1.409 | 1.475 | 6.714 |
| C | 8.391 | 6.251 | 6.238 | | 7.596 | 3.770 | 6.223 |
| C | 0.153 | 5.034 | 5.955 | | 7.052 | 2.376 | 6.360 |
| C | 0.343 | 7.449 | 6.534 | | 0.106 | 4.116 | 6.031 |
| O | 8.230 | 3.924 | 5.551 | | 6.402 | 2.193 | 7.611 |
| TE | | -133.98 | | | | 134.51 | |
| H→C2 | | | | H→C3 | | | |
| H | 0.964 | 3.597 | 6.164 | | 7.061 | 4.910 | 5.772 |
| H | 0.789 | 5.367 | 6.282 | | 5.399 | 5.479 | 5.972 |
| H | 7.257 | 2.181 | 5.350 | | 7.696 | 2.634 | 6.295 |
| H | 7.079 | 5.164 | 6.090 | | 4.656 | 3.033 | 6.485 |
| H | 7.879 | 4.433 | 4.674 | | 5.815 | 4.448 | 4.594 |
| C | 7.726 | 4.334 | 5.770 | | 5.698 | 3.375 | 6.487 |
| C | 6.948 | 3.058 | 5.952 | | 6.655 | 2.336 | 6.544 |
| C | 0.295 | 4.409 | 6.480 | | 6.006 | 4.615 | 5.668 |
| O | 5.916 | 2.985 | 6.632 | | 6.465 | 1.106 | 6.829 |
| TE | | -134.10 | | | | -135.09 | |
| Propenol | | | | Propanal | | | |
| H | 6.762 | 3.581 | 5.873 | | 7.291 | 5.220 | 4.045 |
| H | 5.820 | 5.173 | 6.089 | | 5.831 | 5.790 | 3.201 |
| H | 5.303 | 1.564 | 5.040 | | 6.035 | 3.417 | 5.598 |
| H | 3.685 | 3.963 | 5.944 | | 4.660 | 6.191 | 5.383 |
| H | 2.850 | 0.864 | 5.618 | | 6.805 | 6.923 | 4.169 |
| H | 4.628 | 1.441 | 6.682 | | 6.159 | 5.779 | 6.267 |
| C | 4.636 | 3.420 | 5.889 | | 5.569 | 5.576 | 5.354 |
| C | 4.501 | 1.942 | 5.696 | | 5.192 | 4.120 | 5.367 |
| C | 5.802 | 4.086 | 5.995 | | 6.426 | 5.894 | 4.118 |
| O | 3.217 | 1.631 | 5.144 | | 4.081 | 3.680 | 5.115 |
| TE | | -133.61 | | | | -134.13 | |
| Acrolein | | | | | | | |
| H | 5.698 | 3.218 | 6.152 | | | | |
| H | 5.673 | 5.081 | 6.139 | | | | |
| H | 3.627 | 1.949 | 6.001 | | | | |
| H | 3.187 | 5.052 | 5.931 | | | | |
| C | 3.757 | 4.124 | 6.034 | | | | |
| C | 3.021 | 2.877 | 5.860 | | | | |
| C | 5.118 | 4.144 | 6.185 | | | | |
| O | 8.678 | 2.060 | 7.767 | | | | |
| TE | | -133.95 | | | | | |

**Table D7S.** Cartesian coordinates (Å) of acrolein, its intermediates and the products adsorbed on *p*(4x1)O/Ag(110)

| H→O | x | y | z | H→C1 | x | y | z |
|---|---|---|---|---|---|---|---|
| H | 10.204 | 7.458 | 6.524 | | 9.887 | 3.035 | 6.315 |
| H | 8.676 | 0.131 | 6.242 | | 9.590 | 4.862 | 6.167 |
| H | 10.000 | 4.852 | 6.149 | | 7.985 | 1.515 | 6.491 |
| H | 7.303 | 6.374 | 6.336 | | 7.157 | 4.498 | 6.329 |
| H | 7.251 | 4.145 | 5.838 | | 6.564 | 2.143 | 5.618 |
| C | 8.395 | 6.294 | 6.403 | | 7.843 | 3.645 | 6.400 |
| C | 8.928 | 5.048 | 6.191 | | 7.196 | 2.295 | 6.518 |
| C | 9.120 | 7.504 | 6.662 | | 9.179 | 3.866 | 6.333 |
| O | 8.207 | 3.949 | 5.779 | | 6.395 | 2.181 | 7.687 |
| TE | | -169.28 | | | | -169.53 | |
| H→C2 | | | | H→C3 | | | |
| H | 9.576 | 3.271 | 6.357 | | 7.160 | 4.991 | 5.891 |
| H | 9.638 | 5.049 | 6.428 | | 5.452 | 5.411 | 6.091 |
| H | 7.235 | 2.178 | 5.295 | | 8.017 | 2.875 | 6.581 |
| H | 7.093 | 5.136 | 6.158 | | 4.935 | 2.887 | 6.552 |
| H | 7.941 | 4.431 | 4.745 | | 5.955 | 4.430 | 4.711 |
| C | 7.703 | 4.286 | 5.817 | | 5.933 | 3.338 | 6.591 |
| C | 6.912 | 3.032 | 5.933 | | 7.004 | 2.440 | 6.770 |
| C | 9.009 | 4.172 | 6.629 | | 6.134 | 4.606 | 5.785 |
| O | 5.977 | 2.858 | 6.717 | | 6.971 | 1.199 | 7.096 |
| TE | | -169.36 | | | | -170.14 | |
| Propenol | | | | Propanal | | | |
| H | 6.759 | 3.584 | 5.871 | | 7.286 | 5.217 | 4.045 |
| H | 5.822 | 5.174 | 6.092 | | 5.825 | 5.791 | 3.207 |
| H | 5.299 | 1.565 | 5.037 | | 6.034 | 3.417 | 5.608 |
| H | 3.682 | 3.968 | 5.945 | | 4.662 | 6.194 | 5.391 |
| H | 2.834 | 0.832 | 5.627 | | 6.806 | 6.921 | 4.171 |
| H | 4.624 | 1.446 | 6.678 | | 6.162 | 5.777 | 6.272 |
| C | 4.631 | 3.425 | 5.882 | | 5.570 | 5.577 | 5.361 |
| C | 4.491 | 1.943 | 5.690 | | 5.191 | 4.121 | 5.368 |
| C | 5.798 | 4.088 | 5.994 | | 6.423 | 5.894 | 4.122 |
| O | 3.217 | 1.617 | 5.143 | | 4.085 | 3.680 | 5.105 |
| TE | | -169.23 | | | | -169.51 | |
| Acrolein | | | | | | | |
| H | 7.401 | 3.437 | 6.274 | | | | |
| H | 7.157 | 5.275 | 6.444 | | | | |
| H | 5.587 | 1.972 | 5.703 | | | | |
| H | 4.727 | 4.980 | 5.906 | | | | |
| C | 5.408 | 4.129 | 5.962 | | | | |
| C | 4.887 | 2.830 | 5.572 | | | | |
| C | 6.718 | 4.289 | 6.303 | | | | |
| O | 3.757 | 2.644 | 5.102 | | | | |
| TE | | -170.70 | | | | | |

**Table D8S.** Cartesian coordinates (Å) of acrolein, its intermediates and the products adsorbed on $O_{oss}$/Ag(111) surface

| H→O | x | y | z | H→C1 | x | y | z |
|---|---|---|---|---|---|---|---|
| H | 4.097 | 6.161 | 8.977 | | 6.267 | 6.257 | 7.349 |
| H | 5.138 | 1.652 | 8.681 | | 7.721 | 5.104 | 7.224 |
| H | 3.297 | 1.667 | 8.936 | | 6.363 | 3.281 | 8.176 |
| H | 5.239 | 4.089 | 8.836 | | 4.151 | 5.452 | 8.173 |
| H | 10.930 | 4.077 | 8.899 | | 3.861 | 3.705 | 7.934 |
| C | 4.238 | 2.217 | 8.915 | | 6.679 | 5.257 | 7.505 |
| C | 4.272 | 3.590 | 8.963 | | 5.932 | 4.275 | 8.017 |
| C | 3.142 | 4.471 | 9.111 | | 4.509 | 4.443 | 8.446 |
| O | 12.024 | 5.777 | 8.678 | | 4.380 | 4.248 | 9.856 |
| TE | | | -181.520 | | | | -181.463 |
| H→C2 | | | | H→C3 | | | |
| H | 3.569 | 4.087 | 8.733 | | 4.166 | 0.936 | 8.824 |
| H | 6.222 | 2.557 | 9.169 | | 4.160 | 1.925 | 7.355 |
| H | 4.636 | 1.773 | 9.052 | | 2.835 | 2.070 | 8.532 |
| H | 5.202 | 4.819 | 8.739 | | 5.782 | 2.957 | 9.091 |
| H | 4.111 | 2.751 | 6.688 | | 3.182 | 4.481 | 8.606 |
| C | 5.147 | 2.705 | 9.331 | | 3.922 | 1.934 | 8.433 |
| C | 4.637 | 3.900 | 8.529 | | 4.689 | 3.028 | 9.139 |
| C | 4.784 | 3.567 | 7.054 | | 4.210 | 4.369 | 9.022 |
| O | 5.584 | 4.096 | 6.303 | | 4.857 | 5.437 | 9.276 |
| TE | | | -181.600 | | | | -182.003 |
| Propenol | | | | Propanal | | | |
| H | 4.373 | 5.258 | 9.065 | | 2.875 | 1.777 | 8.383 |
| H | 2.535 | 4.149 | 7.993 | | 4.902 | 3.302 | 8.321 |
| H | 4.493 | 0.982 | 8.211 | | 4.202 | 1.097 | 7.422 |
| H | 2.824 | 1.766 | 8.447 | | 2.799 | 1.829 | 6.608 |
| H | 5.399 | 3.122 | 7.399 | | 4.750 | 3.445 | 6.544 |
| H | 3.408 | 4.538 | 6.491 | | 2.662 | 4.357 | 8.664 |
| C | 3.871 | 1.874 | 8.151 | | 3.473 | 1.916 | 7.470 |
| C | 4.349 | 3.039 | 7.698 | | 4.191 | 3.275 | 7.474 |
| C | 3.541 | 4.291 | 7.556 | | 3.222 | 4.404 | 7.686 |
| O | 4.196 | 5.440 | 8.116 | | 11.792 | 5.314 | 6.904 |
| TE | | | -185.883 | | | | -186.443 |
| Acrolein | | | | | | | |
| H | 4.642 | 1.017 | 7.871 | | | | |
| H | 2.843 | 1.460 | 8.032 | | | | |
| H | 5.184 | 3.451 | 7.595 | | | | |
| H | 10.855 | 3.701 | 7.936 | | | | |
| C | 3.875 | 1.790 | 7.888 | | | | |
| C | 4.163 | 3.093 | 7.739 | | | | |
| C | 3.103 | 4.106 | 7.770 | | | | |
| O | 3.288 | 5.311 | 7.630 | | | | |
| TE | | | -178.161 | | | | |

**Table D9S.** Cartesian coordinates (Å) of TS's, acrolein hydrogenation on $O_{oss}$/Ag(111) surface

| H→O | x | y | z | H→C1 | x | y | z |
|---|---|---|---|---|---|---|---|
| H | 4.528 | 6.145 | 10.256 | | 4.630 | 5.403 | 10.104 |
| H | 5.142 | 1.626 | 8.489 | | 3.784 | 6.295 | 7.153 |
| H | 3.323 | 1.872 | 8.576 | | 5.433 | 6.717 | 6.402 |
| H | 5.571 | 4.001 | 8.799 | | 6.527 | 5.042 | 7.890 |
| H | 11.250 | 4.378 | 8.561 | | 3.579 | 4.551 | 8.810 |
| C | 4.318 | 2.310 | 8.632 | | 4.862 | 6.122 | 7.114 |
| C | 4.542 | 3.649 | 8.755 | | 5.449 | 5.221 | 7.913 |
| C | 3.532 | 4.705 | 8.679 | | 4.675 | 4.373 | 8.835 |
| O | 3.810 | 5.930 | 8.736 | | 5.126 | 3.248 | 9.222 |
| TE | | | -180.732 | | | | -179.618 |
| H→C2 | | | | H→C3 | | | |
| H | 3.903 | 4.226 | 10.168 | | 3.646 | 1.246 | 9.995 |
| H | 6.569 | 2.320 | 9.316 | | 4.361 | 1.307 | 7.874 |
| H | 4.918 | 1.639 | 9.248 | | 2.864 | 2.016 | 8.507 |
| H | 5.684 | 4.655 | 8.936 | | 5.738 | 3.063 | 8.973 |
| H | 3.864 | 2.739 | 7.264 | | 3.135 | 4.490 | 8.593 |
| C | 5.499 | 2.539 | 9.482 | | 3.913 | 1.833 | 8.735 |
| C | 4.998 | 3.801 | 8.863 | | 4.672 | 3.059 | 9.133 |
| C | 4.493 | 3.633 | 7.476 | | 4.159 | 4.385 | 8.975 |
| O | 4.852 | 4.376 | 6.573 | | 4.816 | 5.466 | 9.178 |
| TE | | | -179.589 | | | | -180.334 |
| HC1; H→O | | | | HO;H→C1 | | | |
| H | 4.993 | 5.319 | 9.923 | | 3.995 | 4.287 | 10.043 |
| H | 4.030 | 5.164 | 7.566 | | 4.529 | 5.272 | 7.226 |
| H | 6.244 | 5.943 | 6.868 | | 5.434 | 1.008 | 8.605 |
| H | 7.660 | 4.740 | 6.794 | | 3.629 | 1.236 | 8.949 |
| H | 6.222 | 2.973 | 7.717 | | 5.617 | 3.327 | 7.777 |
| H | 3.745 | 3.408 | 7.515 | | 2.564 | 3.559 | 8.367 |
| C | 6.615 | 4.929 | 7.041 | | 4.584 | 1.682 | 8.674 |
| C | 5.822 | 3.975 | 7.536 | | 4.646 | 2.956 | 8.124 |
| C | 4.396 | 4.192 | 7.944 | | 3.570 | 3.828 | 8.049 |
| O | 4.250 | 4.130 | 9.337 | | 3.609 | 5.043 | 7.465 |
| TE | | | -183.437 | | | | -183.976 |
| HC3; H→C2 | | | | HC2; H→C3 | | | |
| H | 9.099 | 6.338 | 10.288 | | 5.141 | 0.076 | 9.897 |
| H | 8.637 | 6.660 | 8.380 | | 7.012 | 0.848 | 8.168 |
| H | 4.536 | 0.439 | 7.317 | | 4.278 | 1.838 | 9.222 |
| H | 3.429 | 0.587 | 8.702 | | 5.945 | 2.311 | 9.854 |
| H | 10.855 | 7.566 | 9.103 | | 5.421 | 0.476 | 7.429 |
| H | 5.060 | 2.593 | 8.543 | | 6.759 | 3.287 | 7.595 |
| C | 4.381 | 0.143 | 8.369 | | 5.332 | 1.551 | 9.337 |
| C | 5.569 | 0.591 | 9.215 | | 5.991 | 1.225 | 7.991 |
| C | 5.899 | 1.988 | 8.966 | | 6.092 | 2.495 | 7.166 |
| O | 7.016 | 2.551 | 9.079 | | 5.490 | 2.682 | 6.126 |
| TE | | | -184.588 | | | | -183.240 |

**Table D10S.** Frequencies ($cm^{-1}$) of acrolein, its intermediates and products adsorbed on Ag(110) surface

| | H→O | H→C1 | H→C2 | H→C1 | acrolein | propenol | propanal |
|---|---|---|---|---|---|---|---|
| 1 | 3664 | 3151 | 3036 | 3055 | 3175 | 3741 | 3055 |
| 2 | 3136 | 3066 | 3002 | 3030 | 3103 | 3161 | 3044 |
| 3 | 3118 | 3044 | 2980 | 2999 | 3087 | 3078 | 2995 |
| 4 | 3049 | 2846 | 2933 | 2929 | 2853 | 3056 | 2960 |
| 5 | 3043 | 2766 | 2870 | 2817 | 1543 | 2934 | 2844 |
| 6 | 1528 | 1568 | 1669 | 1486 | 1501 | 2848 | 2833 |
| 7 | 1426 | 1423 | 1440 | 1452 | 1392 | 1616 | 1689 |
| 8 | 1364 | 1398 | 1424 | 1435 | 1322 | 1440 | 1462 |
| 9 | 1291 | 1298 | 1381 | 1372 | 1237 | 1422 | 1460 |
| 10 | 1245 | 1269 | 1265 | 1309 | 1147 | 1367 | 1389 |
| 11 | 1135 | 1206 | 1189 | 1288 | 968 | 1273 | 1375 |
| 12 | 1094 | 1121 | 1132 | 1199 | 928 | 1250 | 1362 |
| 13 | 972 | 1016 | 1032 | 1076 | 907 | 1188 | 1284 |
| 14 | 929 | 989 | 989 | 1018 | 878 | 1128 | 1235 |
| 15 | 849 | 933 | 957 | 938 | 658 | 1024 | 1103 |
| 16 | 788 | 911 | 893 | 900 | 543 | 995 | 1098 |
| 17 | 619 | 900 | 856 | 819 | 305 | 930 | 1041 |
| 18 | 527 | 677 | 589 | 555 | 277 | 916 | 901 |
| 19 | 431 | 455 | 513 | 344 | 233 | 901 | 870 |
| 20 | 391 | 363 | 349 | 296 | 163 | 640 | 623 |
| 21 | 288 | 252 | 316 | 261 | 127 | 450 | 531 |
| 22 | 262 | 194 | 190 | 221 | 92 | 340 | 305 |
| 23 | 227 | 145 | 165 | 176 | 56 | 253 | 206 |
| 24 | 136 | 133 | 143 | 142 | 18 | 187 | 139 |
| 25 | 105 | 71 | 92 | 104 | | 121 | 120 |
| 26 | 81 | 48 | 86 | 62 | | 89 | 101 |
| 27 | 6 | 47 | 34 | 26 | | 54 | 82 |
| 28 | | | | | | 36 | 77 |
| 29 | | | | | | 20 | 55 |
| 30 | | | | | | 6 | 34 |

**Table D11S.** Frequencies ($cm^{-1}$) of transition states of acrolein hydrogenation over Ag(110) forming propenol and propanal as products

| | H→O | H→C1 | H→C2 | H→C3 | HC1; H→O | HO; H→C1 | HC3; H→C2 | HC2; H→C3 |
|---|---|---|---|---|---|---|---|---|
| 1 | 3179 | 3167 | 3193 | 3101 | 3148 | 3703 | 3049 | 3093 |
| 2 | 3085 | 3094 | 3095 | 3046 | 3069 | 3107 | 3041 | 3028 |
| 3 | 3061 | 3075 | 3046 | 3012 | 3059 | 3097 | 3018 | 2974 |
| 4 | 2932 | 2841 | 2822 | 2738 | 2875 | 3030 | 2971 | 2886 |
| 5 | 1502 | 1599 | 1711 | 1520 | 2853 | 2947 | 2953 | 2875 |
| 6 | 1461 | 1445 | 1455 | 1476 | 1574 | 1512 | 1535 | 1682 |
| 7 | 1361 | 1386 | 1383 | 1390 | 1433 | 1441 | 1498 | 1415 |
| 8 | 1301 | 1299 | 1316 | 1327 | 1405 | 1364 | 1480 | 1411 |
| 9 | 1229 | 1255 | 1231 | 1237 | 1301 | 1254 | 1390 | 1394 |
| 10 | 1175 | 1155 | 1190 | 1183 | 1274 | 1233 | 1344 | 1366 |
| 11 | 970 | 1120 | 1089 | 1113 | 1209 | 1189 | 1300 | 1269 |
| 12 | 926 | 990 | 988 | 1019 | 1125 | 1085 | 1231 | 1201 |
| 13 | 883 | 925 | 943 | 967 | 1013 | 986 | 1117 | 1144 |
| 14 | 819 | 913 | 866 | 914 | 993 | 959 | 1070 | 1065 |
| 15 | 727 | 879 | 690 | 866 | 937 | 910 | 993 | 991 |
| 16 | 635 | 780 | 652 | 734 | 918 | 844 | 961 | 939 |
| 17 | 548 | 616 | 567 | 570 | 907 | 799 | 956 | 929 |
| 18 | 370 | 510 | 520 | 521 | 827 | 703 | 750 | 802 |
| 19 | 315 | 332 | 334 | 338 | 689 | 595 | 610 | 596 |
| 20 | 284 | 290 | 279 | 252 | 559 | 517 | 570 | 505 |
| 21 | 251 | 192 | 202 | 233 | 445 | 404 | 507 | 436 |
| 22 | 182 | 133 | 130 | 182 | 371 | 353 | 452 | 339 |
| 23 | 138 | 84 | 83 | 105 | 258 | 313 | 325 | 241 |
| 24 | 90 | 50 | 69 | 78 | 214 | 282 | 315 | 151 |
| 25 | 56 | 18 | 48 | 41 | 149 | 219 | 213 | 109 |
| 26 | 45 | 12 | 40 | 17 | 133 | 123 | 191 | 90 |
| 27 | 1028i | 820i | 848i | 833i | 91 | 91 | 135 | 71 |
| 28 | | | | | 55 | 68 | 80 | 42 |
| 29 | | | | | 31 | 52 | 74 | 10 |
| 30 | | | | | 694i | 823i | 388i | 859i |

**Table D12S.** Frequencies ($cm^{-1}$) of transition states of acrolein hydrogenation over $O_{oss}$/Ag(111) surface forming propenol and propanal as products

| | H→O | H→C1 | H→C2 | H→C3 | HC1; H→O | HO; H→C1 | HC3; H→C2 | HC2; H→C3 |
|---|---|---|---|---|---|---|---|---|
| 1 | 3233 | 3172 | 3087 | 3163 | 3154 | 3670 | 3038 | 3056 |
| 2 | 3134 | 3093 | 3045 | 3086 | 3078 | 3193 | 3002 | 3039 |
| 3 | 3119 | 3082 | 3027 | 3070 | 3065 | 3154 | 2995 | 2951 |
| 4 | 2830 | 2930 | 2848 | 2888 | 2949 | 3099 | 2930 | 2820 |
| 5 | 1547 | 1617 | 1674 | 1471 | 2904 | 3053 | 2822 | 2807 |
| 6 | 1526 | 1402 | 1398 | 1439 | 1650 | 1531 | 1571 | 1738 |
| 7 | 1399 | 1275 | 1356 | 1333 | 1424 | 1460 | 1514 | 1685 |
| 8 | 1325 | 1230 | 1242 | 1303 | 1412 | 1368 | 1446 | 1424 |
| 9 | 1262 | 1095 | 1108 | 1213 | 1350 | 1278 | 1435 | 1371 |
| 10 | 1141 | 997 | 990 | 1179 | 1299 | 1258 | 1369 | 1363 |
| 11 | 992 | 969 | 963 | 969 | 1275 | 1237 | 1355 | 1252 |
| 12 | 939 | 956 | 934 | 941 | 1210 | 1100 | 1252 | 1234 |
| 13 | 921 | 894 | 849 | 918 | 1122 | 954 | 1124 | 1138 |
| 14 | 884 | 816 | 825 | 882 | 1002 | 925 | 1061 | 1069 |
| 15 | 724 | 646 | 781 | 620 | 977 | 915 | 1002 | 1002 |
| 16 | 559 | 584 | 529 | 555 | 932 | 821 | 921 | 972 |
| 17 | 534 | 506 | 507 | 497 | 922 | 759 | 898 | 894 |
| 18 | 494 | 476 | 382 | 392 | 906 | 638 | 854 | 848 |
| 19 | 287 | 372 | 336 | 334 | 734 | 563 | 574 | 751 |
| 20 | 268 | 342 | 228 | 273 | 647 | 507 | 547 | 554 |
| 21 | 217 | 196 | 167 | 218 | 435 | 478 | 364 | 489 |
| 22 | 187 | 119 | 97 | 125 | 340 | 292 | 280 | 353 |
| 23 | 108 | 95 | 90 | 106 | 199 | 269 | 244 | 220 |
| 24 | 62 | 73 | 79 | 73 | 165 | 182 | 174 | 118 |
| 25 | 40 | 37 | 55 | 47 | 127 | 119 | 166 | 110 |
| 26 | 34 | 23 | 28 | 20 | 118 | 93 | 138 | 83 |
| 27 | 838i | 639i | 904i | 524i | 69 | 77 | 71 | 61 |
| 28 | | | | | 51 | 31 | 64 | 47 |
| 29 | | | | | 22 | 13 | 26 | 26 |
| 30 | | | | | 917i | 634i | 513i | 1176i |